1-1-2006

Quantum dot-polymer nanocomposites : new materials for dispersion, encapsulation, and electronic applications.

Kevin N. Sill
University of Massachusetts Amherst

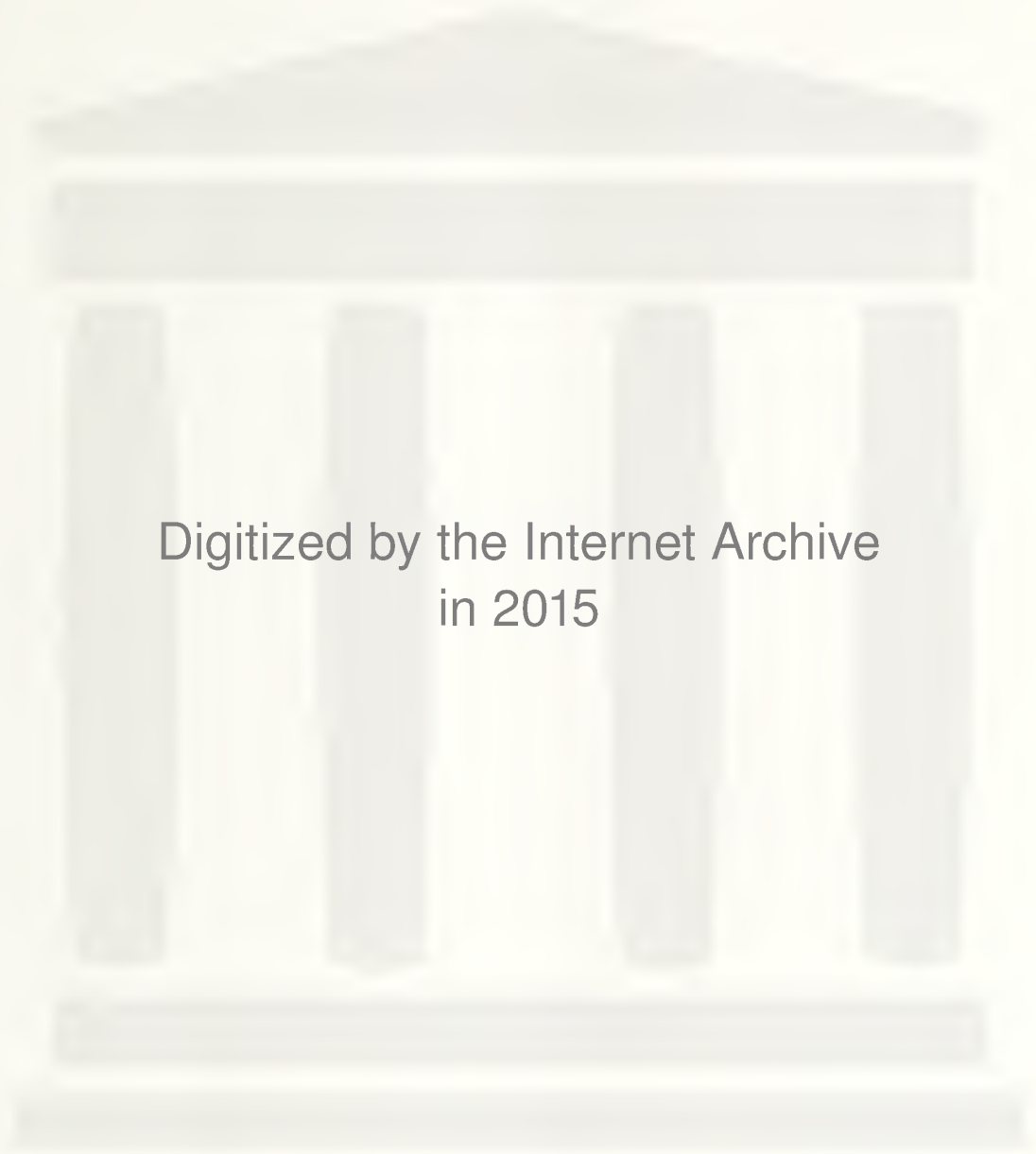

QUANTUM DOT - POLYMER NANOCOMPOSITES: NEW MATERIALS FOR DISPERSION, ENCAPSULATION, AND ELECTRONIC APPLICATIONS

A Dissertation Presented

by

KEVIN N. SILL

Submitted to the Graduate School of the
University of Massachusetts Amherst in partial fulfillment
of the requirements for the degree of

DOCTOR OF PHILOSOPHY

September 2006

Polymer Science and Engineering

INFORMATION TO USERS

The quality of this reproduction is dependent upon the quality of the copy submitted. Broken or indistinct print, colored or poor quality illustrations and photographs, print bleed-through, substandard margins, and improper alignment can adversely affect reproduction.

In the unlikely event that the author did not send a complete manuscript and there are missing pages, these will be noted. Also, if unauthorized copyright material had to be removed, a note will indicate the deletion.

ProQuest Information and Learning Company
300 North Zeeb Road
P.O. Box 1346
Ann Arbor, MI 48106-1346

QUANTUM DOT - POLYMER NANOCOMPOSITES: NEW MATERIALS FOR DISPERSION, ENCAPSULATION, AND ELECTRONIC APPLICATIONS

A Dissertation Presented

by

KEVIN N. SILL

Approved as to style and content by:

_____

Todd S. Emrick, Chair

_____

E. Bryan Coughlin, Member

_____

Paul M. Lahti, Member

_____

Shaw L. Hsu, Department Head
Polymer Science and Engineering

QUANTUM DOT - POLYMER NANOCOMPOSITES: NEW MATERIALS FOR DISPERSION, ENCAPSULATION, AND ELECTRONIC APPLICATIONS

A Dissertation Presented

by

KEVIN N. SILL

Approved as to style and content by:

Todd S. Emrick, Chair

E. Bryan Coughlin, Member

Paul M. Lahti, Member

Shaw L. Hsu, Department Head
Polymer Science and Engineering

ACKNOWLEDGMENTS

I would like to thank my advisor Prof. Todd Emrick for his supervision during my graduate career. I would also like to thank Prof. E. Bryan Coughlin and Prof. Paul Lahti for serving on my dissertation committee. All provided me with the necessary guidance and advice throughout my graduate studies. In addition, Prof Mike Barnes offered a great deal of knowledge and advice during the late stages of my graduate career.

Many thanks are due to Chip Breitenkamp, Rebecca Breitenkamp, and Dr. Habib Skaff. These three above all else challenged me to excel during my time at UMass. They truly made the graduate school experience both rewarding and memorable.

I would like to thank Bryan Parrish for keeping me on an even keel at school. Bryan was always my first call when I needed to get some perspective. I would like to thank the rest of the Emrick group that have helped me along the way. Prof. Denise Junge offered a great deal of guidance and entertainment during her summers at UMass. Dr. Maisie Joralemon joined the group late in my time at UMass but was a great groupmate. Dr. Ken Ellzey was the ultimate "senior" group member and could always provide some archaic procedure to try. Rui Hong and Qingling Zhang were quiet group members, but when they spoke up during group meeting it was most likely a very good idea. I'll also mention Liz Glogowski and Ravi Tangirala for teaching me a bit more patience.

The technical staff at UMass also deserves much credit. Dr. Charlie Dickinson has been an excellent teacher in the use and application of NMR spectroscopy. His

advice and knowledge will be missed. Dr. Steven Eyles offered his assistance many times during his supervision of the mass spectrometry laboratory and the size-exclusion chromatography laboratory. Lou Raboin has spent countless hours attempting to teach a chemist how to be a microscopist, and Dr. Evgenia Pekarskaya has lent her TEM expertise on a number of occasions.

People at institutions other than UMass have also had a profound effect upon my graduate career. Prof. André Striegel has counseled and guided me in all aspects of my life, particularly my scientific career, since the age of 17 and I have benefited greatly from his advice. I would also like Dr. Josh Orlicki, the person who was my undergraduate mentor at the University of Illinois. His patient explanations and instructions provided a solid foundation for my graduate career. In addition, I would like to thank Prof. Jeffrey Moore for his guidance and advice during my undergraduate and graduate studies.

Finally, I would like to thank my friends and family for their support. Brandon Underwood has always been a source of support and friendship. My parents Morton and Linda Sill have always supported me in my every endeavor and I thank them for all that they have done over the years. Finally, I thank my wife Stephanie Barnes for her unwavering love and support thoughout the entire graduate school process.

ABSTRACT

QUANTUM DOT - POLYMER NANOCOMPOSITES: NEW MATERIALS FOR DISPERSION, ENCAPSULATION, AND ELECTRONIC APPLICATIONS

September 2006

KEVIN N. SILL, B.S., UNIVERSITY OF ILLINOIS

M.S., UNIVERSITY OF MASSACHUSETTS AMHERST

Ph.D., UNIVERSITY OF MASSACHUSETTS AMHERST

Directed by: Professor Todd S. Emrick

Tremendous advances in the synthesis and functionalization of nanoparticles over the past twenty years have resulted in remarkable discoveries in the field of nanotechnology. One such development is found in quantum dots, semiconductor nanoparticles that exhibit unique optical and electronic properties not found in the bulk. Research efforts associated with the combination of quantum dots and polymers center on uniting the mechanical or processing properties of the polymer with the optical properties of the quantum dot. Simply blending polymers with nanoparticles typically leads to nanoparticle aggregation, which negates the inherent advantageous properties of the quantum dots. The development of organic and polymer ligands for nanoparticle surface modification enables the preparation of dispersed nanocomposites that retain, or even enhance, the original nanoparticle properties.

Presented here is the synthesis of functionalized nanoparticles that are tailored for the growth of polymers directly from the particle surface. Initial studies focused on the preparation of nanoparticle-polymer hybrid materials where the nanoparticles were

evenly dispersed throughout the polymer. A method was developed to cross-link polymers grafted from the nanoparticle in an encapsulating shell, with the goal of minimizing nanoparticle degradation. In addition, polymerization chemistry from quantum dot surfaces was modified and optimized to produce conjugated polymer-quantum dot composites. The coupling of these two electronically active components gave composite materials with very unique optical properties that hold potential as displays, sensors, and light-emitting materials.

TABLE OF CONTENTS

LIST OF TABLES

LIST OF FIGURES

LIST OF SCHEMES

LIST OF ACRONYMS

ATRP	atom transfer radical polymerization
BCB	benzocyclobutane
CdO	cadmium oxide
CdS	cadmium sulfide nanoparticles
CdSe	cadmium selenide nanoparticles
CdSe-PKV	cadmium selenide nanoparticles with poly(N-dodecylcarbazole vinylene) grafted from the particle surface
CdSe-PPV	cadmium selenide nanoparticles with poly(*p*-phenylene vinylene) grafted from the particle surface
CdSe-PS	cadmium selenide nanoparticles with polystyrene grafted from the particle surface
CdSe-oxyPPV	Cadmium selenide nanoparticles with octyl ether poly(*p*-phenylene vinylene) grafted from the particle surface
CdSe/ZnS	cadmium selenide nanoparticles with a zinc sulfide overcoat, a core-shell nanoparticle
CdTe	cadmium telluride nanoparticles
DMAP	4-dimethylaminopyridine
DOPO	di-*n*-octylphosphine oxide
DOPO-Br	4-bromobenzyl-di-*n*-octylphosphine oxide
DOSPO	di-*n*-octyl-stryrenyl phosphine oxide
DPPE	bis(diphenylphosphino) ethane
DPPP	bis(diphenylphosphino) propane
EA	electron affinity
E_g	band gap energy

EI	electron impact ionization
eV	electron volt
FAB	fast atom bombardment ionization
FRET	Förster resonance energy transfer
FWHM	full width at half peak maximum
HDA	1-hexadecyl amine
HRMS	high-resolution mass spectrometry
InP	indium phosphide nanoparticles
IP	ionization potential
MALDI-TOF	matrix assisted laser desorption ionization – time of flight mass spectrometry
M_n	number average molecular weight
M_w	weight average molecular weight
NMR	nuclear magnetic resonance spectroscopy
NMRP	nitroxide mediate radical polymerization
oligoPPV	short chain oligomers (average DP ~ 4) of di-octyl substituted poly(*p*-phenylene vinylene)
oxyPPV	poly(*p*-phenylene vinylene) with octyl ether substitutents
PAA	poly(acrylic acid)
PbSe	lead selenide nanoparticles
Pd_2dba_3	tris(dibenzylideneacetone)dipalladium
PDI	polydispersity index
$Pd(OAc)_2$	palladium acetate
$Pd(PPh_3)_4$	tetrakis(triphenylphosphino)palladium

PEG	poly(ethylene glycol)
PKV	poly(N-dodecylcarbazole vinylene)
PL	photoluminescence
PMMA	poly(methyl methacrylate)
PPV	poly(*p*-phenylene vinylene)
PS	polystyrene
PS-co-BCB	random copolymer of styrene and 4-vinyl benzocyclobutane
PVP	poly(4-vinyl pyridine)
TEM	transmission electron microscopy
TEMPO	2,2,6,6-tetramethyl-1-piperidinyloxy
TLC	thin layer chromatography
TOP	tri-*n*-octyl phosphine
TOPO	tri-*n*-octyl phosphine oxide
RAFT	reversible addition-fragmentation chain transfer polymerization
R_g	radius of gyration
ROMP	ring-opening metathesis polymerization
UV-Vis	ultraviolet-visible spectroscopy
ZnSe	zinc selenide nanoparticles

CHAPTER 1

INTRODUCTION

1.1 Nanotechnology and Nanoparticles

Efforts in nanoscience and nanotechnology are broad and often interdisciplinary, encompassing the fields of chemistry, biology, physics, engineering and materials science, with an emphasis on the understanding, development, fabrication, characterization and application of materials on the nanometer size scale.[1-9] For example, key components of the microelectronics industry are enabled by processes performed at the nanoscale. These nanoscale materials are prepared by either "top-down" or "bottom-up" approaches. The top-down technique involves the downward scaling of bulk materials to nanoscale dimensions. For example, conventional photolithography for the generation of nanoscale surface features is performed in a top-down fashion by irradiation and selective dissolution of polymer films using nanoscale masks.[10] Commercial computer processors currently utilize a 45 nm lithographic process while state-of-the-art photolithographic techniques allow for features down to 20 nm.[11-13] Other lithographic techniques such as electron beam or soft X-ray lithography allow for the creation of lines less than 10 nm wide.[14]

Alternatively, bottom-up approaches involve preparation of nanoscale materials from chemical precursors. Nanoparticles of many compositions can be prepared with dimensions from 1 to 100 nm. Nanoparticles are composed of a variety of materials such as clay, iron, carbon, gold and a host of metals and metal amalgams.[15-20] Each distinct nanoparticle carries its own unique properties that often differ from the properties of the

bulk material. Based upon composition, the core of the nanoparticle can possess magnetic, semiconducting or catalytic properties that make them prime candidates in applications such as data storage, photovoltaics or catalysis. Quantum confined particles, or quantum dots, are one such example where material properties are dependent upon the size of the particle.[21] Other examples of this unique behavior include gold nanoparticles, which exhibit a size-dependent absorption spectrum based upon the vibration of the particle's atomic lattice structure, known as plamson resonance;[22] iron oxide particles that can exhibit varying degrees of magnetic susceptibility solely based upon particle size and crystal structure;[23] and palladium particles, which possess a very large surface area to mass ratio that is beneficial in catalysis.[24]

Many nanoparticle syntheses give products that consist of an inorganic core and an organic periphery, such as that depicted in **Figure 1**. Many nanoparticle syntheses utilize surfactants with polar head groups such as amines, carboxylic acids, thiols, phosphonic acids, phosphines or phosphine oxides and apolar tails such as *n*-alkanes. Alkane chains attached to the nanoparticles provide solubility in a range of organic solvents, and are convenient for their chemical and thermal stability. Exceptions to these generalizations do exist, as iron oxide nanoparticles can be prepared in slightly basic conditions at room temperature without additional ligands.[25]

Rapid developments in nanoparticle synthesis and characterization over the past twenty years have driven tremendous advances in the field. One important challenge in nanoscience is the synthesis of composite materials consisting of nanoparticles and polymers that are designed to maximize the contributions of both components. While there remains significant interest in the use of nanoparticles as fillers in polymer

materials to enhance physical and mechanical properties, a primary goal of nanotechnology has been the incorporation of these materials into a polymer matrix for the preparation of functional hybrid materials.[26-30] These composite materials are expected to allow for the combination of the processability of the polymer with the optical, electronic or magnetic properties of the nanoparticle to give functional materials with features on the nanometer size scale. Research efforts are underway that focus on precise structures of nanoparticles in polymers, including their assembly in arrays and along interfacial boundaries. The introduction of precise organic chemistry on nanoparticle materials has led to developments in the growth of polymers from nanoparticle surfaces, allowing one to tailor the properties of the particles by the choice of polymer and its inherent functionality. This dissertation will describe the use of organic ligands to tailor nanoparticles, particularly cadmium selenide quantum dots, with functional ligands, and the use of these ligand-functionalized nanoparticles for the growth of polymers from the nanoparticle surface.

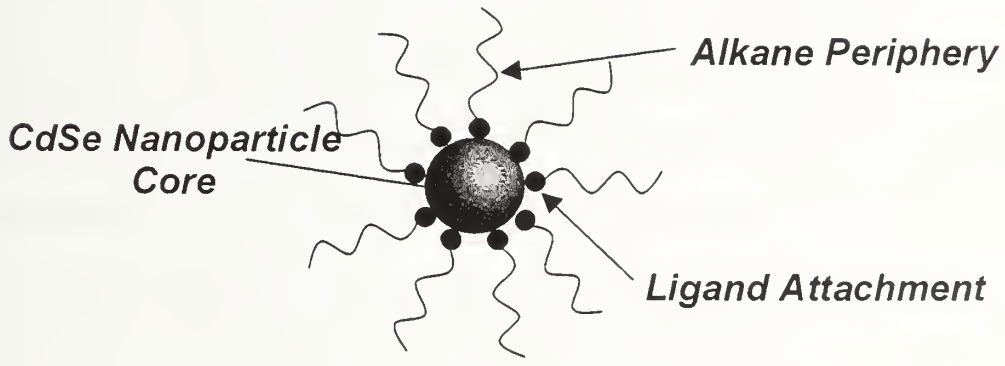

Figure 1. Schematic illustration of ligand-stabilized nanoparticles.

1.2 Cadmium Selenide Quantum Dots

Semiconductor nanoparticles are generating interest across materials science and biology.[31-33] These nanoparticles, also termed quantum dots, are unique in that their properties that are intermediate between the conventional molecular and bulk systems.[34-39] This phenomenon is due to quantum confinement, the case where the lattice structure of the particle is smaller than the Bohr-exciton radius (5.4 nm)[40] of the bulk material. When an exciton (an electron-hole pair) is created it is confined to a space smaller than its equilibrium distance. This confinement leads to discrete energy states, where the energy of confinement is dissipated by the emission of light. The wavelength of emitted light scales directly with particle size, leading to a predictable relationship between nanoparticle size and the wavelength of light emitted. Examples of quantum dots include cadmium sulfide (CdS)[41], cadmium telluride (CdTe)[18], zinc sulfide (ZnS)[42], zinc selenide (ZnSe)[43], indium phosphide (InP)[44], lead selenide (PbSe)[45] and a host of other materials.

Of particular interest for this dissertation are 2-10 nm cadmium selenide (CdSe) nanoparticles that exhibit photoluminescence in the visible region of light (**Figure 2**), a result of their 1.8-2.8 nm band gap.[46] Since 1993, CdSe nanocrystals have been prepared through the use of a high temperature, inverse micelle synthesis.[47-54] This synthetic method involves the use of appropriate Cd and Se precursors in the presence of surfactant and ligand molecules. Typically, tri-*n*-octyl phosphine oxide (TOPO) and CdO are heated under an inert atmosphere to greater than 300 °C resulting in complexation of cadmium by the phosphine oxide. A solution of selenium in tri-*n*-octyl phosphine is injected rapidly into the hot cadmium solution, initiating nanocrystal nucleation and growth (**Figure 3**) to give nanocrystals with a low size distribution (~ 10%). The

quantum confined nature of the particles, along with the narrow distribution of particle size gives CdSe nanoparticles with a very narrow fluorescence emission profile, approximately 20-30 nm full width at half peak maximum (FWHM), and solution fluorescence quantum yields of 70-80%. The nature of the ligand binding to the nanocrystal surface, and the organic periphery that results from this binding, serves to passivate otherwise dangling bonds on the nanoparticle surface, protect the nanoparticles from surface oxidation, and allow for dispersion of the nanoparticles in common organic solvents. However, this chemically inert alkane periphery does not allow for further modification of the nanoparticle periphery; however, methods have been developed that allow for the functionalization of CdSe nanoparticles.[55,56]

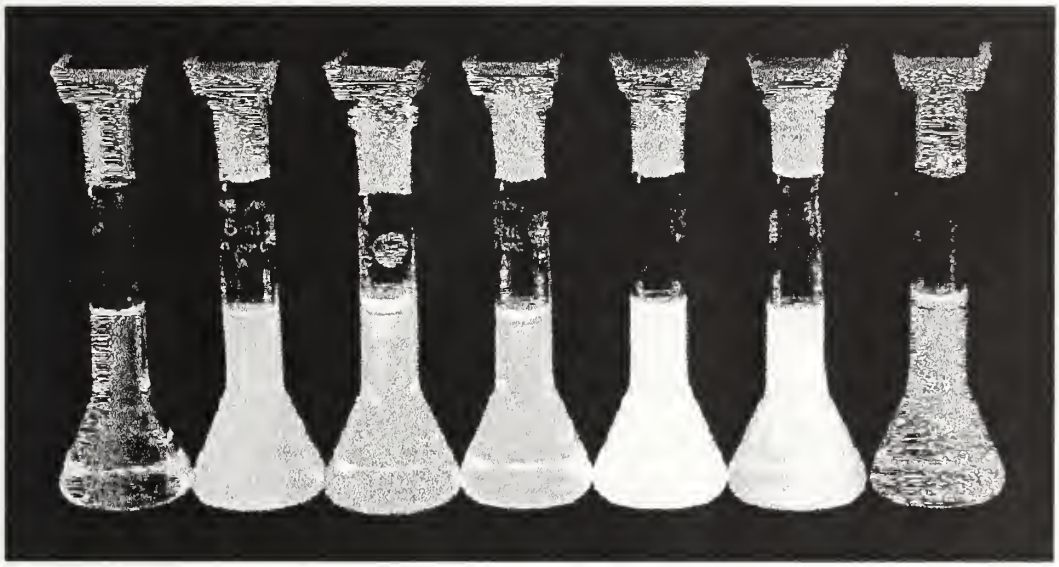

Figure 2. Full color emission of CdSe quantum dots of ~ 1.5 (left) to 4.5 nm (right) diameter. (Fair use image from http://www.chemie.uni-hamburg.de/pc/Weller/)

Multiple research groups have investigated the atomic structure and ligand coverage of CdSe nanoparticles prepared by the high-temperature, inverse-micelle synthesis. Murray and Bawendi utilized computer modeling and X-ray diffraction to determine that 2.0, 3.7, and 8.0 nm CdSe nanoparticles are comprised of approximately

275, 1,000, and 10,000 atoms in a wurtzite structure, respectively.[57] Further X-ray diffraction studies by Bawendi and coworkers have shown that of the 1,000 atoms in 3.7 nm CdSe nanoparticle, approximately 300 atoms are present on the surface of the nanoparticle surface. In addition, it was determined by ^{31}P NMR that approximately 150-170 of the 300 surface atoms were coordinated with a TOPO ligand, resulting in a ligand coverage of ~55%.[58] Rutherford backscattering spectroscopy, which uses low mass ions to probe the chemical composition of a surface, performed by Rosenthal and coworkers revealed that due to the preferential binding of TOPO to Cd atoms, the surface coverage consists of a 1:1.2 ratio of Se-to-Cd atoms, and suggests that the TOPO ligand coverage is closer to 70%.[59]

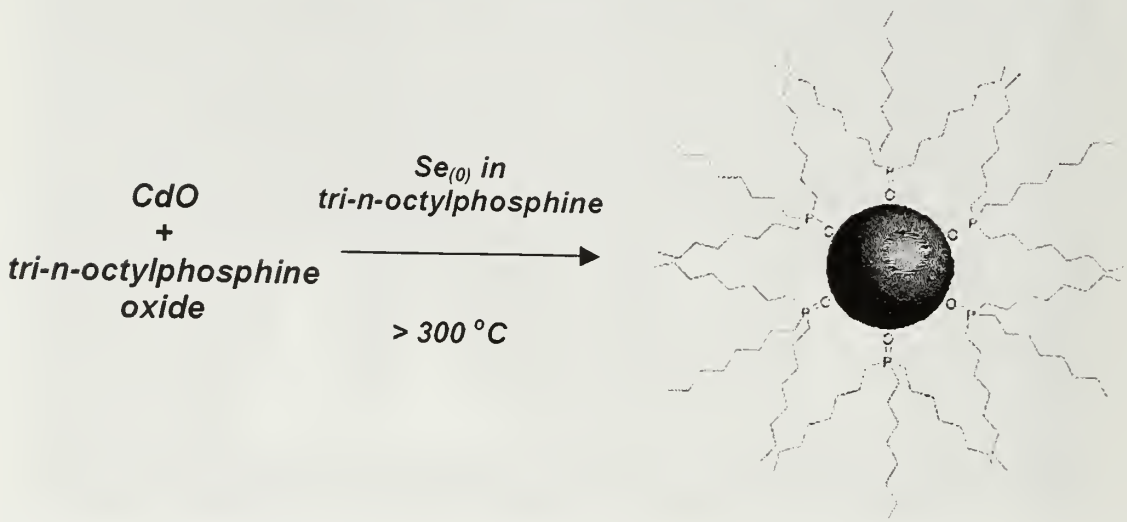

Figure 3. Typical CdSe nanoparticle synthesis.

1.3 Polymer-Nanoparticle Materials

1.3.1 Historical Perspective of Polymer-Nanoparticle Blends

The integration of nanoparticles into polymers has been of significant theoretical and experimental interest to the polymer and engineering communities for many years.

Micron and sub-micron sized fillers have been used for some time in conjunction with polymer materials, in an effort to enhance the physical and mechanical properties relative to the polymers alone. In the mid 19th century Charles and Nelson Goodyear showed that vulcanized rubber could be toughened by the addition of zinc oxide or magnesium sulfate.[60] Bakelite™ represented the first mass-produced synthetic polymer composite, a silicate clay reinforced phenolic resin pioneered by Leo Baekeland in the early 1900's.[61] More recently, it was found that rubber particles embedded in nylon and other polymer matrices afford composites with outstanding impact resistance.[62]

However, significant challenges are associated with blending polymers and nanoparticles to afford homogeneous dispersion of inorganic particles within the polymer (**Figure 4**). For a random dispersion of nanoparticles within a polymer film to be achieved, the particles must be compatible enthapically with the surrounding polymer matrix. The currently available commercial polymers and nanoparticles leave few choices in this regard, such that blends nearly always lead to phase separation and aggregation of the nanoparticles.[63] A number of approaches have been investigated and will be discussed below.

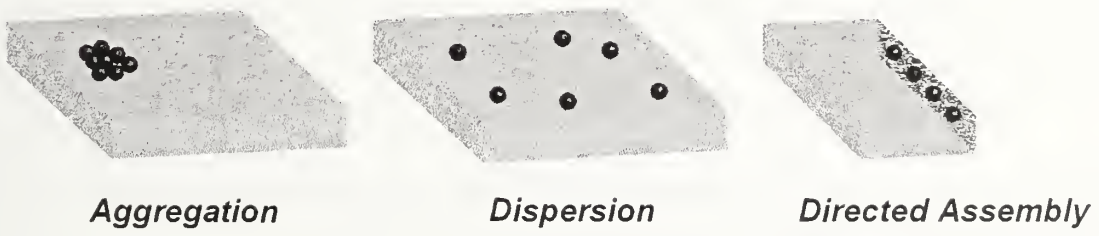

Figure 4. Schematic illustration of nanoparticle phase behavior in polymeric materials.

1.3.2 The Graft-to Approach to Nanoparticle-Polymer Composite Materials

The two most common routes to polymer functionalization include the "graft-to" approach which attaches polymers to nanoparticles, and the "graft-from" method, which focuses on polymerization from a nanoparticle surface. The typical graft-to approach is carried out by the attachment of polymers with ligand-functionalized chain-ends to nanoparticles through ligand exchange chemistries. While this procedure is commonly for simplicity, less than optimum grafting density may result due to steric shielding that arises upon placement of each successive polymer chain onto the nanoparticle. An example of this grafting-to method involves the ligand exchange of pyridine-functionalized poly(ethylene glycol) (PEG) for TOPO on CdSe nanoparticles to afford a water soluble, PEG functionalized quantum dot (**Figure 5**).[64]

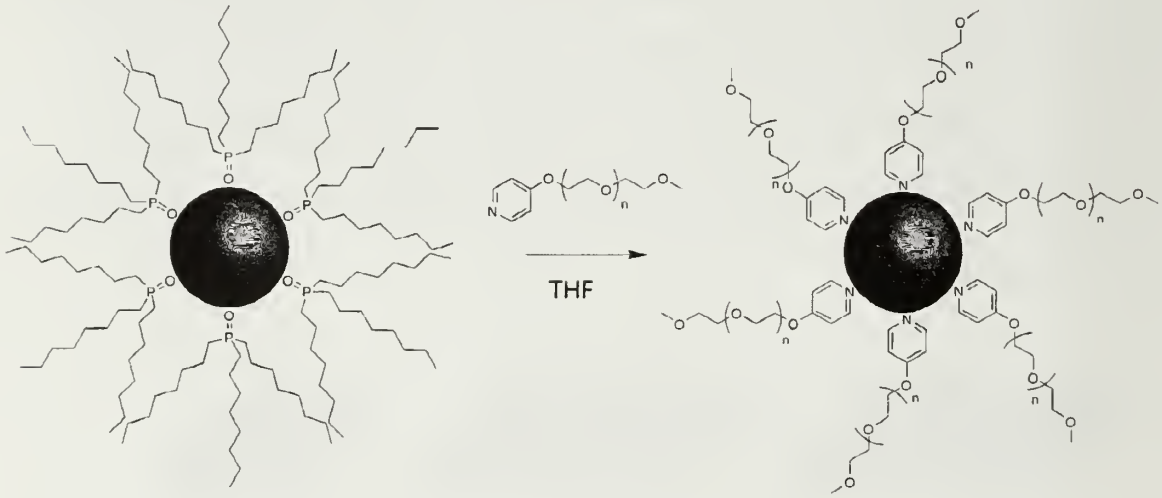

Figure 5. Ligand exchange of TOPO-covered CdSe with 4-hydroxypyridine-poly(ethylene glycol) ligands according to Skaff and Emrick.

Another derivative of the graft-to approach involves the use of polymers with pendant functionality as multi-dentate ligands. For example, palladium nanoparticles are stabilized by poly(N-vinyl pyrrolidone), and have been shown to be active catalysts for

Suzuki couplings in aqueous media.[65] Bawendi and coworkers have performed ligand exchange with ethylene glycol-phosphine oxide copolymers and CdSe to give highly luminescent, water soluble quantum dots.[66,67] Winnik and coworkers have prepared composite materials from TOPO covered CdSe/ZnS particles following ligand exchange with poly(dimethylaminoethyl methacrylate).[63]

The third graft-to approach allows for the preparation of the polymer-nanoparticle composite by synthesizing the particle in the presence of an end-functionalized polymer ligand (**Figure 6**). For example. Hedrick and coworkers have prepared CdS particles with thiol-functionalized polycaprolactone ligands.[68] McCormick and coworkers utilized acrylate based copolymers with a thiol end group to prepare water soluble gold. silver. platinum or rhodium nanoparticles.[69] Gold nanoparticles dispersed in polystyrene films were prepared following the synthesis of gold nanoparticles with polystyrene thiol ligands.[70] Knoll and coworkers prepared gold nanoparticles functionalized with electroactive polyaniline.[71] In addition. catalytically active palladium particles were prepared in a two phase synthesis with poly(N.N'-dihexylcarbodimide) and palladium (IV) chloride.[72] While this approach results in an efficient, one-pot synthesis of a variety of nanoparticles. the polymer ligand must be amenable to the nanoparticle growth conditions. a considerable problem for semiconductor nanoparticles prepared by high temperature methods.

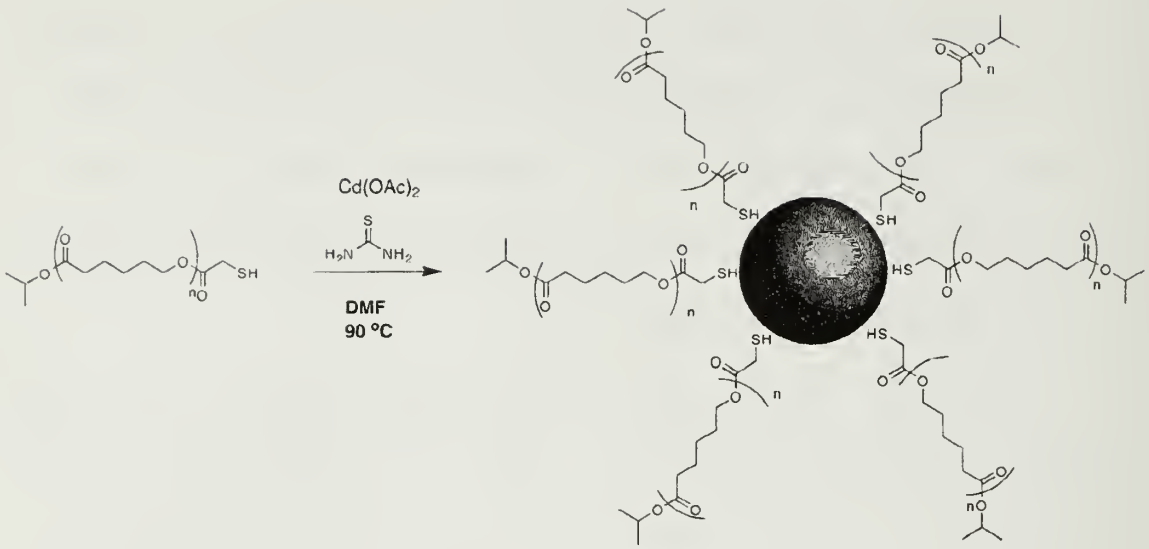

Figure 6. The direct preparation of CdS quantum dots in the presence of thiol functionalized polycaprolactone as reported by Hedrick and coworkers.

1.3.3 The Graft-from Approach to Nanoparticle-Polymer Composites

The attachment of polymerization initiators to nanoparticle surfaces, followed by polymer growth outward from the surface, describes the "graft-from" technique. This is proving to be an excellent approach in which polymerization initiators can be attached to nanoparticles, followed by polymerization to prepare a variety of nanoparticle-polymer hybrid materials. Critical to this "grafting-from" process is the compatibility of the nanoparticle with the polymerization conditions chosen, such that neither the attachment of functional ligands, nor the polymerization process, appreciably alters the inherent properties of the nanoparticles. While these requirements require thoughtful synthesis, much progress has been made in recent years. It should be noted that nanoparticle surfaces differ from flat surfaces as substrates in the "grafting-from" process, as higher surface curvature of the spherical nanoparticle may reduce steric crowding during chain growth, which may lead to more effective polymerization from the nanoparticles.

Polymerization techniques utilized in the "grafting-from" method include controlled radical polymerization, living anionic polymerization, and ring-opening metathesis polymerization (ROMP). Mirkin and coworkers demonstrated the technique by the surface functionalization of gold nanoparticles with norbornene derivatives that were used to prepare polynorbornene grafts by ROMP (**Figure 7**).[73] Jordan and coworkers used ω-functionalized self-assembled monolayers of thiolates on gold nanoparticles to initiate living cationic ring-opening polymerizations of 2-oxazoline monomers.[74] Möhwald has reported atom transfer radical polymerization (ATRP) of 2-(dimethylamino)ethyl methacrylate from the gold nanoparticles as another polymerization technique from gold nanoparticles.[75]

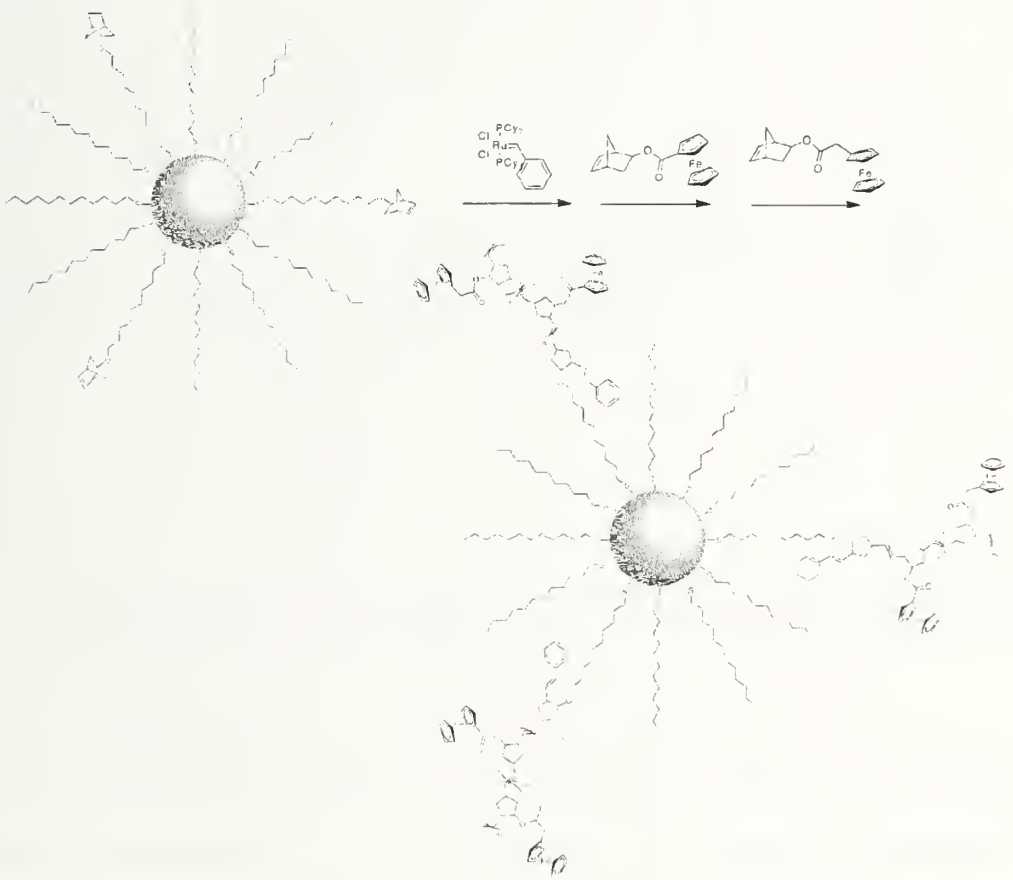

Figure 7. The preparation of norborne based block copolymers from the surface of gold nanoparticles by Mirkin and coworkers.

In the case of SiO_2 nanoparticles, surface-initiated anionic polymerization has been reported using 1,1-diphenylethylene with a chlorosilane end-group to functionalize the nanoparticles, followed by anionic polymerization of styrene.[76] Additionally, Zydowicz has reported nitroxide mediated radical polymerization (NMRP) from silica nanoparticles.[77] The Patten group has reported ATRP from silica and core-shell CdS/SiO_2 nanoparticles, and have demonstrated the ability to grow well-defined PS or PMMA layers from isobutryl-bromide modified inorganic surfaces (**Figure 8**).[78,79] Recently, Patten and coworkers have also reported ATRP of acrylate type monomers from magnetic iron oxide nanoparticles.[80] Takahara and coworkers have copolymerized styrene and 3-vinylpyridine from nitroxide functionalized magnetite particles.[81,82]

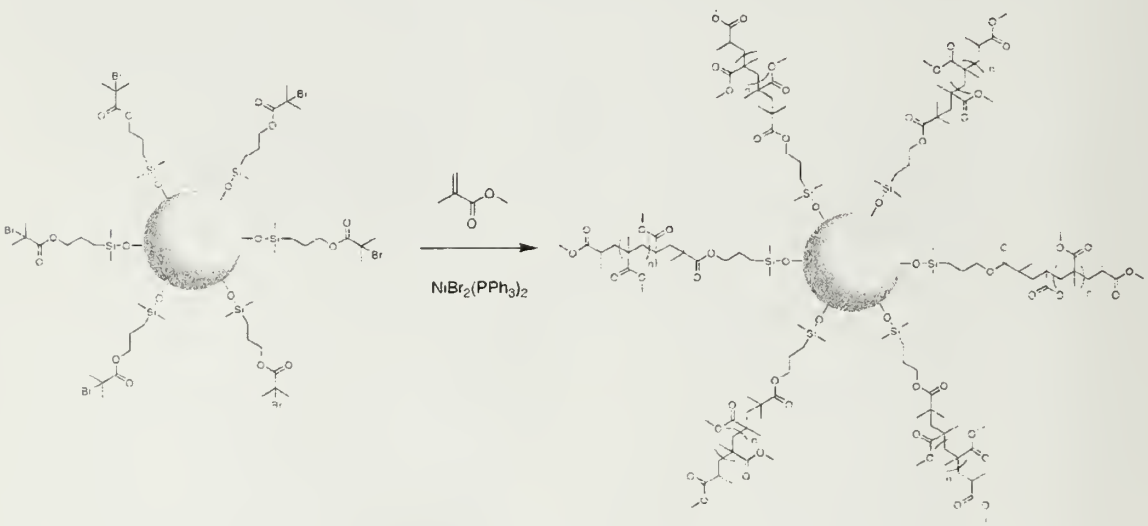

Figure 8. Atom transfer radical polymerization of methyl methacrylate from isobutryl-bromide functionalized silica nanoparticles as reported by Patten.

The nanoparticles described above represent a robust group of nanoparticles that are generally stable to acidic, basic, and radical environments. These particles contrast with semiconducting nanoparticles which are typically more susceptible to oxidation and particle degradation. Research from the Emrick and Coughlin labs provided the first

example of CdSe-polyolefin materials prepared by the ROMP of norbornene from CdSe.[83] To achieve this goal, CdSe was functionalized with a styrenic derivative that was capable of performing a ligand exchange with bis-tricyclohexylphosphine benzylidine ruthenium dichloride (Grubbs' catalyst) to afford a catalyst on the surface of the CdSe particle as illustrated in **Figure 9**. The norbornene was successfully polymerized from the surface of the catalyst functionalized CdSe nanoparticles allowing for a dispersion of nanoparticles within the polyolefin matrix. It is also important to note that the optical properties of the CdSe particles were not destroyed during this process as the photoluminescence of the particle was maintained. This work offered proof-of-concept for grafting from CdSe and was the basis for the work described in Chapter 2.

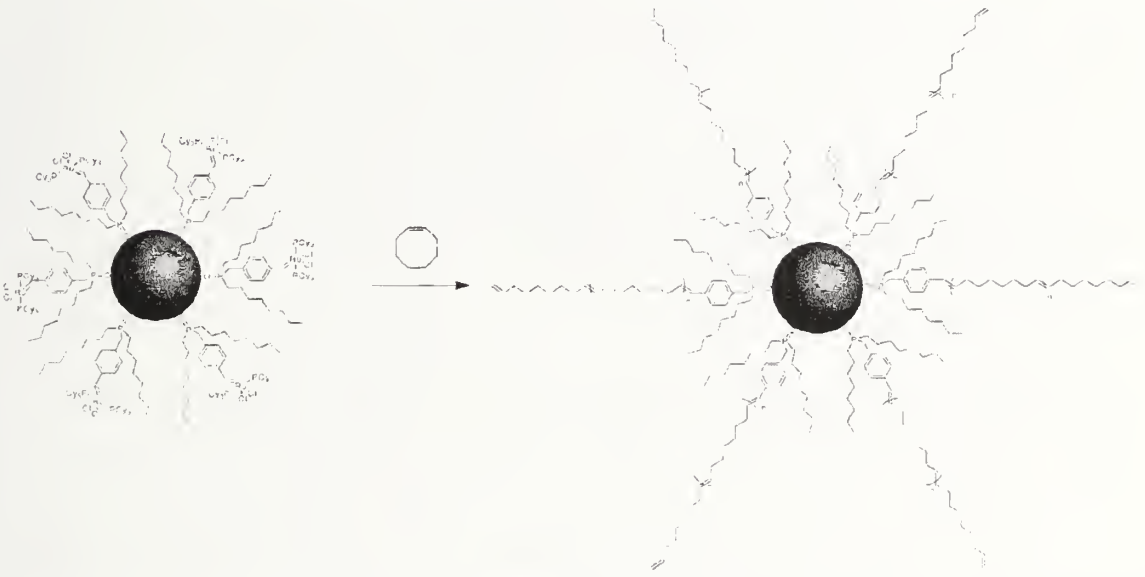

Figure 9. Ring-opening metathesis polymerization of cyclooctene from ruthenium-benzylidene CdSe quantum dots.

1.3.4 Self Assembly and Precise Placement of Nanoparticles in a Polymer Matrix

While a majority of research on nanoparticle-polymer composites focuses on dispersion, the next logical progression is the precise placement of nanoparticles within a

functional material. (**Figure 3**) Well-ordered nanoparticles within polymers is expected to provide access to new materials that combine the unique physical properties of the particles with the superior processability of the polymers. The ability to control the assembly of nanoparticles within materials promises advances in information storage, nano-electronics, and quantum computing.

One approach towards this goal involves the use of block copolymer phase behavior to dictate the location of the nanoparticle within a polymer matrix. Theoretical studies for these self-assembly events has been developed by Balasz and coworkers over the past decade.[84-87] These calculations are driven by a combination of self-consistent field theory, which is preferred for diblock copolymers, and density functional theory, which is optimal for studying ordered colloidal particles. The theory accounts for key parameters such as nanoparticle size, chain length of the polymer blocks, and the relevant interaction parameters, including those between nanoparticles and block A, nanoparticles and block B, and block A with block B. These models show that nanoparticles can be directed to the center or the edges of phase separated lamella or spherical domains by choosing systems with the appropriate parameters. For example, nanoparticles that exhibit a preference for one polymer phase over the other will tend to reside in the favored phase. A particle with neutral interactions for either phase will tend to assemble to the polymer-polymer interface to mediate interfacial interactions.

Multiple groups have produced experimental evidence consistent with the proposed theory. Thomas and coworkers sequestered CdSe nanoparticles to a phosphine oxide rich domain in a polynorbornene diblock copolymer.[88] A more recent report from Thomas has illustrated the ability to sequester two different types of nanoparticles to two

specific locations in a diblock copolymer. Specifically, when 3.5 nm gold nanoparticles and 21 nm silica particles are blended with poly(styrene-*b*-(ethylene-*co*-propylene)), the alkyl covered gold particles are driven to the diblock copolymer interface while the silica particles are sequestered to the center of the poly(ethylene-*co*-propylene) domain.[89] Research by Lopes demonstrated the self-assembly of various nanoparticles (e.g. gold, silver, indium, and lead) within a PS-PMMA diblock copolymer matrix under non-equilibrium conditions. Under appropriate annealing conditions, the polymer matrix will phase separate into an ordered lamella structure with the nanoparticles residing exclusively in the polystyrene phase due to the more favorable gold-polystyrene interactions.[90]

Several different approaches that do not involve nanoparticle-polymer self-assembly events to prepare these ordered hybrid materials have also been discovered. One such approach to nanoparticle-polymer assemblies was reported by Russell and coworkers using templates prepared from diblock copolymers.[91] These templates consist of a cylindrical PMMA phase within a PS matrix, where the cylinder diameter is on the order of 15-20 nm. CdSe nanoparticles were driven into these cylinders by capillary forces present upon withdrawal of the templates from dilute solutions of CdSe nanocrystals. Recently, an improvement to this dipping method was reported through the use of electrophoretic deposition of CdSe nanoparticles into similar block copolymer templates.[92] This approach offers control over the density of particles deposited into the template, and complete coverage, at least one particle per cylinder, was reported. Additionally, Kotov and coworkers have prepared "nanorainbows" using a multilayer approach, where a thin polymer film of poly(diallyldimethylammonium chloride)

containing cadmium telluride nanoparticles is deposited onto a quartz slide.[93] Subsequent deposition of larger cadmium telluride nanoparticles with progressively longer wavelengths (e.g. yellow, orange, and red) were then deposited in layer-by-layer fashion. This resulted in a multilayer film that has a color gradient oriented normal to the surface, a material of interest in photonic and electronic devices.

1.4 Composites of Conjugated Polymers and Quantum Dots

One application of quantum dot-polymer composites that offers exceptional promise is the use of these materials in photovoltaic devices since the tunable, narrow fluorescence emission and the wide adsorption window inherent in quantum dots offer the potential to provide tremendous advances to photovoltaic materials. The combination of semiconducting nanoparticles with electroactive polymers offer a truly unique system where the band gaps of the individual components can be tuned to allow for specific energy transfer events. An idealized example would integrate quantum dots into an electroactive polymer that possesses a larger band gap allowing for energy transfer from the polymer to the nanoparticle, resulting in emission exclusively from the quantum dot core. Conversely, the use of a polymer with a band gap smaller than the quantum dot would allow for excitons generated in the particle core to transfer to the polymer for charge separation and transport as required for use in solar cell applications.

While energy transfer events between these two components is not yet fully understood, several research groups have performed theoretical and experimental studies of energy transfer events.[94-100] The two theories of energy transfer mechanisms generally involve charge separation and transport and Förster resonance energy transfer (FRET). Photo induced charge separation in conjugated polymers is improved by the inclusion of

an electron-accepting species, such as a CdSe nanoparticle. For this energy transfer to be efficient, the interface between the conjugated polymer and the nanoparticle must be maximized. However, aggregation of CdSe nanoparticles is typically found in blends of CdSe nanoparticles and conjugated polymers, representing an area of potential improvement for energy transfer. Förster resonance energy transfer involves dipole-coupling in non-radiative energy transfer of excitions.[101] The efficiency of FRET is determined by the spectral overlap of the donor and acceptor, the distance between the two moieties, and the relative orientation of the donor and acceptor's dipole moments. FRET efficiency is typically defined as a distance, R_0, which is the distance between the donor and acceptor that will allow for 50% energy transfer efficiency. It is important to note that the energy transfer process between conjugated polymers and CdSe nanoparticles is likely complex and may incorporate elements of both of the above energy transfer mechanisms.

Pioneering work in this field was reported in 1994 when Colvin and Alivisatos described the electroluminescence from blends of CdSe and PPV.[102] Since that time, Greenham and Alivisatos have extensively studied photophysical principles responsible for the energy transfer events between the two components.[94-96] Bawendi and coworkers blended CdSe nanoparticles with biphenyloxadiazole functionalized polymers for use in device applications; however, 60 vol. % CdSe was necessary to obtain electroluminescence spectra characteristic of the quantum dot.[103] Similar quantum dot loadings were necessary to obtain photoluminescence from CdSe/ZnS core shell nanoparticles when blended with polyfluorene in a study conducted by Anni and coworkers.[98]

Quantum dots other than CdSe have been incorporated into nanoparticle-polymer blends as Shaheen has described energy transfer events between InP and poly(3-hexyl thiophene)[104] while Coffer has reported the doping of PPV with europium-silica nanoparticles for device applications.[105] A photovoltaic device from blended materials of PbSe in PPV was reported by Selmic,[106] while an infrared detector based upon PbS blended with PPV was described by Sargent.[107] In addition, solar cell applications for blends of PPV with CdTe were reported by Nann and Kumar.[108] However, the recurring problem of phase separation in nanoparticle-polymer blends severely limits the efficiency of the energy transfer process due to self-quenching events and inter-dot coupling.

Recently, a shift from the aggregated blends has been made to the dispersion of quantum dots in an electroactive polymer matrix. This dispersion may offer a distinct advantage over aggregation in photovoltaic applications where intimate contact between individual quantum dots and polymer chains is crucial for energy transfer events. Published concurrently with the results presented herein were results from the groups of Alivisatos and Fréchet, where dispersions of CdSe quantum dots were dispersed in a polythiophene matrix. In this work, a hexamer of polythiophene was end functionalized with an amine group then placed on the nanoparticle surface with ligand exchange chemistry (**Figure 10**).[109] These hybrid materials exhibited drastically different results when compared with a simple blend of CdSe and polythiophene. Similar research was presented by Advincula where oligomeric dendrons of polythiophene were functionalized with a phosphonic acid then placed on CdSe quantum dots.[110]

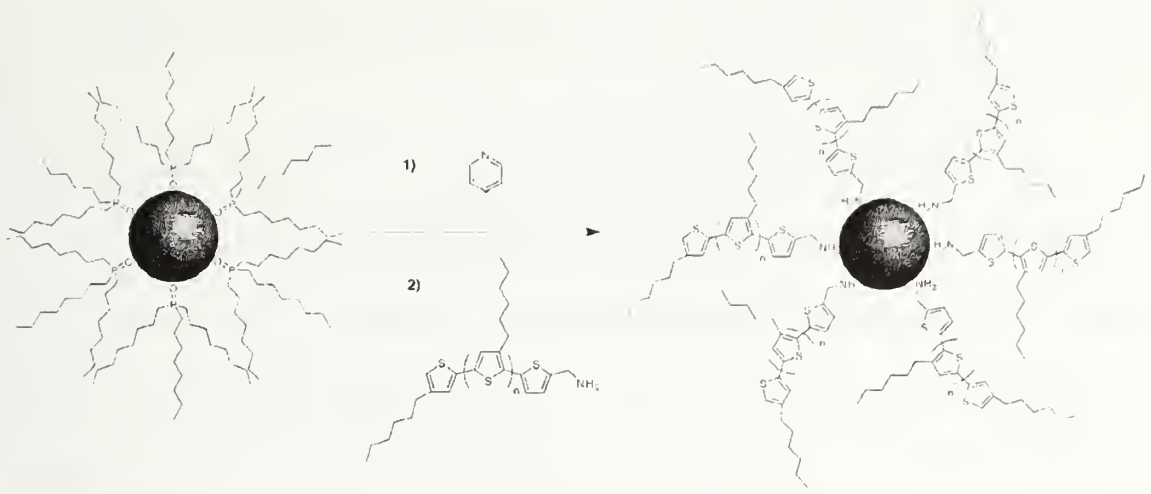

Figure 10. Ligand exchange of TOPO-covered CdSe nanoparticles with amino-functionalized poly(3-hexylthiophene) according to Alivisatos and Fréchet.

1.5 Thesis Outline

Chapter 2 describes the synthesis of nitroxide functionalized quantum dots for surface-initiated controlled free radical polymerization. Characterization of these composites utilized transmission electron microscopy, as well as solution state fluorescence and UV-Vis spectroscopy. It was found that the nanoparticle-polymer composites exhibited dispersion of quantum dots within the polymer film without degradation of the quantum dot's optical properties. The incorporation of CdSe-polymer composites into diblock copolymers is also discussed.

Chapter 3 describes the cross-linking of a polymer shell around CdSe nanoparticles, with the goal of improving the stability of the nanoparticles in the presence of various chemical environments. A thermally cross-linkable benzocyclobutane monomer was prepared and used in a graft-from copolymerization. Optimization of solvent and temperature gave intra-particle cross-linking to afford discrete particles surrounded by a chemically cross-linked polymer shell. Electron microscopy and

fluorescence spectroscopy were utilized to compare these materials to their uncross-linked counterparts.

The preparation of CdSe-poly(phenylene vinylene) hybrid materials is the focus of Chapter 4. The preparation of CdSe in a functional ligand and its use in the polymerization of conjugated polymers from these novel particles is described. The morphological and optical properties of the hybrid materials are vastly different from that of simple blends of the two components. Collaborations with Eastman Kodak Company (Rochester, NY) and Professor Mike Barnes (Department of Chemistry, University of Massachusetts, Amherst) allowed for the investigation of these materials with solid state, single molecule, time resolved and time evolution fluorescence spectroscopy.

1.6 References

(1) Mohanty, P. *Nature* **2005**, *437*, 325-326.

(2) Service, R. F. *Science* **2005**, *309*, 36-36.

(3) Yan, H. *Science* **2004**, *306*, 2048-2049.

(4) Gerstner, E. *Nature* **2003**, *425*, 244-244.

(5) Service, R. F. *Science* **2002**, *298*, 2322-2323.

(6) Appell, D. *Nature* **2002**, *419*, 553-555.

(7) Niemeyer, C. M. *Science* **2002**, *297*, 62-63.

(8) De Franceschi, S.; Kouwenhoven, L. *Nature* **2002**, *417*, 701-702.

(9) Tseng, G. Y.; Ellenbogen, J. C. *Science* **2001**, *294*, 1293-1294.

(10) Ito, T.; Okazaki, S. *Nature* **2000**, *406*, 1027-1031.

(11) Bailey, T. C.; Johnson, S. C.; Sreenivasan, S. V.; Ekerdt, J. G.; Willson, C.G.; Resnick, D. J. *J. Photopolym. Sci. Tech.* **2002**, *15*, 481-486.

(12) Chou, S. Y.; Krauss, P. R.; Renstrom, P. J. *Science* **1996**, *272*, 85-87.

(13) Hachman, M. 2006.

(14) Chao, W. L.; Harteneck, B. D.; Liddle, J. A.; Anderson, E. H.; Attwood, D. T. *Nature* **2005**, *435*, 1210-1213.

(15) Kim, H.; Achermann, M.; Balet, L. P.; Hollingsworth, J. A.; Klimov, V. I. *J. Am. Chem. Soc.* **2005**, *127*, 544-546.

(16) Konya, Z.; Puntes, V. F.; Kiricsi, I.; Zhu, J.; Alivisatos, A. P.; Somorjai, G. A. *Nano Letters* **2002**, *2*, 907-910.

(17) Pan, C.; Pelzer, K.; Philippot, K.; Chaudret, B.; Dassenoy, F.; Lecante, P.; Casanove, M. J. *J. Am. Chem. Soc.* **2001**, *123*, 7584-7593.

(18) Rogach, A. L.; Katsikas, L.; Kornowski, A.; Su, D. S.; Eychmuller, A.; Weller, H. *Berichte Der Bunsen-Gesellschaft-Physical Chemistry Chemical Physics* **1996**, *100*, 1772-1778.

(19) Fendler, J. H. *Chem. Mater.* **1996**, *8*, 1616-1624.

(20) Brust, M.; Walker, M.; Bethell, D.; Schiffrin, D. J.; Whyman, R. *Chem. Commun.* **1994**, 801-802.

(21) Eychmuller, A. *J. Phys. Chem. B* **2000**, *104*, 6514-6528.

(22) Link, S.; El-Sayed, M. A. *J. Phys. Chem. B* **1999**, *103*, 4212-4217.

(23) Huber, D. L. *Small* **2005**, *1*, 482-501.

(24) Li, P. H.; Wang, L.; Li, H. J. *Tetrahedron* **2005**, *61*, 8633-8640.

(25) Babes, L.; Denizot, B.; Tanguy, G.; Le Jeune, J. J.; Jallet, P. *J. Coll. Inter. Sci.* **1999**, *212*, 474-482.

(26) Zeng, Q. H.; Yu, A. B.; Lu, G. Q.; Paul, D. R. *J. Nanosci. Nanotech.* **2005**, *5*, 1574-1592.

(27) Shenhar, R.; Norsten, T. B.; Rotello, V. M. *Adv. Mater.* **2005**, *17*, 657-669.

(28) Advincula, R. C. *J. Disp. Sci. Tech.* **2003**, *24*, 343-361.

(29) Schmidt, G.; Malwitz, M. M. *Curr. Opin. Coll. Inter. Sci.* **2003**, *8*, 103-108.

(30) Godovsky, D. Y. In *Biopolymers* 2000; Vol. 153, p 163-205.

(31) Murray, C. B.; Kagan, C. R.; Bawendi, M. G. *Ann. Rev. Mater. Sci.* **2000**, *30*, 545-610.

(32) Penner, R. M. *Acc. Chem. Res.* **2000**, *33*, 78-86.

(33) Khairutdinov, R. F. *Colloid Journal* **1997**, *59*, 535-548.

(34) Yu, H.; Li, J. B.; Loomis, R. A.; Gibbons, P. C.; Wang, L. W.; Buhro, W. E. *J. Am. Chem. Soc.* **2003**, *125*, 16168-16169.

(35) Yu, D.; Wang, C. J.; Guyot-Sionnest, P. *Science* **2003**, *300*, 1277-1280.

(36) Nirmal, M.; Brus, L. *Acc. Chem. Res.* **1999**, *32*, 407-414.

(37) Alivisatos, A. P. *J. Phys. Chem.* **1996**, *100*, 13226-13239.

(38) Alivisatos, A. P. *Science* **1996**, *271*, 933-937.

(39) Bandaranayake, R. J.; Wen, G. W.; Lin, J. Y.; Jiang, H. X.; Sorensen, C. M. *Appl. Phys. Lett.* **1995**, *67*, 831-833.

(40) Fu, H.; Wang, L.-W.; Zunger, A. *Physical Review B* **1999**, *59*, 5568.

(41) Karayigitoglu, C. F.; Tata, M.; John, V. T.; McPherson, G. L. *Coll. Surf. A* **1994**, *82*, 151-162.

(42) Calandra, P.; Longo, A.; Liveri, V. T. *J. Phys. Chem. B* **2003**, *107*, 25-30.

(43) Teredesai, P. V.; Deepak, F. L.; Govindaraj, A.; Sood, A. K.; Rao, C. N. R. *J. Nanosci. Nanotech.* **2002**, *2*, 495-498.

(44) Battaglia, D.; Peng, X. G. *Nano Lett.* **2002**, *2*, 1027-1030.

(45) Yu, W. W.; Falkner, J. C.; Shih, B. S.; Colvin, V. L. *Chem. Mater.* **2004**, *16*, 3318-3322.

(46) Lee, J.; Sundar, V. C.; Heine, J. R.; Bawendi, M. G.; Jensen, K. F. *Adv. Mater.* **2000**, *12*, 1102-1105.

(47) Bunge, S. D.; Krueger, K. M.; Boyle, T. J.; Rodriguez, M. A.; Headley, T. J.; Colvin, V. L. *J. Mater. Chem.* **2003**, *13*, 1705-1709.

(48) Crouch, D. J.; O'Brien, P.; Malik, M. A.; Skabara, P. J.; Wright, S. P. *Chem. Commun.* **2003**, 1454-1455.

(49) Nakamura, H.; Yamaguchi, Y.; Miyazaki, M.; Maeda, H.; Uehara, M.; Mulvaney, P. *Chem. Commun.* **2002**, 2844-2845.

(50) Qu, L. H.; Peng, Z. A.; Peng, X. G. *Nano Lett.* **2001**, *1*, 333-337.

(51) Manna, L.; Scher, E. C.; Alivisatos, A. P. *J. Am. Chem. Soc.* **2000**, *122*, 12700-12706.

(52) Peng, X. G.; Manna, L.; Yang, W. D.; Wickham, J.; Scher, E.; Kadavanich, A.; Alivisatos, A. P. *Nature* **2000**, *404*, 59-61.

(53) Brus, L. *J. Phys. Chem. Solids* **1998**, *59*, 459-465.

(54) Murray, C. B.; Norris, D. J.; Bawendi, M. G. *J. Am. Chem. Soc.* **1993**, *115*, 8706-8715.

(55) Lover, T.; Henderson, W.; Bowmaker, G. A.; Seakins, J. M.; Cooney, R. P. *Inorg. Chem.* **1997**, *36*, 3711-3723.

(56) Kalyuzhny, G.; Murrary, R. W. *J. Phys. Chem. B* **2005**, *109*, 7012-7021.

(57) Murray, C. B.; Norris, D. J.; Bawendi, M. G. *J. Am. Chem. Soc.* **1993**, *115*, 8706-8715.

(58) Becerra, L. R.; Murray, C. B.; Griffin, R. G.; Bawendi, M. G. *J. Phys. Chem.* **1994**, *100*, 3297-3300.

(59) Taylor, J.; Kippeny, T.; Rosenthal, S. J. *J. Clust. Sci.* **2001**, *12*, 571-582.

(60) Goodyear, C. *Dinglers Polytechnisches Journal* **1856**, *CXXXIX*, 376-390.

(61) Baekeland, L. H. *Scientific American Supplement* **1909**, *68*, 322.

(62) Sheldon, R. P. *Composite Polymeric Materials*; Applied Science Publishers LTD: Essex, England, 1982.

(63) Wang, F.; Han, M. Y.; Mya, K. Y.; Wang, Y.; Lai, Y. H. *J. Am. Chem. Soc.* **2005**, *127*, 10350-10355.

(64) Skaff, H.; Emrick, T. *Chem. Commun.* **2003**, 52-53.

(65) Li, Y.; Hong, X. M.; Collard, D. M.; El-Sayed, M. A. *Org. Lett.* **2000**, *2*, 2385-2388.

(66) Kim, S.; Bawendi, M. G. *J. Am. Chem. Soc.* **2003**, *125*, 14652-14653.

(67) Kim, S. W.; Kim, S.; Tracy, J. B.; Jasanoff, A.; Bawendi, M. G. *J. Am. Chem. Soc.* **2005**, *127*, 4556-4557.

(68) Carrot, G.; Scholz, S. M.; Plummer, C. J. G.; Hilborn, J.; Hedrick, J. *Chem. Mater.* **1999**, *11*, 3571-3577.

(69) Lowe, A. B.; Sumerlin, B. S.; Donovan, M. S.; McCormick, C. L. *J. Am. Chem. Soc.* **2002**, *124*, 11562-11563.

(70) Corbierre, M. K.; Cameron, N. S.; Sutton, M.; Mochrie, S. G. J.; Lurio, L. B.; Ruhm, A.; Lennox, R. B. *J. Am. Chem. Soc.* **2001**, *123*, 10411-10412.

(71) Tian, S.; Liu, J.; Zhu, T.; Knoll, W. *Chem. Mater.* **2004**, *16*, 4103-4108.

(72) Hu, J.; Liu, Y. *Langmuir* **2005**, *21*, 2121-2123.

(73) Watson, K. J.; Zhu, J.; Ngyen, S. T.; Mirkin, C. A. *J. Am. Chem. Soc.* **1999**, *121*, 462-463.

(74) Jordan, R.; West, N.; Ulman, A.; Chou, Y. M.; Nuyken, O. *Macromolecules* **2001**, *34*, 1606-1611.

(75) Hongwei Duan, M. K. D. W. D. G. K. H. M. *Angew. Chemie Inter. Ed.* **2005**, *44*, 1717-1720.

(76) Zhou, Q.; Wang, S.; Fan, X.; Advincula, R.; Mays, J. *Langmuir* **2002**, *18*, 3324-3331.

(77) Bartholome, C.; Beyou, E.; Bourgeat-Lami, E.; Chaumont, P.; Zydowicz, N. *Macromolecules* **2003**, *ASAP Articles*.

(78) Farmer, S. C.; Patten, T. E. *Chem. Mater.* **2001**, *13*, 3920-3926.

(79) von Werne, T.; Patten, T. E. *J. Am. Chem. Soc.* **1999**, *121*, 7409-7410.

(80) Gravano, S. M.; Dumas, R.; Liu, K.; Patten, T. E. *J. Polym. Sci. Part A* **2005**, *43*, 3675-3688.

(81) Matsuno, R.; Yamamoto, K.; Otsuka, H.; Takahara, A. *Chem. Mater.* **2003**, *15*, 3-5.

(82) Matsuno, R.; Yamamoto, K.; Otsuka, H.; Takahara, A. *Macromolecules* **2004**, *37*, 2203-2209.

(83) Skaff, H.; Ilker, M. F.; Coughlin, E. B.; Emrick, T. *J. Am. Chem. Soc.* **2002**, *124*, 5729-5733.

(84) Lee, J. Y.; Thompson, R. B.; Jasnow, D.; Balazs, A. C. *Macromolecules* **2002**, *35*, 4855-4858.

(85) Thompson, R. B.; Ginzburg, V. V.; Matsen, M. W.; Balazs, A. C. *Macromolecules* **2002**, *35*, 1060-1071.

(86) Lee, J. Y.; Thompson, R. B.; Jasnow, D.; Balazs, A. C. *Physical Review Letters* **2002**, *89*, art. no.-155503.

(87) Thompson, R. B.; Ginzburg, V. V.; Matsen, M. W.; Balazs, A. C. *Science* **2001**, *292*, 2469-2472.

(88) Fogg, D. E.; Radzilowski, L. H.; Dabbousi, B. O.; Schrock, R. R.; Thomas, E. L.; Bawendi, M. G. *Macromolecules* **1997**, *30*, 8433-8439.

(89) Bockstaller, M. R.; Lapetnikov, Y.; Margel, S.; Thomas, E. L. *J. Am. Chem. Soc.* **2003**, *125*, 5276-5277.

(90) Lopes, W. A. *Phys. Rev. E* **2002**, *65*, 031606.

(91) Misner, M. J.; Skaff, H.; Emrick, T.; Russell, T. P. *Adv. Mater.* **2003**, *15*, 221-224.

(92) Zhang, Q.; Xu, T.; Butterfield, D.; Misner, M. J.; Ryu, D. Y.; Emrick, T.; Russell, T. P. *Nano Lett.* **2005**, *5*, 357-361.

(93) Mamedov, A. A.; Belov, A.; Giersig, M.; Mamedova, N. N.; Kotov, N. A. *J. Am. Chem. Soc.* **2001**, *123*, 7738-7739.

(94) Greenham, N. C.; Peng, X.; Alivisatos, A. P. *Synth. Met.* **1997**, *84*, 545-546.

(95) Ginger, D. S.; Greenham, N. C. *Phys. Rev. B* **1999**, *59*, 10622-10629.

(96) Greenham, N. C.; Peng, X.; Alivisatos, A. P. *Phys. Rev. B* **1996**, *54*, 17628-17633.

(97) Milliron, D. J.; Alivisatos, A. P.; Pitois, C.; Edder, C.; Frechet, J. M. J. *Adv. Mater.* **2003**, *15*, 58.

(98) Anni, M.; Manna, L.; Cingolani, R.; Valerini, D.; Creti, A.; Lomascolo, M. *App. Phys. Lett.* **2004**, *85*, 4169-4171.

(99) Javier, A.; Yun, C. S.; Sorena, J.; Strouse, G. F. *J. Phys. Chem. B* **2003**, *107*, 435-442.

(100) Burda, C.; Green, T. C.; Link, S.; El-Sayed, M. A. *J. Phys. Chem. B* **1999**, *103*, 1783-1788.

(101) Lakowicz, J. R. *Principles of Fluorescence Spectroscopy*; 2nd ed.; Plenum Publishing, 1999.

(102) Colvin, V. L.; Schlamp, M. C.; Alivisatos, A. P. *Nature* **1994**, *370*, 354-357.

(103) Mattoussi, H.; Radzilowski, L. H.; Dabbousi, B. O.; Fogg, D. E.; Schrock, R. R.; Thomas, E. L.; Rubner, M. F.; Bawendi, M. G. *J. Appl. Phys.* **1999**, *86*, 4390-4399.

(104) Selmarten, D.; Jones, M.; Rumbles, G.; Yu, P.; Nedeljkovic, J.; Shaheen, S. *J. Phys. Chem. B* **2005**, *109*, 15927-15932.

(105) Ji, J.; Coffer, J. L. *J. Phys. Chem. B* **2002**, *106*, 3860-3863.

(106) Qi, D.; Fischbein, M.; Drndic, M.; Selmic, S. *Appl. Phys. Lett* **2005**, *86*, 093103.

(107) McDonald, S. A.; Konstantantos, G.; Zhang, S.; Cyr, P. W.; Klem, E. J. D.; Levina, L.; Sargent, E. H. *Nature Mater.* **2005**, *4*, 138-141.

(108) Kumar, S.; Nann, T. *J. Mater. Res.* **2004**, *19*, 1990-1994.

(109) Liu, J.; Tanaka, T.; Sivula, K.; Alivisatos, A. P.; Frechet, J. M. J. *J. Am. Chem. Soc.* **2004**, *126*, 6550-6551.

(110) Locklin, J.; Patton, D.; Deng, S.; Baba, A.; Millan, M.; Advincula, R. C. *Chem. Mater.* **2004**, *16*, 5187-5193.

CHAPTER 2

FUNCTIONALIZED CADMIUM SELENIDE NANOPARTICLES FOR CONTROLLED FREE RADICAL POLYMERIZATION

2.1 Nitroxide Mediated Radical Polymerization

Free radical polymerization is a rapid and versatile polymerization technique of central importance to polymer chemistry in both fundamental studies and the commercial polymer industry.[1-7] A number of commodity polymers are prepared by radical polymerization due to its ease of use. While free radical polymerization is used effectively in many cases, it typically gives polymers with a rather high polydispersity index (PDI) of about 2. In this sense, free radical polymerization lacks many aspects of control found in living ionic techniques.[8]

In the 1990's, a number of polymerization methods were developed to stabilize the reactive radical chain end of free radical polymerization. One such method is known as nitroxide mediated radical polymerization (NMRP).[9,10] It was found that the addition of the stable free radical 2,2,6,6-tetramethyl-1-piperidinyloxy (TEMPO) to the thermally initiated polymerization of styrene resulted in a reduction of the PDI from ~2 in conventional free radical polymerization to 1.2-1.4. During the polymerization, the TEMPO radical forms a thermally reversible bond with the propagating carbon centered radical. When the carbon-oxygen nitroxide bond is formed, propagation is not possible and the chain is considered dormant. At temperatures around 125 °C, the C-O bond undergoes homolytic cleavage to give a nitroxide free radical and a carbon centered radical at the polymer chain end. The polymer chain end radical can propagate by

reaction with monomers in solution. (**Scheme 1**) The equilibrium of the nitroxide strongly favors the bound state (K_{eq}=4 x 10^{-10}), which greatly reduces the number of free radicals in polymerization.[11] Since nitroxide is bound to the polymer chain end during an overwhelming majority of the polymerization, termination reactions such as radical combination and disproportionation are nearly eliminated leading to all polymer chains having roughly the same molecular weight, giving the polymer sample a low PDI. The use of a unimolecular initiator, a preformed nitroxide-containing moiety, allows for the monomer-to-initiator ratio to be precisely pre-determined giving the ability to target particular molecular weights with NMRP, much like living anionic polymerization.

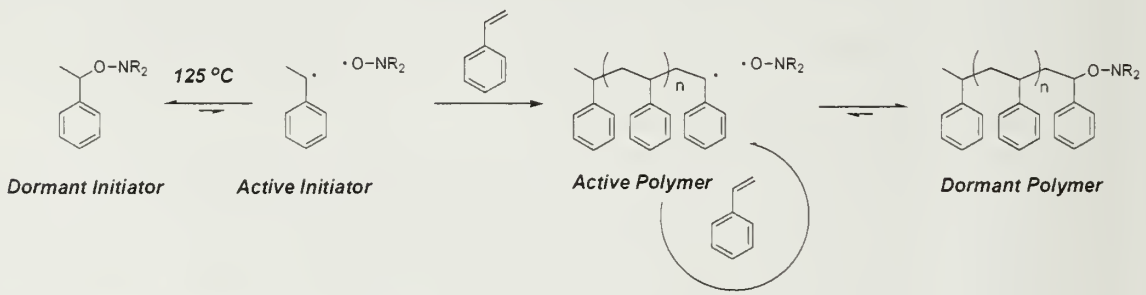

Scheme 1. Mechanism for Nitroxide Mediated Radical Polymerization

Several different types of controlled free radical polymerization have been developed in recent years. For example, Matyjaszewski[12] helped pioneered the field of atom transfer radical polymerization (ATRP) while Moad and Rizzardo[13] have introduced reversible addition-fragmentation chain transfer polymerization (RAFT). Each polymerization technique leads to controlled molecular weights and low PDIs for various vinyl monomers and each technique has certain merits and drawbacks. ATRP exhibits excellent control over a variety of monomers but requires the addition of copper halides and ligating species that are not always readily separable from the

polymeric product. RAFT is also amenable to a range of monomers but suffers from low thermal stability and requires the addition of a radical initiator. Meanwhile, Hawker has provided numerous advances in NMRP including the synthesis and evaluation of a library of nitroxide functionalized initiators, the discovery of monomers amenable to NMRP, and the preparation of random and block copolymers using NMRP.[14] The strength of NMRP is that no additional radical sources, ligands or metals are needed for controlled polymerization; however, NMRP struggles with the polymerization of acrylate monomers.

2.2 Nitroxide Mediated Polymerization from CdSe Nanoparticles

2.2.1 Phosphine Oxide – Nitroxide Ligand Design and Synthesis

NMRP was chosen as the polymerization method in this graft-from approach since the radical initiators or amine containing ligands required for RAFT or ATRP are not necessary in nitroxide-based polymerizations, eliminating any potential interactions with the CdSe nanoparticle surface. In addition, the dominant-active equilibrium of NMRP keeps the concentration of free radicals low, and thus lowers the chance of radical coupling and degradation of the CdSe nanoparticle surface. Growth of polymer chains directly from the surface of CdSe nanoparticles requires attachment of nitroxide-containing ligands to the nanoparticle surface. TEMPO was chosen as the nitroxide functionality due to its commercial availability and extensive prior research on its behavior in living free radical polymerization. As shown by Hawker and coworkers, Jacobsen's catalyst ((R,R)-(-)-N,N'-bis(3,5-di-t-butylsalicylidene)-1,2-cyclohexanediaminomanganese (III) chloride) provides a convenient route to nitroxide

derivatives.[15] In this reaction, (**Scheme 2**) the manganese catalyst reacts adds to the styrenic olefin to form a benzyl radical adduct. The benzyl radical is trapped by TEMPO to form the carbon-oxygen nitroxide bond. The desired product is formed following hydride displacement of the manganese moiety with sodium borohydride. With this reaction in mind, the initial synthetic design involved nitroxide functionalization of di-*n*-octyl-stryrenyl phosphine oxide (DOSPO).[16] (**Scheme 3**) Unfortunately, application of this reaction to DOSPO gave an inseparable mixture of products and resulted in the abandonment of this approach.

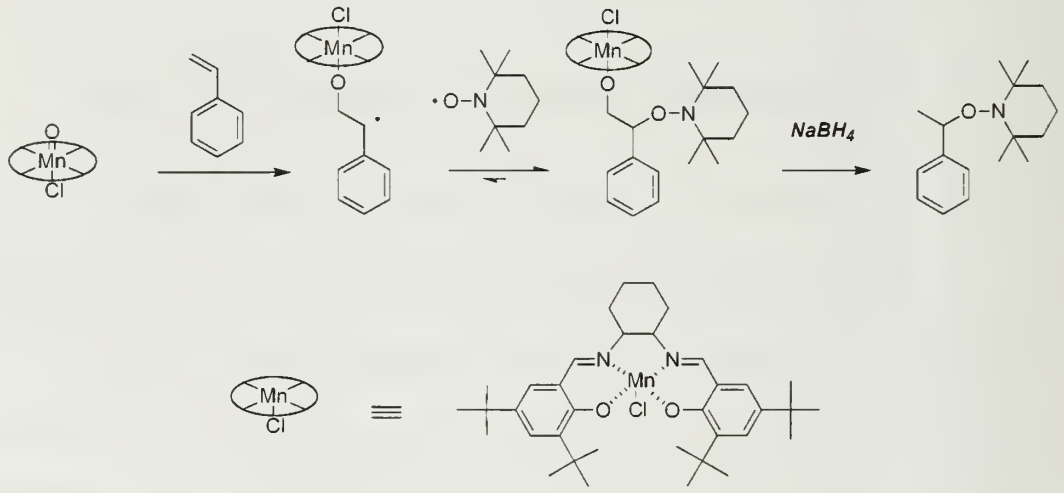

Scheme 2. Mechanism for the use of Jacobsen's Catalyst in the conversion of styrenic derivatives to benzyl nitroxides as proposed by Hawker

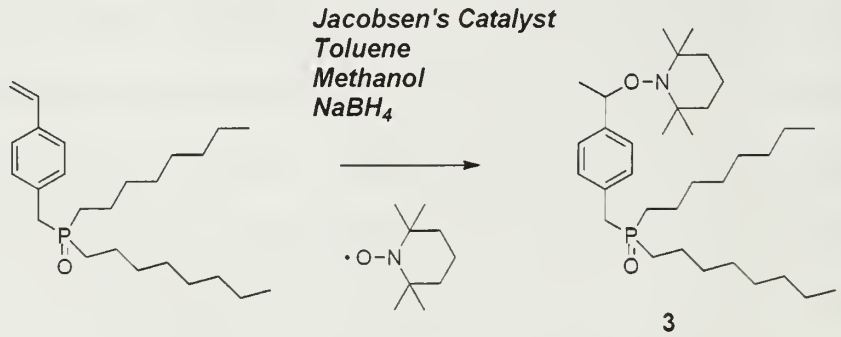

Scheme 3. Proposed conversion of DOSPO to nitroxide-functionalized ligand 3. Compound 3 was formed but could not be isolated from the reaction solution.

An alternative strategy was devised involving the synthesis of a previously reported[16] benzyl chloride functionalized TEMPO derivative, followed by nucleophilic substitution of the benzyl chloride with di-*n*-octylphosphine oxide (DOPO) as shown in **Scheme 4**. DOPO was prepared by Grignard reaction of *n*-octyl magnesium bromide with dibutyl phosphite according to previous literature procedure.[17] The TEMPO substituted benzyl chloride **2** was prepared from 4-vinyl benzyl chloride **1** utilizing the manganese catalyzed nitroxide synthesis described above in 67 % yield following purification by silica gel column chromatography and recrystallization from hexanes. The substitution reaction proceeded as planned and nitroxide ligand **3** was isolated in 89 % yield as a colorless oil following purification by silica gel column chromatography. Evidence for the formation of the desired product was shown in the ^{1}H NMR spectrum where the benzyl proton resonance exhibited an upfield shift (from δ 4.59 ppm to δ 3.11 ppm) and splitting of the benzyl protons signal by the adjacent phosphine oxide.

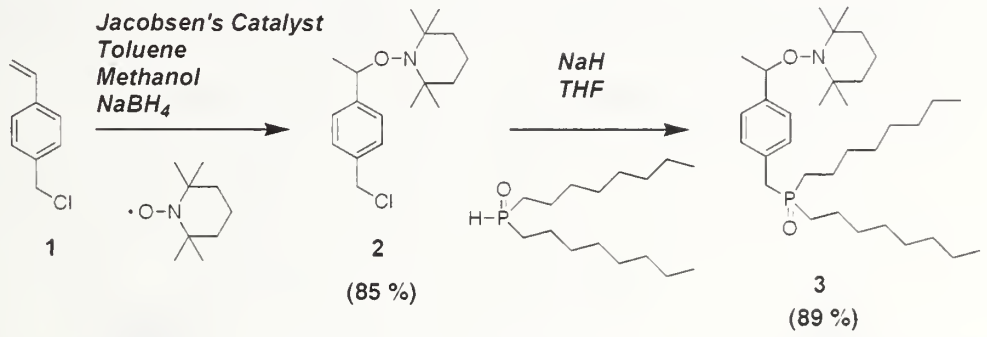

Scheme 4. Synthesis of nitroxide functionalized phosphine oxide 2 from 4-vinyl benzyl chloride.

2.2.2 Ligand Exchange to Afford Nitroxide Functionalized CdSe

The ligands on TOPO-covered CdSe nanoparticles can be removed using a large excess of ligands such as pyridine.[18,19] This "stripping" step results in CdSe

nanoparticles with a weak ligand coverage that are readily precipitated into hexanes, effectively removing any unbound pyridine and residual phosphine oxide. The pyridine-functionalized nanoparticles represent a reactive intermediate towards other functional ligands, as the pyridine coverage can be displaced easily with a stronger binding ligand such as a phosphine oxide or a thiol. One significant drawback to this approach is that the pyridine-capped intermediate is highly susceptible to oxidization of surface atoms and subsequent degradation of the nanoparticle's optical properties. The surface oxidation is manifested in both the UV-Vis and fluorescence spectra where blue shifts of peak maxima are commonly observed.[20]

For the synthesis of the nitroxide-functionalized nanoparticles **5**, ligand exchange with pyridine functionalized CdSe **4** with phosphine oxide **3** was performed at room temperature (**Scheme 5**). This is preferred as significant particle degradation was observed when ligand exchange was performed at elevated temperature (40 – 60 °C). The degradation is believed to be a result of radical formation at higher temperatures, leading to an increase of radicals that degrade the CdSe surface.

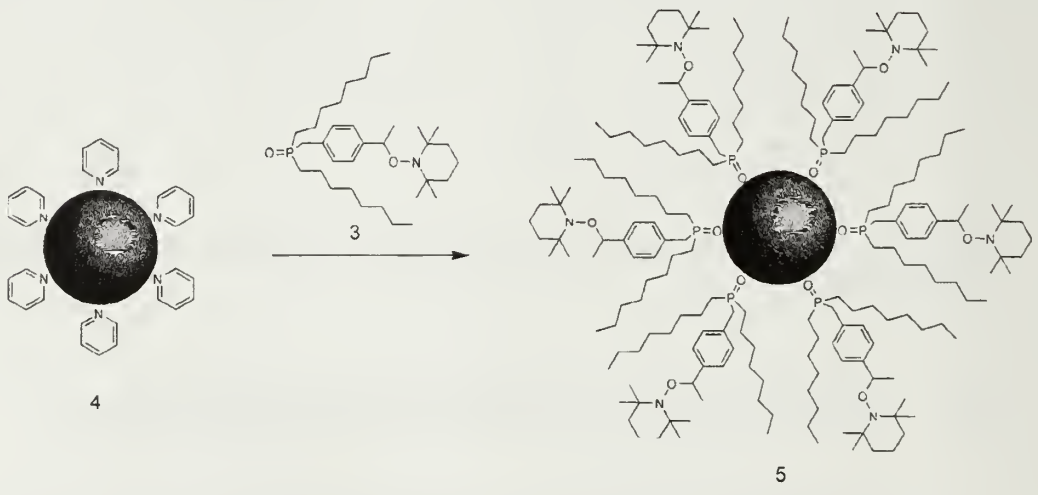

Scheme 5. Ligand exchange of pyridine functionalized CdSe 4 with ligand 3 to give nitroxide functionalized CdSe particles 5.

After allowing 24 hours for the ligand exchange, the solution was concentrated and the nitroxide-functionalized particles were precipitated with methanol and stored in styrene at -20 °C. It was found that multiple precipitations resulted in irreversible nanoparticle sedimentation, thus only one precipitation was utilized in the purification of these quantum dots. ^{1}H NMR spectroscopy of **5** showed resonances corresponding to that of the ligand, and the ^{31}P NMR spectrum showed one resonance at δ 48.14 ppm, corresponding to the phosphine oxide of the ligand; no TOPO phosphorous signal, expected at δ 46 ppm, was observed. Characterization of functionalized CdSe nanoparticles **5** by UV-Vis spectroscopy exhibited only a very small blue shift (3-5 nm). Similarly, the fluorescence peak maximum shifted from 528 nm to 525 nm as shown in **Figure 11**. The transmission electron micrographs of **5** appeared identical to those of TOPO covered CdSe.

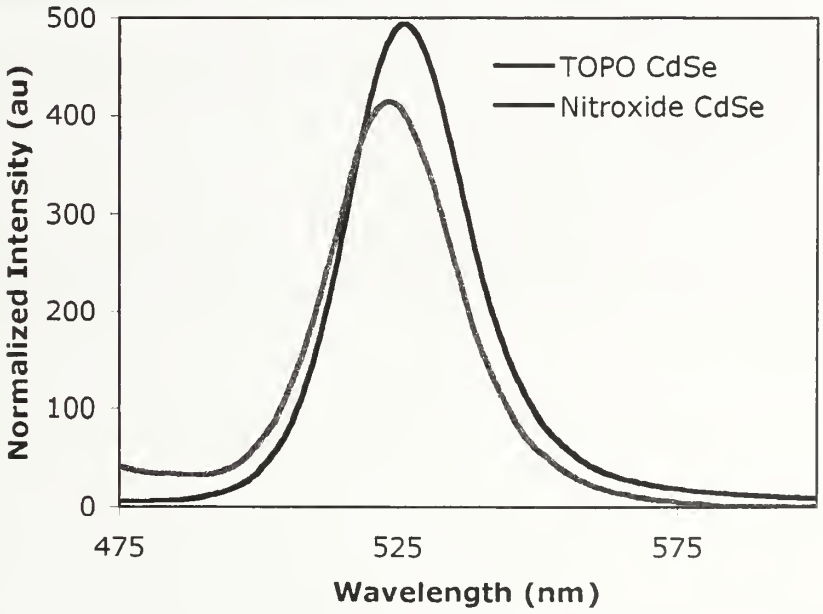

Figure 11. Solution state fluorescence emission spectra (ex @ 400 nm) of as synthesized TOPO covered CdSe and nitroxide CdSe following ligand exchange.

2.2.3 Polymerizations and Copolymerizations from Nitroxide Functionalized CdSe Nanoparticles

The graft-from polymerizations were performed shortly after ligand exchange as storage of the functionalized CdSe nanoparticles for extended periods (3 days or longer) typically led to irreversible nanoparticle precipitation. The styrene solution of **5** was transferred to a reaction vial and degassed by freeze-pump-thaw techniques. After multiple degassing cycles, the solutions were heated to 125 °C for 12 to 24 hours according to **Scheme 6**. In addition to bulk polymerization, this process is also amenable to solution polymerization in either toluene or xylenes for 48 h at 125 °C. During this heating phase, the nitroxide C-O bond undergoes reversible homolytic cleavage to give a benzyl radical, allowing for propagation of the polymer chain from the surface of the nanoparticle. There appears to be very little surface degradation of the CdSe nanoparticle as evidenced by minimal blue shifts of the band-edge adsorption maximum in the UV-Vis spectrum. In a contrasting control experiment involving TOPO covered CdSe, severe degradation, as evidenced by the loss of their characteristic red color, is noted within 15 minutes under conventional radical polymerization conditions (1 % AIBN in 1 mL styrene with 5 mg CdSe), illustrated in **Figure 12**.

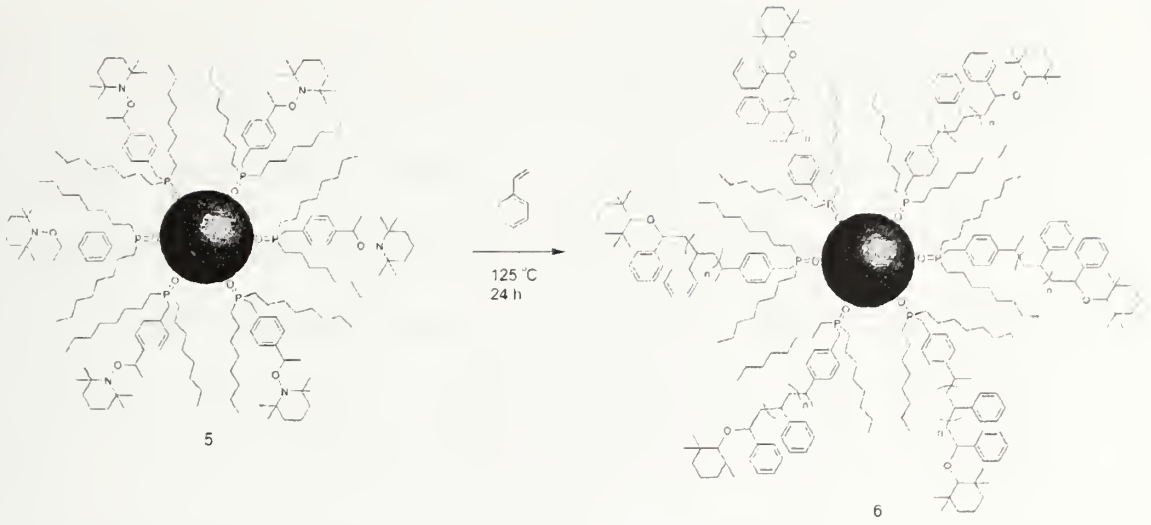

Scheme 6. Polymerization of styrene from nitroxide CdSe 5 to give CdSe-PS hybrid material 6.

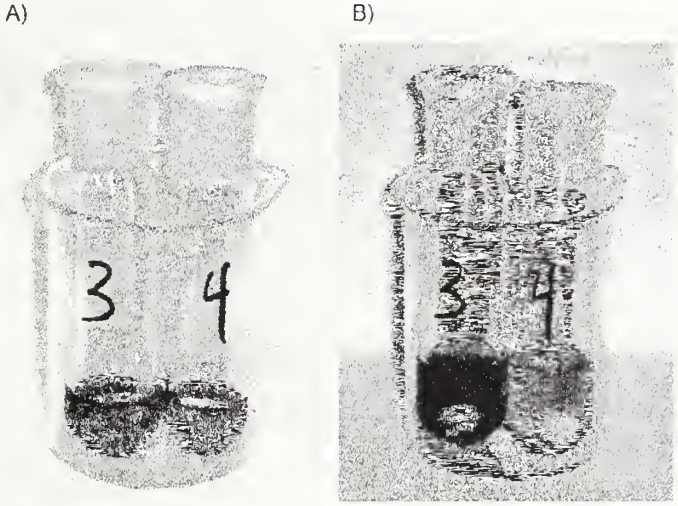

Figure 12. Nitroxide covered (3) and TOPO covered CdSe (4) before (A) and after (B) heating to 125 °C for 12 h in the presence of styrene. (Volume change in the after image is due to the addition of toluene following polymerization.)

Copolymerizations of styrene and methyl methacrylate were also performed in either solution or in the bulk. A range of copolymer compositions was prepared by varying the monomer feed ratio. Following polymerization, the CdSe-polymer composite material **6** was isolated as a pale red powder following precipitation into methanol. The powder was dispersible in good solvents for polystyrene or PS-*r*-PMMA

such as toluene, chloroform and THF. The ^{1}H NMR spectra of these materials appeared to be identical to that of the particular polymer grafted from the particle, as resonances for both the phosphine oxide ligand and the TEMPO overlap with the polymer signals.

Characterization of the polymer grafts by size exclusion chromatography required removal of the polymers from the nanoparticle surface. Failure to remove the chain and separate it from the particle may allow for sedimentation of bare CdSe within the column pores and eventually render the column useless. Therefore, the cadmium selenide core was chemically degraded with 4-dimethylaminopyridine (DMAP), and the free polymers isolated by precipitation.

		Feed Ratio		Final Polymer	
Mn	PDI	% Styrene	% MMA	% Styrene	% MMA
9300	1.3	100	-	100	-
13400	1.29	100	-	100	-
22600	1.35	100	-	100	-
75500	1.34	100	-	100	-
125900	1.76	100	-	100	-
56800	1.46	80	20	78	22
27500	1.44	70	30	73	27
47400	1.40	60	40	60	40
14000	1.41	60	40	55	45
108000	1.76	50	50	56	44
103000	2.00	40	60	45	55
10500	1.38	40	60	45	55
18400	1.35	30	70	32	68
7400	1.74	10	90	7	93

Table 1. Molecular weight characterization data for "graft-from" polymerizations. M_n and PDI were calculated from SEC while percent incorporation was calculated from ^{1}H NMR.

Molecular weights of the grafted polystyrene chains ranged from 7,000 to 150,000 with PDI ranges of ca. 1.3-2.0. (**Table 1**) It was found that polymers with lower percent conversions (ca. 50 %) were likely to have lower PDI values compared to those allowed to proceed to near complete conversion.[21,22] For the PS-PMMA

copolymers. PDIs were slightly higher, (1.4-1.8) when compared to polystyrene homopolymers of comparable molecular weight. The percent incorporation in the random copolymer were calculated from the integrations of the ^{1}H NMR resonances of aromatic region of polystyrene versus the methyl ester of poly(methyl methacrylate) (PMMA) and tracked well the feed ratio as the percentages of incorporation.

2.3 Characterization of CdSe-Polymer Hybrid Materials

A primary goal of grafting polymers from the surface of CdSe nanoparticles is to achieve dispersion of the nanoparticles in a polymer matrix. The blending of TOPO-covered CdSe nanoparticles with polymers leads to phase separation and aggregation of the nanoparticles due to the poor enthalpic compatibility of the polymer and nanoparticles. This aggregation leads to self-quenching events between nanoparticles, resulting in a loss of the nanoparticle's unique optical and electronic properties.

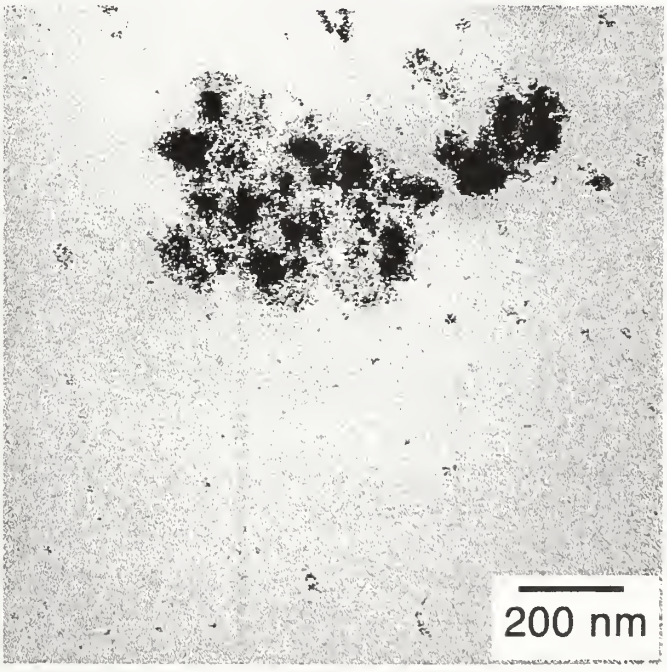

Figure 13. TEM micrograph showing aggregation of TOPO covered CdSe when blended with 80,000 g/mol PS.

Transmission electron microscopy was utilized to determine the morphology of these hybrid materials with respect to the blended materials. The micrograph shown in **Figure 13** illustrates a control experiment where 80,000 g/mol polystyrene was mixed with TOPO-covered CdSe nanoparticles in chloroform, then drop-cast onto a carbon coated grid. The resulting aggregated morphology is typically associated with the attempted blending of nanoparticles and polymers. A completely different morphology is observed in TEM micrographs of CdSe-PS hybrid materials prepared by the graft-from technique. In these cases, an even dispersion of nanoparticles is evident in the micrograph shown in **Figure 14**. This dispersion is also seen when the composites are blended with additional polystyrene.

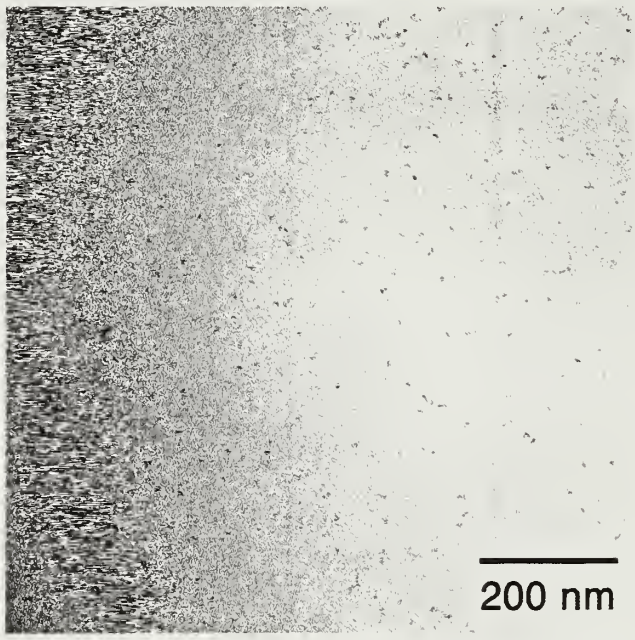

Figure 14. TEM micrograph of CdSe-PS hybrid. The PS grafted from the surface has a molecular weight of 80,000 g/mol.

The optical properties of the CdSe nanoparticles following controlled radical polymerization was a point of concern throughout the project. As previously discussed, the CdSe nanoparticle surface is highly sensitive to radicals, leading to oxidation and

nanoparticle degradation.[23-25] After a surface cadmium atom is oxidized, its electrons are no longer available to the particle core, thus shrinking the effective particle size and in turn increasing the particle's band gap, leading to a blue shift of the corresponding peak in the UV-Vis spectrum. Initial evidence for the preservation of the nanoparticle's optical properties was the persistence of the characteristic red color following polymerization (**Figure 12**). This initial observation was confirmed as the UV-Vis band-edge adsorption peak was shifted from 529 nm to 527 nm following polymerization. The 2-3 nm blue indicates that very little oxidation occurred during the polymerization step. (**Figure 15**)

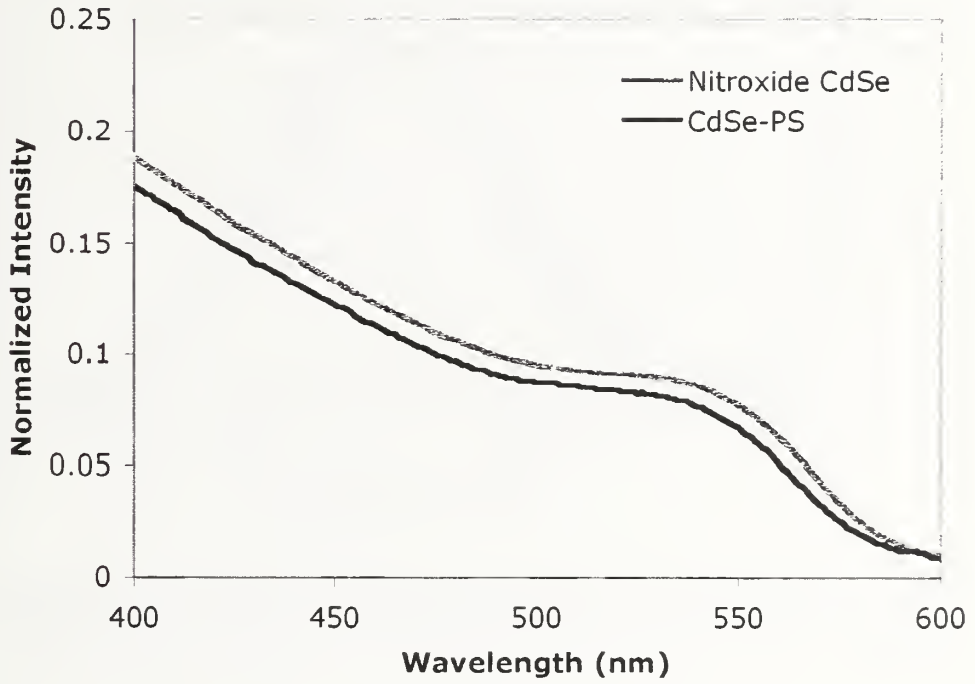

Figure 15. UV spectra illustrating the band edge adsorption of CdSe before (Nitroxide CdSe) and after (CdSe-PS) polymerization.

Photoluminescence spectra (PL) were collected with an excitation wavelength of 400 nm from chloroform solutions. Excellent agreement with the UV-Vis spectra was present as 2-3 nm blue shifts were associated with the CdSe fluorescence peak

maximum following polymerization. However, a striking increase in fluorescence intensity was observed after fluorescence spectra of the hybrid material **6** were compared to that of the starting nitroxide functionalized CdSe **5** as illustrated in **Figure 16.** Quantum yields of 3 to 8% relative to Rhodamine 6G were calculated for the composite material, compared to 0.4 to 1% for the starting nitroxide CdSe, equaling an order of magnitude increase in photoluminescence intensity.

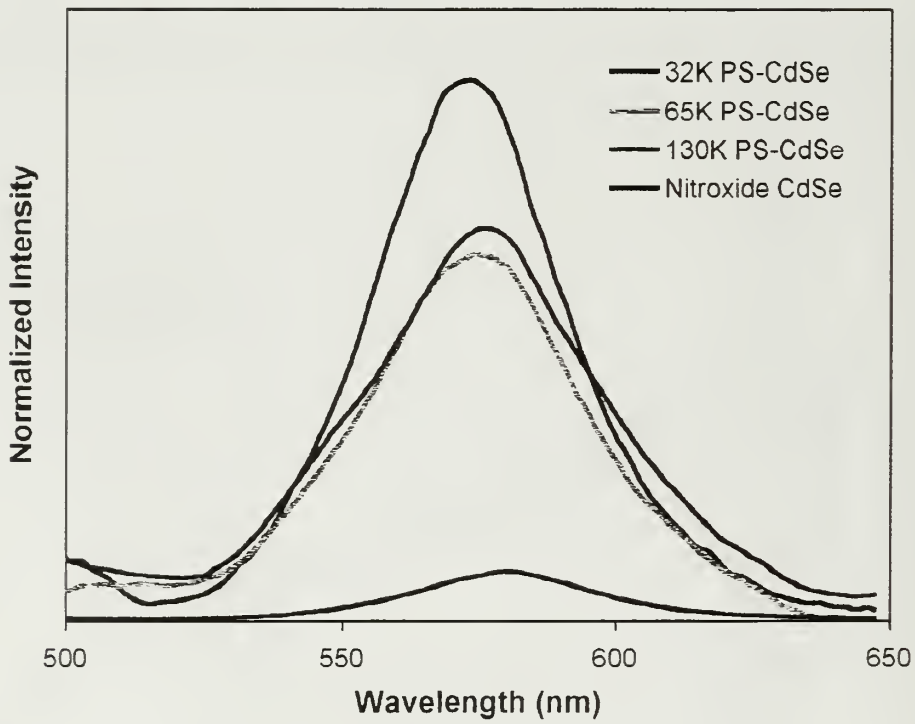

Figure 16. Solution state fluorescence emission spectra (Ex @ 400 nm) before and after polymerization for a variety of molecular weight polymers grafted from the particle.

Initial explanations for this profound increase in fluorescence involved theories of particle annealing. Previous research has illustrated that prolonged heating of CdSe nanoparticles at temperatures greater than 100 °C can effectively anneal the crystal structure, eliminating structural defects thus leading to an increase in quantum yield.[26]

A control experiment to evaluate the effect of thermal annealing on CdSe photoluminescence was performed with TOPO capped CdSe as heating **5** in the absence of a vinyl monomer led to nanoparticle degradation. Briefly, TOPO covered CdSe was stirred in xylenes at 125 °C under an inert atmosphere for 24 h. However, this annealing step accounted for an average of a two-fold increase in PL intensity and 3-5 nm blue shifts.

A second hypothesis considered involves the ligand coverage of the nanoparticle surface; particularly the number of ligands bound the surface at any given time. Surface cadmium atoms that do not have an associated ligating species represents a surface defect that contributes to a decrease in the photoluminescence intensity. Thus, as the number of vacant sites is reduced, the effective photoluminescence increases. In the experiments presented above, all polystyrene grafted from the nanoparticle surface is above the chain entanglement weight. This entanglement likely influences the equilibrium between bound and unbound phosphine oxides, resulting in a increased number of phosphine oxides bound to the particle surface at any given time. Therefore, it is believed that the increase in PL quantum yield is a cooperative effect of both CdSe annealing and the shifting of the ligand equilibrium to the bound state.

2.4 Incorporation of CdSe-Polymer Hybrids into Polystyrene-Poly(methyl methacrylate) Block Copolymers

Following the successful dispersion of nanoparticles in a polymer matrix, a logical progression involves the controlled placement of nanoparticles at specific regions or locations within a polymer matrix. This control over nanoparticle location is

a prerequisite for applications such as data storage or display applications where the ability to address individual particles or a specific group of particles, would be necessary. While a daunting task, the Balasz group has developed self-consistent field theory that predicts that the location of the nanoparticle in a block copolymer assembly can be controlled by ligand functionality.[27] Consider the following simplified example, in a diblock copolymer composed of polymer A and polymer B, nanoparticles with ligand functionality similar to A would reside in the A block, and those with functionality similar to B would reside in the B block. A nanoparticle with no preference for either the A or B domains would be driven to the interface between A and B to mediate interfacial interactions. Kramer and coworkers recently demonstrated an elegant example of this theory with gold nanoparticles in a polystyrene-*b*-poly(vinyl pyridine) diblock copolymer assembly.[28] The gold particles functionalized with short polystyrene chains were located in the center of the PS block, while the PVP covered gold particles resided in the PVP phase. In addition, the placement of gold near the interface or at the interface was precisely controlled through the use of mixed monolayers of PS and PVP on the gold surface.

Experiments aimed towards the results described above were attempted by blending the CdSe-PS or CdSe-(PS-*r*-PMMA) composite materials with PS-PMMA diblock copolymers. Initial experiments involved the use of 80.000 g/mol PS grafted from CdSe blended with PS-PMMA (85.000 and 91.000 g/mol respectively). Briefly, 5 wt % CdSe polymer composite was dissolved with an appropriate diblock copolymer in toluene. After solvent evaporation, the samples were dried, microtomed,

and examined with electron microscopy. A representative example of our results is shown in **Figure 17**. It is clearly evident that phase separation between the diblock copolymer and the nanoparticle composite has occurred, as all nanoparticles are present in domains where the lamella morphology has been disturbed. Additional experiments performed with smaller molecular weights grafted from the particle (14.000 g/mol) also led to similar results as shown in **Figure 18**.

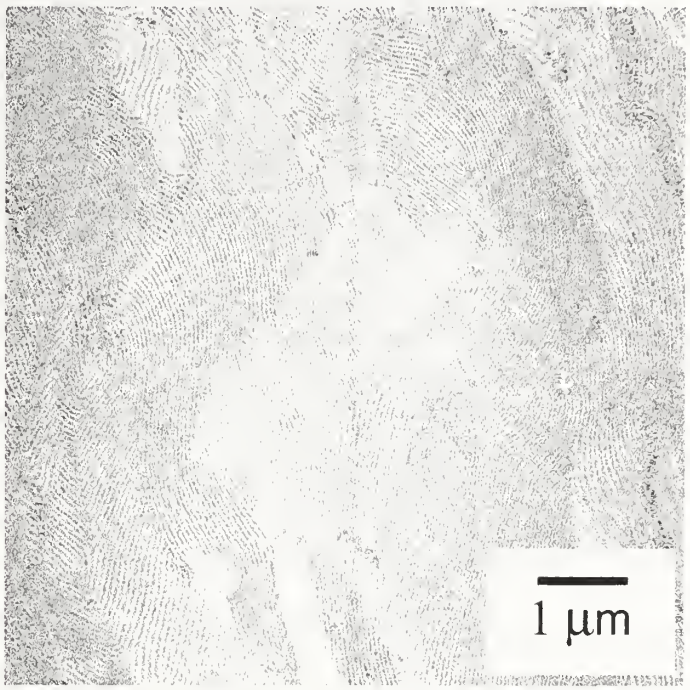

Figure 17. TEM micrograph illustrating the phase separation between CdSe-PS and PS-b-PMMA following blending. (CdSe-PS = 80,000 g/mol)

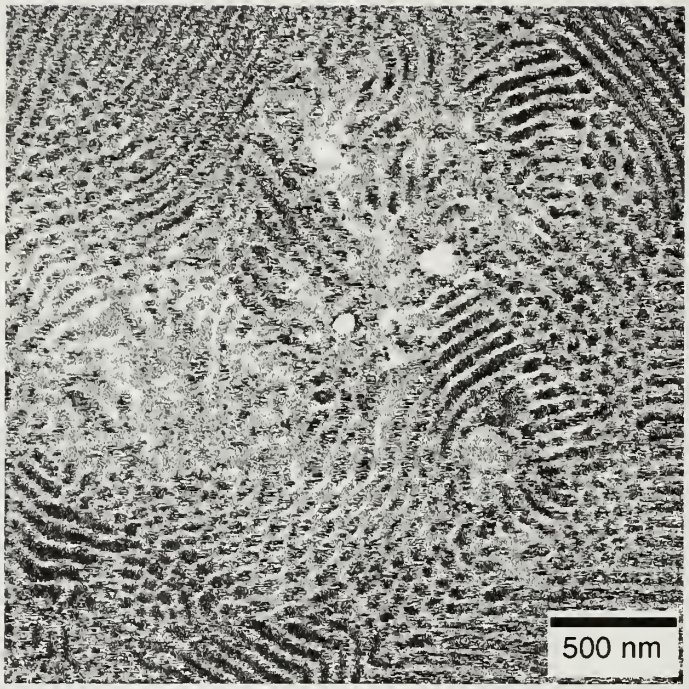

Figure 18. TEM micrograph illustrating the phase separation between CdSe-PS and PS-b-PMMA following blending. (CdSe-PS = 14,000 g/mol)

While these results were initially surprising, they are easily explained when one considers the size of the hybrid material when compared to the diblock copolymer. If the CdSe-PS hybrid material is approximated as a 50-arm star with each arm having a molecular weight of 80.000 g/mol then our molecular weight for the hybrid material can be estimated to be 4.000.000 g/mol.[29] Several research groups have examined both theoretical and experimental relationships between the molecular weight and radius of gyration (R_g) for multi-arm star polymers versus linear polymer chains.[30,31] Using these values, the apparent molecular weight for the hybrid can be calculated to roughly 800,000 g/mol. This apparent molecular weight corresponds to the molecular weight of a linear polymer chain that would exhibit similar solution properties (viscosity and R_g) at theta conditions. Therefore, if we consider an experiment where 5 wt % 800,000 g/mol polystyrene is blended with a 175.000 g/mol diblock copolymer, phase separation

and disruption of the lamella structure would be expected.[32-34] This disruption of the morphological structure occurs since the R_g for the hompolymer additive (~ 35 nm) is comparable to the d spacing for the diblock copolymer (~ 50 nm). These experiments demonstrate the importance of the molecular weight of the polymers grafted from the surface of the nanoparticle and their behavior in polymer microstructures.

2.5 Summary

Phosphine oxide ligands containing nitroxide moieties were synthesized and placed on CdSe nanoparticles by ligand exchange chemistry. These functionalized nanoparticles were utilized as multifunctional initiators for nitroxide mediated radical polymerization from the surface of the nanoparticle. The composite materials exhibited dispersion of the CdSe nanoparticles throughout the polymer film. Moreover, the CdSe nanoparticle's inherent optical properties were not degraded, but in the case of fluorescence, enhanced by the graft-from polymerization method.

2.6 Experimental Details

2.6.1 General Methods and Materials

Solvents were purchased from VWR and all other reagents were purchased from Aldrich and used as supplied unless otherwise noted. THF was dried over sodium/benzophenone and distilled before use. All reactions were run under a N_2 atmosphere unless otherwise noted. NMR spectra were obtained on a Bruker DPX 300 MHz or a Bruker 400 MHz Spectrospin spectrometer. Chemical shifts are expressed in parts per million (δ) using residual solvent protons as the internal standard. $CHCl_3$ (δ 7.26 for ^1H. 77.23 for ^{13}C) was used as an internal standard for $CDCl_3$. Gel permeation

chromatography (GPC) measurements were performed in tetrahydrofuran (THF) at 1.0 mL/min using a Knauer K-501 Pump with a K-2301 refractive index detector and K-2600 UV detector, and a column bank consisting of two Polymer Labs PLGel Mixed D columns and one PLGel 50 Å column (1.5 x 30 cm) at 35 °C. Molecular weights are reported relative to polystyrene standards. Matrix assisted laser desorption ionization - time of flight (MALDI-TOF) mass spectrometry was performed on a Brüker Reflex III spectrometer on the CdSe composite samples without the use of a matrix. High-resolution electron impact (EI) mass spectrometry was performed on a JOEL MStation JMS700 spectrometer. Fluorescence measurements were recorded on a Perkin-Elmer LS-55 fluorescence spectrophotometer and UV-Vis measurements were made on a Perkin-Elmer Lambda 25 spectrophotometer. Fluorescence spectra were normalized to the optical density at the excitation wavelength. Transmission electron microscopy and electron diffraction were performed on a JEOL 100CX microscope at 100,000 magnification (46 cm camera length).

2.6.2 Di-*n*-octylphosphine oxide

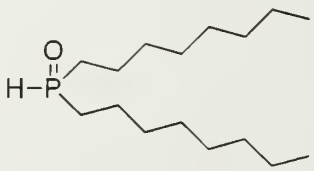

To a 5 L three-necked flask equipped with stirbar, stopper, reflux condenser and addition funnel was added magnesium (54.6 g, 2.25 mol) and diethyl ether (500 mL). The flask was cooled to 0 °C then bromooctane (444 g, 2.3 mol) in diethyl ether (1500 mL) was added drop wise over 4 hours. Upon complete addition, the ice bath was removed and the solution heated to 35 °C for 16 hours. The solution was cooled to 0 °C

then dibutyl phosphite (196 g, 1 mol) in diethyl ether (1000 mL) was added drop wise over 4 hours. The reaction was heated to reflux for 16 hours following the addition. The solution was again cooled to 0 °C then quenched with an aqueous solution of 25 % sulfuric acid (1 L) over 4 hours. The layers were separated and the aqueous layer extracted with ether (3 x 1 L). The combined organic layers were dried over $MgSO_4$, filtered and concentrated. Pure product was obtained as a white powder following two recrystallizations from hexanes (220 g, 80 % yield). ^{1}H NMR (300 MHz, $CDCl_3$, δ) 6.85 (d, J_{PH}=445.7 Hz, P-*H*, 1 H), 1.77 (m, P-CH_2, 4 H), 1.61 (m, P-CH_2-CH_2-, 4 H), 1.27 (m, -CH_2-, 20 H), 0.87 (t, J_{HH}=6.8 Hz, -CH_3, 6 H).

2.6.3 TEMPO-benzyl chloride 2

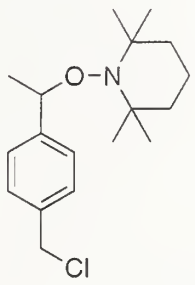

To a 1 L beaker was added 4-vinyl benzyl chloride **1** (3.61 g, 23.6 mmol), TEMPO (2.45 g, 15.7 mmol), (R,R)-(-)-N,N'-bis(3,5-di-*t*-butylsalicylidene)-1,2-cyclohexanediaminomanganese (III) chloride (1.50 g, 2.36 mmol), toluene (50 mL) and ethanol (50 mL). A slow stream of air was bubbled into the solution then sodium borohydride (1.78 g, 47.2 mmol) was slowly added to the stirred solution. After 16 h, additional ethanol (25 mL), toluene (25 mL) and sodium borohydride (1.78 g, 47.2 mmol) was added and stirred an additional 8 hours. The solution was diluted with dichloromethane and filtered over celite. The solvent was evaporated and the residue purified by silica gel column chromatography (10 % CH_2Cl_2 in hexanes eluting to 35 %

CH_2Cl_2 in hexanes). Pure product was obtained by crystallization of the chromatographed material with a mixture of acetone, isopropanol and water giving colorless crystals (3.10 g, 10.5 mmol, 67 %, mp 49-50 °C). ^{1}H NMR (400 MHz, $CDCl_3$, δ) 7.33 (m, Ar-*H*, 4 H), 4.78 (quart, J_{HH}=6.7 Hz, Ar-C*H*-, 1 H), 4.59 (s, Ar-CH_2-Cl, 2 H), 1.48 (br-s, $(CH_3)_2$-C-CH_2, 4 H), 1.45 (d, J_{HH}=6.7 Hz, Ar-CH-CH_3, 3 H), 1.37 (br-s, CH_2-CH_2-CH_2-, 2 H), 1.28 (br-s, C-CH_3, 3 H), 1.16 (br-s, C-CH_3, 3 H), 1.02 (br-s, C-CH_3, 3 H), 0.67 (br-s, C-CH_3, 3 H). ^{13}C NMR (100 MHz, $CDCl_3$, δ) 146.39, 136.05, 128.54, 127.11, 82.95, 59.90, 46.50, 40.55, 34.65, 23.78, 20.54, 17.42.

2.6.4 Benzyl-nitroxide phosphine oxide 3

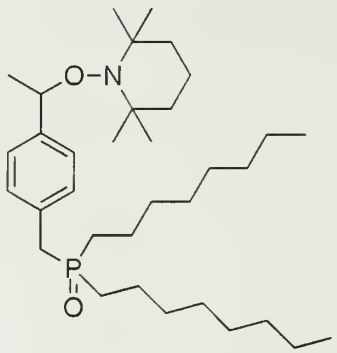

Di-*n*-octylphosphine oxide (1.21 g, 4.40 mmol) and NaH (0.12 g, 4.84 mmol) were stirred in THF (18 mL) at room temperature. The solution was heated to reflux and benzyl chloride **2** (1.50 g, 4.84 mmol) was added. The mixture was heated to reflux with stirring and aliquots removed for evaluation by ^{31}P NMR until the reaction reached completion (ca. 16h). The mixture was allowed to cool, quenched with water and extracted with CH_2Cl_2 (3 x 50 mL). The organic layers were dried over magnesium sulfate, filtered and evaporated under reduced pressure. The residue was purified by flash column chromatography (SiO_2, CH_2Cl_2 followed by 3% MeOH in CH_2Cl_2) to afford a colorless oil (2.14 g, 3.91 mmol, 89%). ^{1}H NMR (300 MHz, $CDCl_3$, δ) 7.18 (d,

J_{HH}=2.17 Hz, 2 H, Ar-*H*), 7.15 (d, J_{HH}=1.79 Hz, 2 H, Ar-*H*), 4.74 (quart, J_{HH}=6.53 Hz, 1 H, Ar-C*H*), 3.11 (d, J_{PH}=14.54, 2 H, Ar-CH_2-P=O), 1.46 (d, J_{HH}=6.70 Hz, 3 H, CH-CH_3), 1.32 (s, 3 H, C-CH_3), 1.26 (m, 28 H, alkyl), 1.16 (s, 3 H, C-CH_3), 1.00 (s, 3 H, C-CH_3), 0.88 (t, J_{HH}=6.42 Hz, 6 H, CH_2-CH_3), 0.58 (s, 3 H, C-CH_3). ^{13}C NMR (75 MHz, $CDCl_3$, δ) 144.77, 131.33, 129.45, 127.65 (Ar, 6 C); 82.92 (CH_3-*C*H, 1 C); 53.61 ((CH_3)$_2$-*C*, 2 C); 40.50 ((CH_3)$_2$-C-*C*H_2, 2 C); 36.25 (P(O)-*C*H_2, 1 C); 31.96, 31.39, 29.45, 27.94, 27.07, 23.39, 21.78 (alkyl *C*H_2, 14 C); 22.81 ((CH_3)$_2$-C, 4 C); 17.36 (TEMPO CH_2-*C*H_2-CH_2, 1 C); 14.28 (alkyl *C*H_3, 2 C).

2.6.5 Preparation of 3-covered CdSe nanoparticles 5

To approximately 25 mg of pyridine functionalized CdSe nanoparticles in THF (3 mL) was nitroxide **3** (250 mg). The solution was stirred at room temperature for 16 h, at which point the solution was optically clear. Anhydrous methanol (4 mL) was added, then the solution concentrated to ca. 3 mL. To this was added anhydrous methanol (4 mL). The solution was centrifuged for 5 min then the supernatant decanted. The nitroxide functionalized nanoparticles were dispersed in styrene (2.5 mL) and stored at -20°C.

2.6.6 General Procedure for Polymerization from Nitroxide CdSe 5

A solution of **5** in styrene (0.4 mL) was added to a reaction tube, purged with N_2, and subjected to five freeze-pump-thaw cycles. The mixture was heated at 125 °C for 4-24 h, depending upon the molecular weight desired. The reaction was cooled and the solid product was dissolved in THF and precipitated into methanol. The product was recovered via filtration to afford a pale red powder.

2.6.7 General procedure for removal of polymer from nanoparticle surface for molecular weight analysis

25 mg of DMAP was added to 15 mg CdSe-polymer product **6** dissolved in THF (1 mL) then stirred at 50 °C for 4 hours. The solution was precipitated into methanol then the milky solution centrifuged for 10 minutes. The supernatant was decanted, and a white solid was collected and dried by N_2 purge.

2.6.8 General procedure for the annealing of CdSe-PS composites with PS-*b*-PMMA diblock copolymers

To a 7 mL vial was added CdSe-PS composite (5 mg) and PS-*b*-PMMA (95 mg). The polymer was dissolved in toluene (2.5 mL) then the vial placed on a bench top and the solvent was allowed to evaporate over 24 h. The vials were then placed in a vacuum oven at 45 °C for 24 h followed by 90 °C for 24 h. The samples were cooled then microtomed to 25 to 40 nm thick slices for electron microscopy.

2.7 References

(1) Colombani, D. *Prog. Polym. Sci.* **1997**, *22*, 1649-1720.

(2) Oneil, G. A.; Torkelson, J. M. *Trends Polym. Sci.* **1997**, *5*, 349-355.

(3) Oneil, G. A.; Wisnudel, M. B.; Torkelson, J. M. *Macromolecules* **1996**, *29*, 7477-7490.

(4) Barton, J. *Prog. Polym. Sci.* **1996**, *21*, 399-438.

(5) Priddy, D. B. In *Polym. Synth.* 1994; Vol. 111, p 67-114.

(6) Gruber, H. F. *Prog. Polym. Sci.* **1992**, *17*, 953-1044.

(7) Corner, T. *Adv. Polym. Sci.* **1984**, *62*, 95-142.

(8) Odian, G. *Principles of Polymerization*; 3rd ed.; Wiley-Interscience: New York, 1991.

(9) Hawker, C. J.; Barclay, G. G.; Orellana, A.; Dao, J.; Devonport, W. *Macromolecules* **1996**, *29*, 5245-5254.

(10) Georges, M. K.; Veregin, R. P. N.; Kazmaier, P. M.; Hamer, G. K. *Macromolecules* **1993**, *26*, 2987-2988.

(11) Li, I.; Howell, B. A.; Matyjaszewski, K.; Shigemoto, T.; Smith, P. B.; Priddy, D. B. *Macromolecules* **1995**, *28*, 6692-6693.

(12) Patten, T. E.; Matyjaszewski, K. *Acc. Chem. Res.* **1999**, *32*, 895-903.

(13) Chiefari, J.; Chong, Y. K.; Ercole, F.; Krstina, J.; Jeffery, J.; Le, T. P. T.; Mayadunne, R. T. A.; Meijs, G. F.; Moad, C. L.; Moad, G.; Rizzardo, E.; Thang, S. H. *Macromolecules* **1998**, *31*, 5559-5562.

(14) Hawker, C. J. *Acc. Chem. Res.* **1997**, *30*, 373-382.

(15) Dao, J.; Benoit, D.; Hawker, C. J. *J. Polym. Sci., Part A: Polym. Chem.* **1998**, *36*, 2161-2167.

(16) Skaff, H.; Ilker, M. F.; Coughlin, E. B.; Emrick, T. *J. Am. Chem. Soc.* **2002**, *124*, 5729-5733.

(17) Williams, R. H.; Hamilton, L. A. *J. Am. Chem. Soc.* **1952**, *74*, 5418-5420.

(18) Kalyuzhny, G.; Murrary, R. W. *J. Phys. Chem. B* **2005**, *109*, 7012-7021.

(19) Lover, T.; Henderson, W.; Bowmaker, G. A.; Seakins, J. M.; Cooney, R. P. *Inorg. Chem.* **1997**, *36*, 3711-3723.

(20) Brus, L. *Curr. Opin. Coll. Inter. Sci.* **1996**, *1*, 197-201.

(21) Kruse, T. M.; Souleimonova, R.; Cho, A.; Gray, M. K.; Torkelson, J. M.; Broadbelt, L. J. *Macromolecules* **2003**, *36*, 7812-7823.

(22) Gray, M. K.; Zhou, H. Y.; Nguyen, S. T.; Torkelson, J. M. *Macromolecules* **2003**, *36*, 5792-5797.

(23) Ipe, B. I.; Lehnig, M.; Niemeyer, C. M. *Small* **2005**, *1*, 706-709.

(24) Bakalova, R.; Ohba, H.; Zhelev, Z.; Nagase, T.; Jose, R.; Ishikawa, M.; Baba, Y. *Nano Letters* **2004**, *4*, 1567-1573.

(25) Burda, C.; Green, T. C.; Link, S.; El-Sayed, M. A. *J. Phys. Chem. B* **1999**, *103*, 1783-1788.

(26) Mattoussi, H.; Cumming, A. W.; Murray, C. B.; Bawendi, M. G.; Ober, R. *J. Phys. Chem.* **1996**, *105*, 9890-9896.

(27) Lee, J. Y.; Thompson, R. B.; Jasnow, D.; Balazs, A. C. *Phys. Rev. Lett.* **2002**, *89*.

(28) Chiu, J. J.; Kim, B. J.; Kramer, E. J.; Pine, D. J. *J. Am. Chem. Soc.* **2005**, *127*, 5036-5037.

(29) Roovers, J. In *Star and Hyperbranched Polymers* New York, 1999, p 285-341.

(30) Schulte-Frohlinde, V.; Holovatch, Y.; von Ferber, C.; Blumen, A. *Phys. Lett. A* **2004**, *328*, 335-340.

(31) Hsu, H. P.; Nadler, W.; Grassberger, P. *Macromolecules* **2004**, *37*, 4658-4663.

(32) Mayes, A. M.; Barker, J. G.; Russell, T. P. *J. Chem. Phys.* **1994**, *101*, 5213-5218.

(33) Mayes, A. M.; Russell, T. P.; Bassereau, P.; Baker, S. M.; Smith, G. S. *Macromolecules* **1994**, *27*, 749-755.

(34) Green, P. F.; Russell, T. P.; Jerome, R.; Granville, M. *Macromolecules* **1988**, *21*, 3266-3273.

CHAPTER 3

CADMIUM SELENIDE/ZINC SULFIDE QUANTUM DOTS WITH A CROSS-LINKED POLYMER SHELL

3.1 Introduction

During the course of experiments with polymer-grafted quantum dots, the degradation of optical properties and nanoparticle aggregation was observed after several months of storage. One possible mechanism for this problem could be the oxidation of surface atoms. When the hybrid material is redissolved, some or all of the polymers grafted from the surface are no longer bound to the nanoparticle, resulting in nanoparticle aggregation. A proposed solution to this undesirable effect is the encapsulation of nanoparticles in a cross-linked polymer environment. Cross-linking the polymer shell of quantum dots was expected to improve their resistance to chemical degradation and afford the creation of unique nanostructured materials.

Several cases of shell cross-linked nanoparticles are reported in the literature, such as the wholly organic polymer nanoparticles developed by Wooley and coworkers. One example of this work is that of polystyrene-*b*-poly(acrylic acid) (PS-*b*-PAA), where the hydrophilic PAA corona is cross-linked by a diamine, or polystyrene-*b*-poly(4-vinyl pyridine) (PS-*b*-PVP), in which the pyridine is quaternized with vinyl benzyl chloride, then radically cross-linked to give the shell cross-linked nanoparticle.[1-3] Taton and coworkers have employed a similar approach to encapsulate alkyl-covered gold nanoparticles by physisosorbtion of PS-*b*-PAA followed by micelle formation. Once assembled, the micelle corona can be cross-linked chemically and gold containing

micelles can be isolated after selective centrifugation to remove empty micelles that do not contain a gold core.[4]

Hawker and coworkers have prepared cross-linked polystyrene nanoparticles, using a benzocyclobutane-functionalized polystyrene copolymers. These functional copolymers can undergo exclusive intrachain cross-linking, without the need for high dilution.[5] The addition of BCB functionalized copolymers to a poor, hot solvent causes the polymer to collapse into a globular conformation followed by intrachain cross-linking through the BCB moiety, as shown in **Figure 19**. The application of this cross-linking chemistry to CdSe-polystyrene hybrid materials is the focus of this chapter.

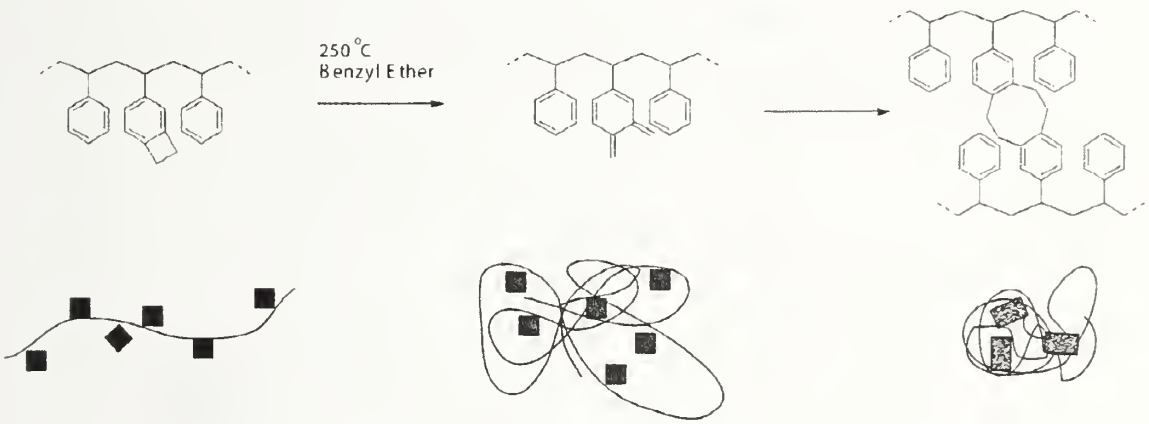

Figure 19. Chemical and schematic illustrations of the synthesis of polymer nanoparticles reported by Hawker and coworkers.

3.2 Polymerization From Cadmium Selenide/Zinc Sulfide Core Shell Nanoparticles

3.2.1 Cadmium Selenide/Zinc Sulfide Core Shell Nanoparticles

The preparation of cadmium selenide quantum dots with an inorganic protective shell was originally reported by Hines and Guyot-Sionnest in followed by simultaneous reports by both the Alivisatos and Bawendi research groups in 1997.[6,7] The passivation of the CdSe core with an overcoat of either CdS or ZnS allows for superior resistance to

oxidation and a dramatic increase in photoluminescence intensity due to the near complete passivation of CdSe surface atoms by the ZnS overcoat. With this inorganic, protective coating, quantum yields of greater than 90 % are routinely reported for CdSe/ZnS core shell quantum dots. The original synthesis of these nanoparticles called for the preparation and isolation of TOPO-covered CdSe followed by the addition of diethyl zinc and hexamethyldisilathane in TOP to give a thin (5-6 monolayers) coating of ZnS on the particle surface. More recently, Rosenzweig and coworkers described a one-pot synthesis of core-shell nanoparticles as shown in **Scheme 7**.[8] The alkyl functionalized CdSe/ZnS are isolated following repeated precipitation into methanol and are readily dispersible in a range of organic solvents such as tetrahydrofuran, chloroform, and hexanes.

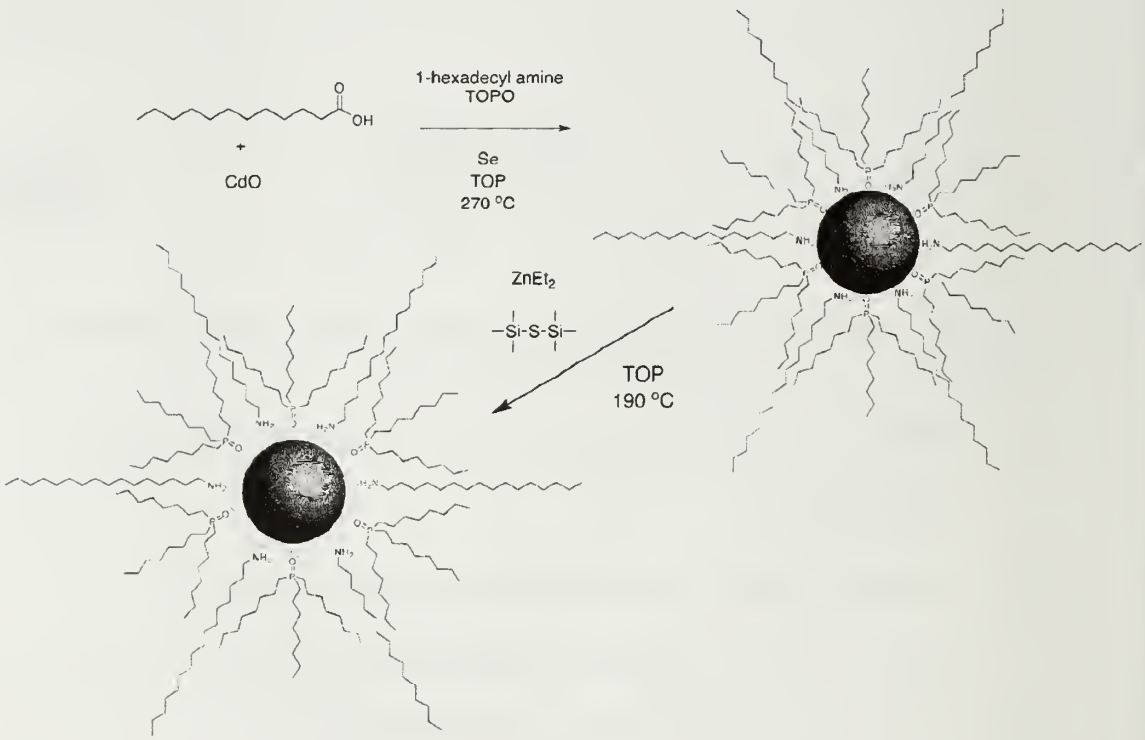

Scheme 7. A one-pot synthesis of TOPO/HDA covered CdSe/ZnS nanoparticles.

3.2.2 Synthesis of a Thermally Active Cross-linkable Monomer

Benzocyclobutane (BCB) has been used as a thermally activated cross-linking agent in multiple areas of polymer chemistry. In addition to the cross-linked polystyrene particles discussed previously, Moore and coworkers have used benzocyclobutane derivatives to cross-link poly(phenyleneterephthalamide).[9] Hawker and Russell have utilized poly(lactic acid)-*b*-styrene-BCB block copolymers to thermally cross-link phase-separated thin films.[10] At high temperatures (> 200 °C), BCB is converted to an ortho-quinoide structure that undergoes inter-molecular Diels-Alder reaction followed by a Cope rearrangement to form the dibenzocyclooctane product as illustrated in **Scheme 8**.[11] The vinyl substituted BCB **10** was chosen as a thermally cross-linkable monomer since the irreversible cross-links are formed in the absence of undesirable side reactions (*e.g.* generation of radical or ionic species which could adversely affect the quantum dot) and without the need for additional cross-linking reagents. Moreover, Hawker has shown this monomer to be amenable to the temperatures and conditions necessary for NMRP.

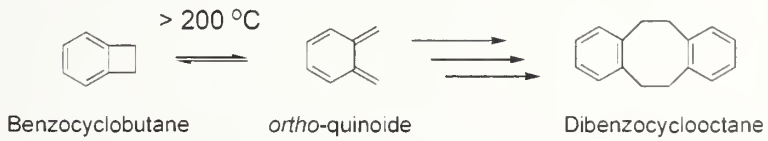

Scheme 8. The thermal initiated dimerization of benzocyclobutane.

BCB-functionalized monomer **10** was prepared in three steps from commercially available 2-methylbenzyl chloride **7**, as shown in **Scheme 9**. Flash vacuum pyrolysis of **7** gave benzocyclobutane **8** in 67 % yield following purification by distillation.[12] The ^{1}H NMR signal at $\delta \sim 3.0$-3.2 ppm, corresponding to the methylene cyclobutane protons, was used to confirm the presence of BCB or BCB derivatives

throughout the synthesis. BCB **8** was converted to 4-carboxyaldehyde benzocyclobutane **9** by Fridel-Crafts addition of α,α`-dichloromethyl methyl ether in 56 % yield.[13] Benzaldehyde **9** was purified by distillation and identified by the ^{1}H NMR signals at δ 9.94 ppm (aldehyde proton) and δ 3.24 ppm (BCB methylene protons). The benzaldehyde intermediate **9** was immediately converted to the styrene since the colorless aldehyde material became yellow and cloudy when stored for extended periods of time, likely a cause of residual HCl (generated from $TiCl_4$). Wittig reaction of **9** with methyl triphenylphosphonium bromide[5] gave vinyl substituted BCB **10** in 28% overall yield. ^{1}H NMR spectroscopy of styrene derivative **10** exhibited characteristic vinyl resonances at δ 6.60, 5.56 and 5.03 ppm and a singlet at δ 3.06 ppm corresponding to the methylene protons of the cyclobutane.

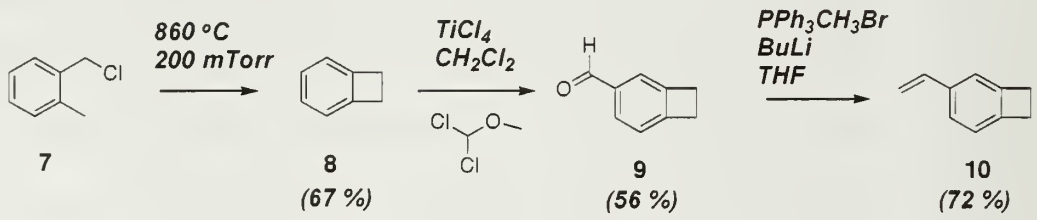

Scheme 9. Synthesis of 4-vinylbenzocyclobutane 10 from 2-methylbenzyl chloride 7.

3.2.3 Thiol-Nitroxide Synthesis and Ligand Exchange with Cadmium Selenide/Zinc Sulfide Core Shell Nanoparticles

Building from the work described in Chapter 2. nitroxide functionalized CdSe/ZnS quantum dots were prepared for the copolymerization of styrene and vinyl-BCB **10**. To achieve this goal, nitroxide functionalized thiol **12** was prepared for these

studies as shown in **Scheme 10**. The thiol was synthesized in addition to the phosphine oxide ligand since it exhibits a stronger affinity for the CdSe/ZnS surface relative to phosphine oxides and ligand exchange with thiols can be performed directly from the CdSe/ZnS TOPO nanoparticles, without the need for a pyridine intermediate.[14] Thiol ligand **12** was prepared from reaction of the TEMPO benzyl chloride derivative **2** with potassium thioacetate to give nitroxide-functionalized thioacetate **11**. Reduction of the thioacetate with LAH gave thiol **12** in 94 % yield. Characterization of **12** by ^{1}H NMR spectroscopy showed the absence of the thioacetate methyl protons (C(O)-CH_3 at δ 2.35 ppm) and a resonance corresponding to the benzyl protons adjacent to the thiol (Ar-CH_2-SH) at δ 3.71 ppm.

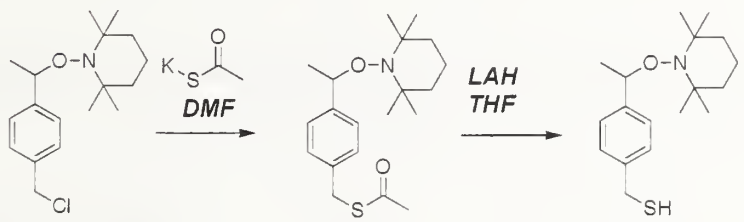

Scheme 10. Synthesis of thiol-nitroxide ligand 12 from benzyl chloride 2, which was prepared in Chapter 2.

Preparation of **12**-functionalized of CdSe/ZnS quantum dots was accomplished by stirring TOPO capped CdSe/ZnS nanoparticles with **12** at room temperature in chloroform according to **Scheme 11**. Evaporation of the chloroform followed by precipitation into methanol, gave the desired nitroxide functionalized CdSe/ZnS nanoparticles **12**. ^{1}H NMR spectroscopy confirmed the presence of thiol nitroxide ligand periphery, and no resonances from either TOPO or TOP were observed in the ^{31}P NMR spectrum of **13**. A slight blue shift in the fluorescence peak maximum was

accompanied by a significant decrease in solution photoluminescence intensity following ligand exchange with thiol **12** as illustrated in **Figure 20**. Preparation of **3**-covered CdSe/ZnS was performed using conditions identical to those described in Chapter 2.

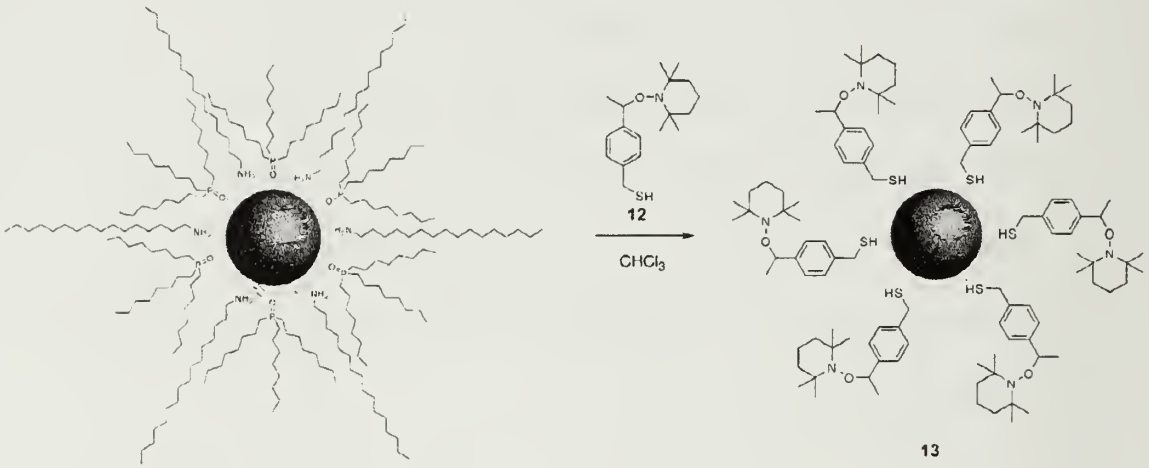

Scheme 11. Ligand exchange of TOPO/HAD covered CdSe/ZnS quantum dots with 12 to give nitroxide functionalized CdSe/ZnS 13.

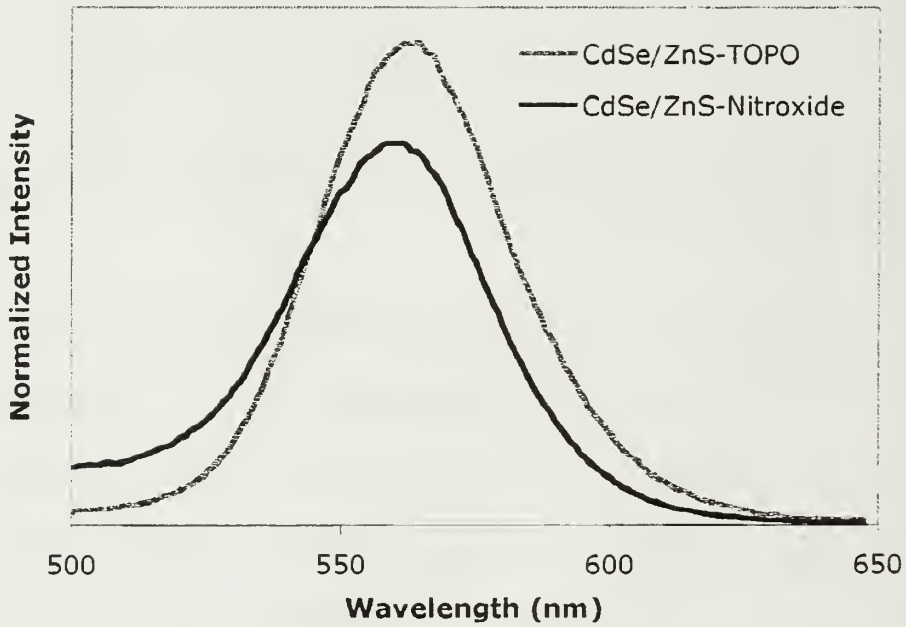

Figure 20. Solution photoluminescence of TOPO covered CdSe/ZnS before (red curve) and after ligand exchange to CdSe/ZnS-nitroxide 13 (blue curve).

3.2.4 Copolymerizations of Styrene and 4-vinylbenzocyclobutane from Cadmium Selenide/Zinc Sulfide Nanoparticles

Trial polymerizations were performed to demonstrate the ability of CdSe/ZnS, capped with either phosphine oxide or thiol nitroxide ligands, to effectively mediate the polymerization of styrenic monomers from the nanoparticle surface. In accord with procedures described in Chapter 2, **12**-functionalized nanoparticles were dissolved in styrene, degassed with multiple freeze-pump-thaw cycles, and heated to 125 °C for 12 h. The nanoparticle polymer hybrid material was isolated by precipitation from methanol. Characterization of the polymer grafts was performed following the removal from the nanoparticle surface by DMAP. Gel permeation chromatography relative to polystyrene standards indicated molecular weights in the range of 10,000 to 100,000 g/mol, depending on the amount of monomer used for a given amount of nitroxide functionalized nanoparticles. Polydispersities of 1.4-1.5 were found for phosphine oxide **3**-functionalized CdSe/ZnS, while PDI ranges of 1.4-1.7 were obtained for the thiol **12**-functionalized CdSe/ZnS. The higher PDI values for the thiol ligand are likely due to the susceptibility of free thiol to chain transfer. The optical properties of the quantum dot were maintained relative to the nitroxide functionalized particles following polymerization, as only a small blue shift is evident in the solution photoluminescence spectrum shown in **Figure 21**.

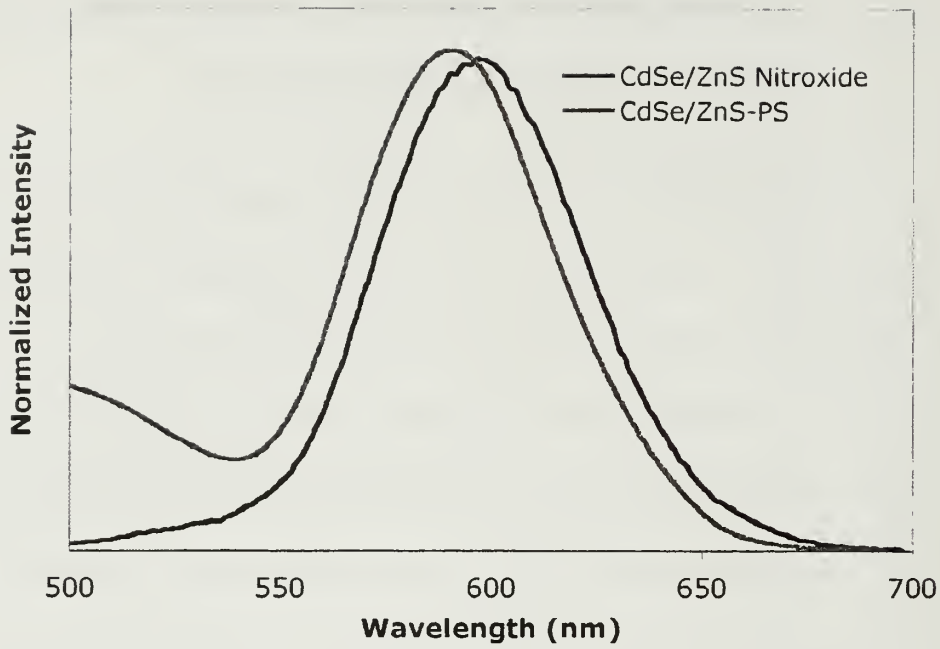

Figure 21. Solution photoluminescence of CdSe/ZnS 13 before polymerization (blue curve) and CdSe/ZnS-PS composite after polymerization (red curve).

12-Functionalized CdSe/ZnS nanoparticles were then used to initiate the copolymerization of styrene and BCB **10** in a 70:30 ratio. (**Scheme 12**) This was done by dispersing the **12**-covered nanoparticles in styrene:BCB **10** mixture, degassing, and heating to 125 °C under nitrogen for 12 hours. (For clarity and reasons that will be discussed later in the chapter, only results from **12**-functionalized CdSe/ZnS will be discussed.) The product, a CdSe/ZnS-(PS-co-BCB) composite material, was isolated in 50 to 60% yield following precipitation into methanol. ^{1}H NMR resonances at δ 7.12 and 6.71 ppm represented the aromatic region of polystyrene while a signal at δ 3.10 ppm confirmed the presence of the BCB moiety in the CdSe/ZnS-(PS-co-BCB) composite. Further characterization of a representative composite was found to have 75,800 g/mol with a PDI of 1.46, and fluorescence maxima at 590 nm compared to 593 nm for the nitroxide functionalized CdSe/ZnS.

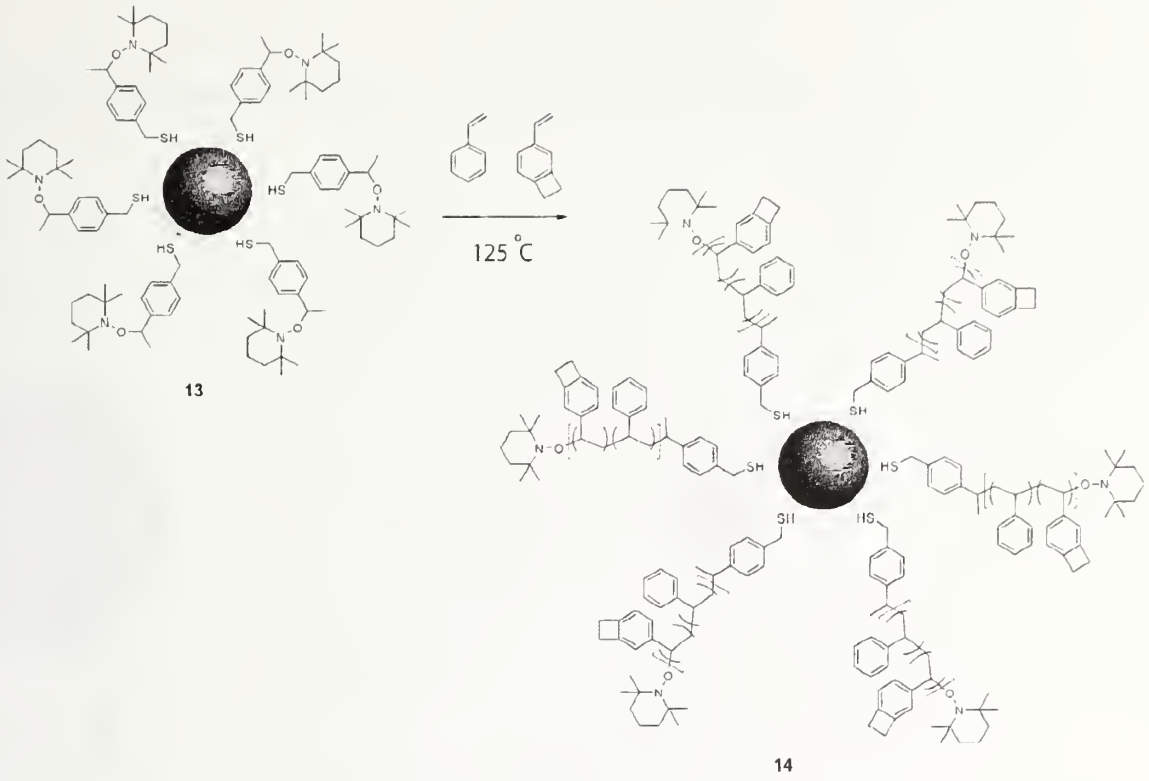

Scheme 12. Copolymerization of styrene and 10 from nitroxide particle 13 to give CdSe/ZnS-(PS-*co*-BCB) composite 14.

3.4 Thermally Activated Cross-linking of CdSe/ZnS-Poly(styrene-*co*-benzocyclobutane) Composite Materials

Initial cross-linking experiments utilized the methods of Harth and coworkers for the preparation of cross-linked organic nanopaticles.[5] The CdSe/ZnS-(PS-co-BCB) composite material was dissolved in benzyl ether then added dropwise to a stirred solution of hot (~ 250 °C) benzyl ether. It was expected that slow addition of the composite into a poor, hot solvent would cause the polymer chain to collapse upon the nanoparticle and cross-link exclusively by an intra-particle mechanism, such that particle-particle coupling would be avoided. (**Scheme 13**) Unfortunately, degradation of the quantum dot occurred during this process, as judged by complete loss of

photoluminescence and absorbance optical properties. A wide range of high boiling solvents and combinations thereof were screened in this high temperature cross-linking procedure (**Table 2**).

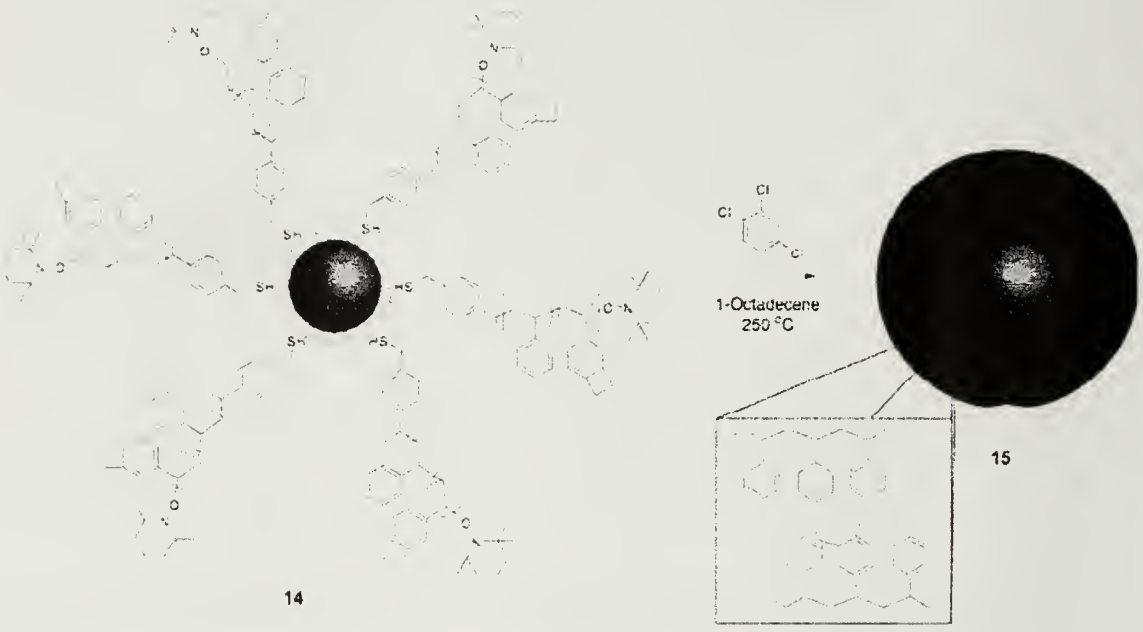

Scheme 13. Schematic illustration of the benzocyclobutane cross-linking reaction converting CdSe/ZnS-(PS-*co*-BCB) composite 14 to shell-cross-linked quantum dots 15.

Polymer Solvent	Crosslinking Solvent	Degrees C	Result
Benzyl Ether	Benzyl Ether	300	No CdSe/ZnS Fluorescence
Benzyl Ether	Benzyl Ether	250	No CdSe/ZnS Fluorescence
Benzyl Ether	Benzyl Ether	225	No CdSe/ZnS Fluorescence
Benzyl Ether	Benzyl Ether	200	No Fluorescence, Little Crosslinking
Benzyl Ether	Benzyl Ether	175	No Fluorescence, No Crosslinking
Benzyl Ether	Silicon Oil	300	No CdSe/ZnS Fluorescence
Benzyl Ether	Silicon Oil	250	No CdSe/ZnS Fluorescence
Benzyl Ether	Hexatriacontane	250	No CdSe/ZnS Fluorescence
Methylene Chloride	Silicon Oil	250	No CdSe/ZnS Fluorescence, Insoluble
1,2,4-Trichlorobenzene	1,2,4-Trichlorobenzene	220	Blue Shifted Flourescence, 7% crosslinking
Benzyl Ether	1,2,4-Trichlorobenzene	220	No CdSe/ZnS Fluorescence
Methylene Chloride	Benzyl Ether	250	No CdSe/ZnS Fluorescence, Insoluble
Methylene Chloride	1-Octadecene	250	Blue Shifted Fluorescence, Insoluble
Benzyl Ether	1-Octadecene	250	No CdSe/ZnS Fluorescence
1,2,4-Trichlorobenzene	1-Octadecene	230	15 nm Blue Shifted Fluorescence

Table 2. A reaction matrix describing various reaction conditions attempted for the synthesis of shell-cross-linked quantum dots 15.

Optimum results were obtained for the cross-linking reaction when a 1,2,4-trichlorobenzene solution of CdSe/ZnS-(BCB-*co*-PS) composite was added to 1-

octadecene at 240 °C. When performed using degassed solvents, the cross-linking reaction proceeded without nanoparticle degradation and only very small blue shifts in quantum dot fluorescence. This relatively small blue shift indicated that the quantum dot was not appreciably affected by the cross-linking reaction. (**Figure 22**) Following the cross-linking reaction, excess solvent was removed *via* Kugelrohr distillation and the shell-cross-linked quantum dots **15** were precipitated into methanol. The resulting material was soluble in a wide range of organic solvents, including hexanes. This unique, increased solubility was noted since the CdSe/ZnS-(PS-*co*-BCB) starting material is insoluble in hexanes. Characterization of **15** by ^{1}H NMR showed the disappearance of BCB resonances at $\delta \sim 3.1$ ppm and the appearance of resonances at $\delta \sim 2.8$ ppm corresponding to the dibenzocyclooctane cross-link, illustrated in **Figure 23**.

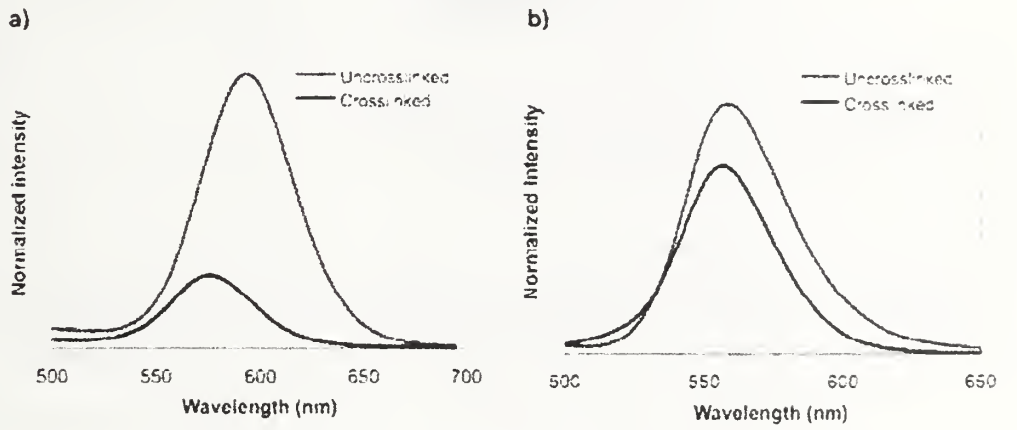

Figure 22. Solution fluorescence emission of CdSe/ZnS-(PS-*co*-BCB) before (red curve) and after (blue curve) the crosslinking reaction for a) reaction run under nitrogen and b) reaction run with degassed solvents under argon

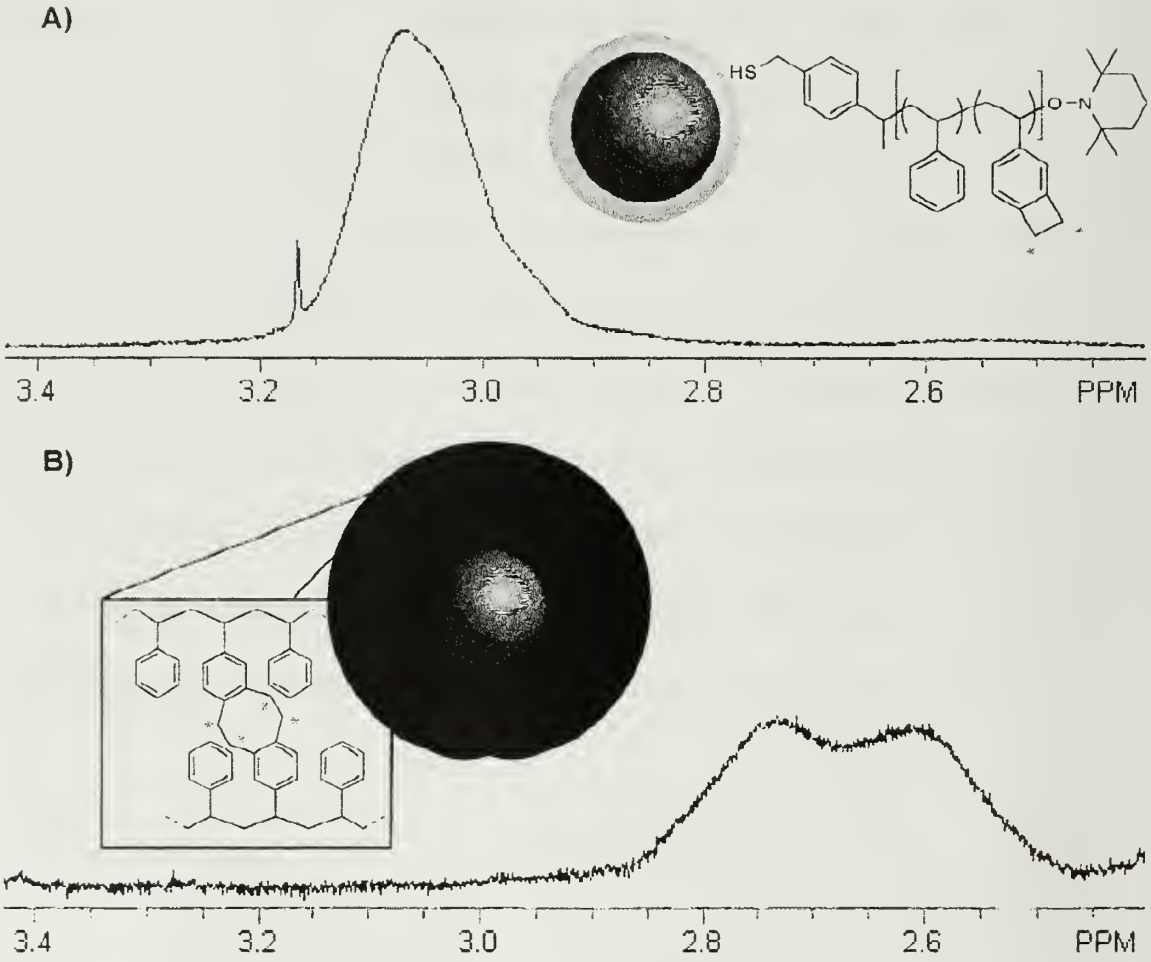

Figure 23. ^{1}H NMR spectrum for A) CdSe/ZnS-(PS-*co*-BCB) 14 before cross-linking and B) shell-cross-linked quantum dots 15 after cross-linking. The red asterisks denote the methylene groups responsible for the resonance.

Optimal results were obtained from composites with individual chains of molecular weight greater than ca. 20.000 g/mol and greater than 20 mole percent BCB. The use of unprotected CdSe nanoparticles (i.e. no inorganic shell) proved incompatible with the cross-linking process, as nanoparticle degradation was consistently observed. Moreover, the nitroxide functionalized phosphine oxide ligand used previously for polymer growth from CdSe nanoparticles, while suitable for use with the CdSe/ZnS core shell particles, did not perform as well as the thiol ligand, as substantial blue shifts

in the quantum dot photoluminescence was observed following cross-linking. The lower affinity of phosphine oxides relative to thiols for the cadmium surface atoms and the poorer ligand coverage compromises the optical properties and likely leads to diffusion of the polymer chain away from the nanoparticle surface before cross-linking occurs.

3.5 Characterization of Shell-Cross-linked Quantum Dots

3.5.1 Electron Microscopy and Electron Diffraction

Transmission electron microscopy was used to characterize these new organic/inorganic shell-cross-linked structures. The micrograph in **Figure 24a** shows the CdSe/ZnS-(PS-*co*-BCB) composite where the 3 nm nanoparticles are dispersed in the polymer matrix, correlating well with our previous results from Chapter 2. **Figure 24b** illustrates the micrographs from the shell cross-linked quantum dots. Two distinct size distributions of particles are present in the micrograph of the shell-cross-linked nanoparticles as shown in the histogram in **Figure 24c**. The larger particles (24-28 nm) are believed to represent the shell-cross-linked quantum dots while the smaller particle distribution (~10 nm) is believed to reflect cross-linked particles that do not contain quantum dots, arising from polymer that was either unbound from the CdSe/ZnS surface following the graft-from step or that became free of the surface at the high temperatures used for cross-linking. Unfortunately, individual quantum dots were not visible inside the cross-linked particles due to the mass thickness contrast of the cross-linked polystyrene and the diffraction contrast of the CdSe/ZnS. The result of a control experiment to demonstrate the size of cross-linked polystyrene is represented in **Figure 24d**. PS-*co*-BCB (M_n ~ 25,000 g/mol) was cross-linked using cross-linking conditions

identical to those used in the preparation of shell-cross-linked quantum dots. resulting in 7-9 nm organic nanoparticles. The size of these polystyrene nanoparticles is in agreement with the sizes previously reported and likely represent the smaller distribution of particles observed in the micrograph of shell-cross-linked quantum dots.

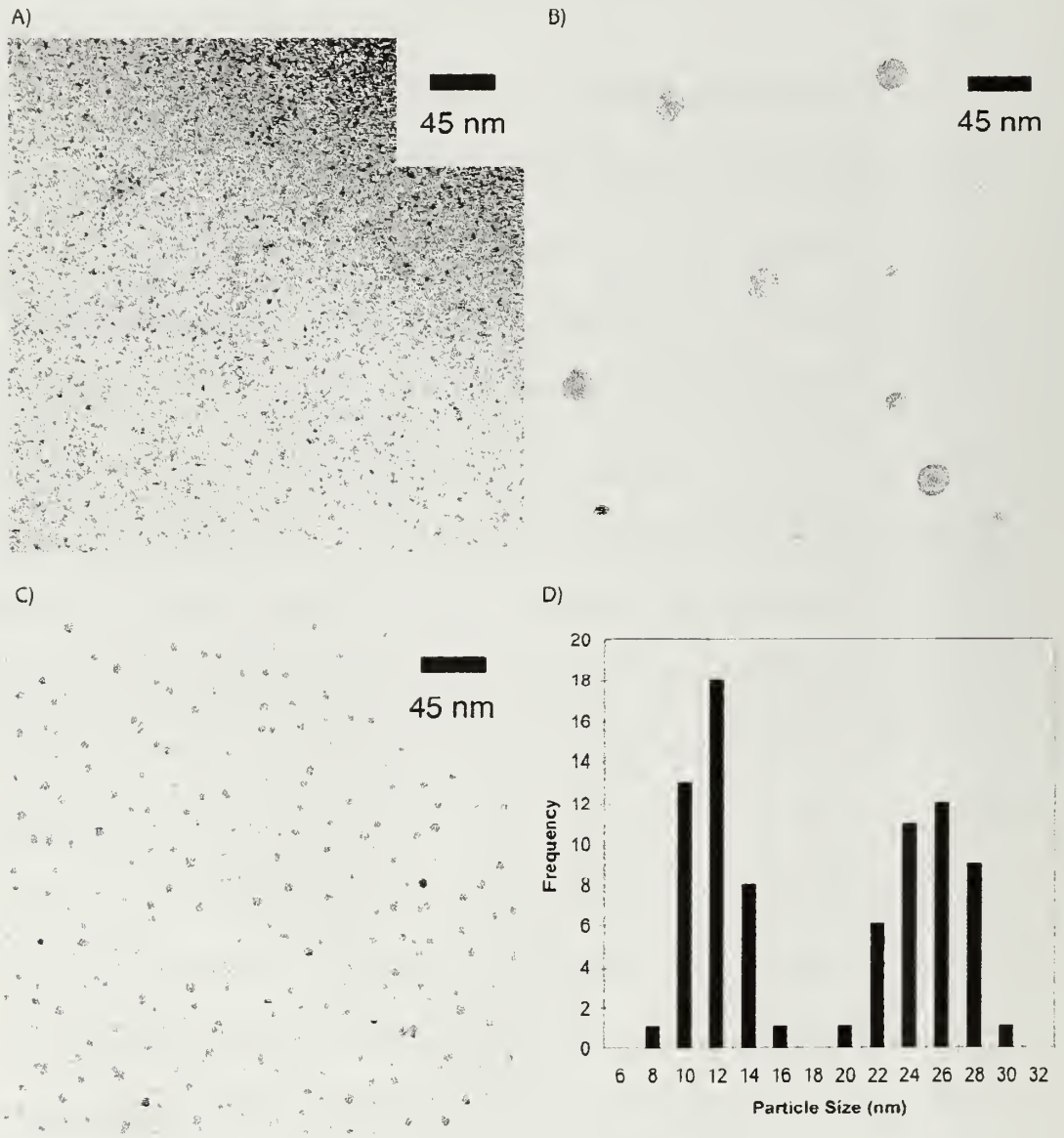

Figure 24. Transmission electron micrographs of A) CdSe/ZnS-(PS-*co*-BCB) 14, B) shell-cross-linked quantum dots 15 and C) the polystyrene cross-linking control experiment. A histogram of particle sizes for shell-cross-linked quantum dots is shown in panel D.

While not visible in the transmission images, electron diffraction of the shell cross-linked quantum dots **15** clearly indicates the presence of a crystalline material with a *d* spacing of 2.11 Å (**Figure 25a**). This value corresponds to the reported value of CdSe (d_{110}, 2.15 Å), suggesting the presence of crystalline CdSe.[15] Electron diffraction of the control experiment (**Figure 25b**) showed only an amorphous halo, confirming the absence of crystalline material in the cross-linked polystyrene beads.

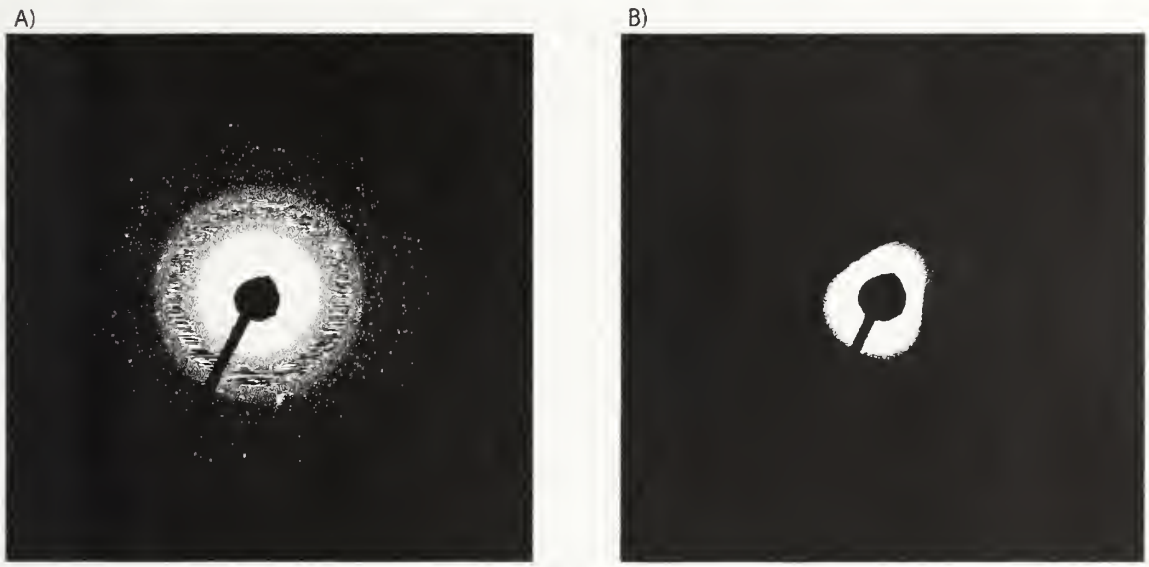

Figure 25. Electron diffraction patterns for A) shell-cross-linked quantum dots 15 and B) the polystyrene control experiment.

The particle size distribution also suggests the existence of the quantum dots within the cross-linked polymer shell. When a single polymer chain is cross-linked into a 10 nm diameter sphere, it occupies a volume of approximately 500 nm^3. When this volume is compared to the 11500 nm^3 occupied by a 27 nm particle, it is obvious that this distribution is not the result of the intermolecular cross-linking between two or three polymer chains. If one were to assume that the larger particles were a result of interchain cross-linking events, then a Gaussian distribution across all particle sizes would be expected, rather than the discrete distributions observed. Based upon the

presence of crystallinity in the electron diffraction image and the distribution of particle sizes, it is surmised that each of the larger cross-linked particles possesses a single quantum dot while the smaller particles are comprised of a single cross-linked polystyrene chain.

It should be noted that these experiments were repeated in the Emrick laboratory by Sang Ho Cha with gold nanoparticle cores. The nitroxide functionalized gold nanoparticles were prepared directly in the nitroxide ligand **12** and the PS-*co*-BCB copolymer grafted from the nanoparticle surface. The resulting Au-(PS-*co*-BCB) composite was cross-linked using conditions identical to those described above. Fortunately, the increased electron density present in the gold core results in improved contrast for electron microscopy. This improved contrast allows for the differentiation of the cross-linked organic shell and the nanoparticle core in the electron micrograph (**Figure 26**). This result offers substantial support for the model of individual nanoparticles inside a cross-linked polymer gel presented for the shell-cross-linked quantum dots.

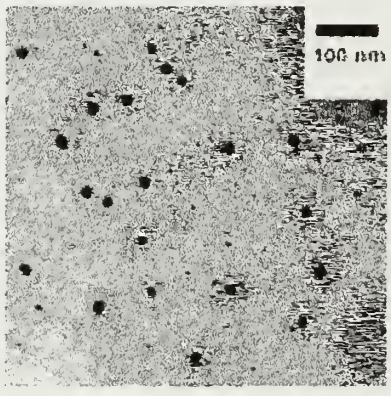

Figure 26. Transmission electron micrographs of shell cross-linked gold nanoparticles illustrating individual nanoparticles inside within polymer shells.

3.5.2 Chemical Degradation of Shell Cross-linked Quantum Dots

Chemical degradation studies were performed using DMAP treatment of the cross-linked composite material vs. uncross-linked to determine the impact of cross-linking on quantum dot properties. DMAP can be used to remove ligands from CdSe nanoparticles and diminish their fluorescence. The permeability of the cross-linked and uncross-linked polymer shells was investigated by mixing these materials with DMAP in a range of solvents and monitoring the fluorescence intensities as a function of time as illustrated in **Figure 27**. When the core-shell materials are stirred with 30 mg DMAP in 4:1 octadecene:$CHCl_3$, a poor solvent combination for polystyrene, no loss in fluorescence intensity or noticeable blue shifts for either the uncross-linked or cross-linked material was observed. However, **Figure 27a** illustrates the experiment performed with a 1:1 mixture of octadecene to $CHCl_3$. In this case, the cross-linked composite exhibits a behavior similar the 4:1 mixture while the uncross-linked composite gradually loses fluorescence over four hours, indicating that DMAP was able to reach the quantum dot surface, resulting in diminishment of fluorescence intensity. Moreover, as shown in **Figure 27b**, fluorescence is lost rapidly in both materials when stirred in a solution of DMAP in $CHCl_3$, a good solvent for polystyrene capable of swelling the cross-linked polymer gel, and providing chemical accessibility to the particle surface. These simple experiments highlight the benefits of shell cross-linking and other limitations associated with organic polymer shells that can be swelled under appropriate conditions.

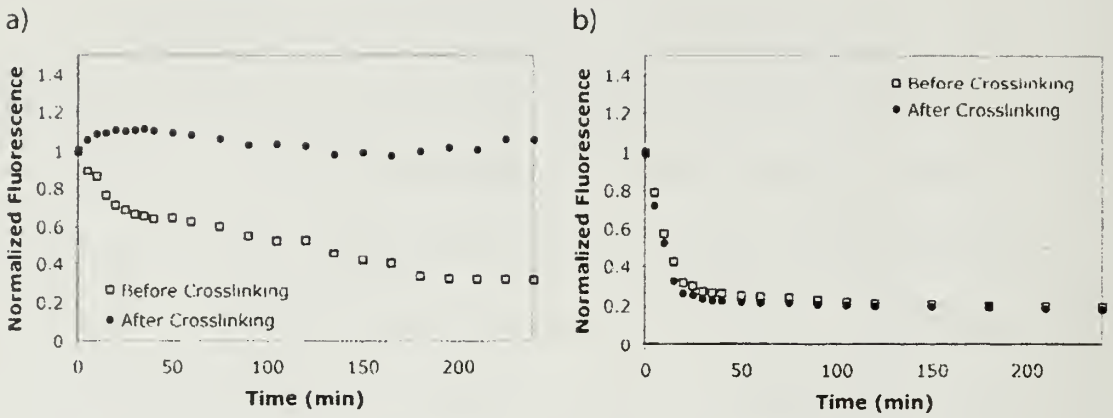

Figure 27. Chemical degradation of CdSe/ZnS-(PS-*co*-BCB) and the shell cross-linked quantum dots. The fluorescence of each material was measured as a function of time following the introduction of 4-dimethylaminopyridine in a) 1:1 octadecene:$CHCl_3$ and b) 100 % $CHCl_3$.

3.6 Summary

CdSe/ZnS core-shell quantum dots were functionalized with a thiol-nitroxide ligand for use in the preparation of nanoparticle-polymer composite materials. 4-vinyl benzocyclobutane was prepared and incorporated as a comonomer in controlled free-radical polymerizations from the CdSe/ZnS surface. Cross-linking conditions were found that allowed for complete conversion of benzocyclobutane to dimer cross-links without adversely affecting the quantum dot's optical properties. The shell cross-linked nanoparticles exhibited improved chemical resistance relative to the native, uncross-linked CdSe/ZnS-polymer composites.

3.7 Experimental Details

3.7.1 General Methods and Materials

Solvents were purchased from VWR and all other reagents from Aldrich and used as supplied unless otherwise noted. THF was dried over sodium/benzophenone and distilled before use. Styrene was washed with 1 N NaOH, dried with $MgSO_4$, and

then distilled over CaH_2 prior to use. All reactions were run under a N_2 atmosphere unless otherwise noted. NMR spectra were obtained on either a Brüker DPX 300 MHz or Brüker Spectrospin 400 MHz spectrometer. Chemical shifts are expressed in parts per million (δ) using residual solvent protons as the internal standard. $CHCl_3$ (δ 7.26 for ^1H, 77.23 for ^{13}C) was used as an internal standard for $CDCl_3$. Gel permeation chromatography (GPC) measurements were performed in tetrahydrofuran (THF) at 1.0 mL/min using a Knauer K-501 Pump with a K-2301 refractive index detector and K-2600 UV detector, and a column bank consisting of two Polymer Labs PLGel Mixed D columns and one PLGel 50 Å column (1.5 x 30 cm) at 35 °C. Molecular weights are reported relative to polystyrene standards. Fluorescence measurements were recorded on a Perkin-Elmer LS-55 fluorescence spectrophotometer and UV-Vis measurements were made on a Perkin-Elmer Lambda 25 spectrophotometer. Fluorescence spectra were normalized to the optical density at the excitation wavelength (400 or 450 nm). Transmission electron microscopy and electron diffraction were performed on a JEOL 100CX microscope at 100K magnification (46 cm camera length). Samples were transferred to the 400 mesh carbon coated copper grids by either drop casting or dip coating from chloroform solutions.

3.7.2 Preparation of TOPO Covered CdSe/ZnS Quantum Dots

To a 3-necked round bottom flask equipped with stir bar, reflux condenser, argon inlet, temperature thermocouple and septa was added CdO (0.016 g) and lauric acid (0.16 g). The reagents were stirred with heating until a clear, colorless solution was present. The solution was cooled, then 1-hexadecylamine (1.94 g) and tri-*n*-

octylphosphine oxide (1.94 g) was added and the reactants heated to 270 °C. Once a clear solution was present, Se (0.08 g) in tri-*n*-octylphosphine (2 mL) was rapidly injected and the temperature reduced to 200 °C. The solution gradually changed from colorless to red over 30 s. After 2 min, diethyl zinc (1 mL, 1.1 M solution in hexanes) and hexamethyldisilathane (0.25 mL) in tri-*n*-octylphosphine (2 mL) was added over 1 min. This solution was stirred at 185 °C for 1 h, then cooled to 50 °C. Methanol (10 mL) was added, the solutions divided into four vials then centrifuged. The supernatant was discarded and the precipitate dissolved in chloroform (3 mL/vial) and centrifuged at 3000 rpm for 5 minutes. The supernatant was recovered and precipitated into methanol (4 mL/vial). This precipitation process was repeated once more then the CdSe/ZnS particles stored in a chloroform solution.

3.7.3 Synthesis of Benzocyclobutane 8

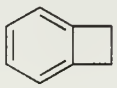

2-methylbenzyl chloride **7** (40 g, 284 mmol) was subjected to flash vacuum pyrolysis under the following conditions. A 500 mL round bottom flask was connected to a 24" long quartz tube, connected to a 250 mL rotary trap. The glassware was attached to a Kugelrohr distillation apparatus such that the round bottom flask containing the starting material was placed in the oven, the quartz tube was situated in a muffle furnace and the cold trap connected to the drive motor and vacuum. The system was evacuated to 200 mTorr, the furnace heated to 850 °C and the trap cooled with liquid nitrogen. Gradually, the oven was warmed from room temperature to 55 °C. After 3 h, all starting material had evaporated and passed through the quartz tube. The

trap was thawed, poured into 250 mL water, and extracted with diethyl ether (3 x 300 mL). The solvent was removed and the residue stirred in DMSO (300 mL) and KOH (40 g) for 24 h at room temperature. This solution was then poured into 400 mL water then extracted with pentane (3 x 250 mL). The combined organic layers were dried over $MgSO_4$, filtered and evaporated. The product was obtained as a colorless liquid following Kugelrohr distillation (14.7 g, 140 mmol, 50 %) ^{1}H NMR (300 MHz, $CDCl_3$, δ) 7.10 (m, Ar-*H*, 4 H), 3.19 (s, Ar-CH_2, 4 H). (75 MHz, $CDCl_3$, δ) 146.36, 127.14, 122.99, 30.19.

3.7.4 Synthesis of 4-carbaldehydebenzocyclobutane 9

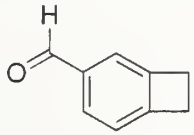

To a flame-dried 2 neck, 250 mL round bottom flask equipped with stir bar, addition funnel and N_2 inlet was added benzocyclobutane **8** (15.0 g, 144.0 mmol) and dichloromethane (100 mL). The solution was cooled with an ice bath and $TiCl_4$ (54.6 g, 288.0 mmol) in dichloromethane (50 mL) was added drop wise over 15 minutes then stirred for an additional 15 minutes. α,α'-Dichloromethylmethyl ether (16.6 g, 144.0 mmol) in dichloromethane (25 mL) was then added drop wise over 15 minutes. After 1 hour, the solution was poured over ice (400 g) and extracted with dichloromethane (3 x 150 mL). The combined organic layers were dried over $MgSO_4$, treated with carbon black, filtered over celite, then the solvent evaporated. Pure product was obtained following Kugelrohr distillation (180 °C) to give a colorless liquid (11.5 g, 86.6 mmol, 60 %). ^{1}H NMR (300 MHz, $CDCl_3$, δ) 9.94 (s, C(O)*H*, 1 H), 7.74 (d-d, J_{HH}=7.5, 1.3

Hz, Ar-*H*, 1 H), 7.58 (s, Ar-*H*, 1 H), 7.21 (d-d, J_{HH}=7.5, 1.4 Hz, Ar-*H*, 1 H), 3.24 (s, Ar-CH_2, 4 H).

3.7.5 Synthesis of 4-vinylbenzocyclobutane 10

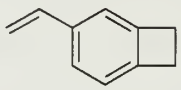

To a 500 mL 2 necked round bottom flask equipped with stir bar, nitrogen inlet and septum was added methyltriphenylphosphonium bromide (43.3 g, 121.2 mmol). The flask was evacuated for 1 hour then backfilled with N_2. THF (200 mL) was added and the stirred solution cooled with a dry ice/acetone bath. *n*-BuLi (116.9 mmol) in hexanes was added drop wise then the flask warmed to room temperature. After 1 h, the solution was again cooled with a dry ice/acetone bath and 4-carbaldehydebenzocyclobutane **9** (11.4 g, 86.6 mmol) was added *via* syringe. The reaction was allowed to warm to room temperature and stirred for 2 hours. The solution was diluted with hexanes (100 mL) then filtered over silica gel. The solvent was removed and the residue purified by silica gel column chromatography (hexanes). Pure product was obtained following Kugelrohr distillation (90 °C) to give a colorless liquid (7.6 g, 58.1 mmol, 67 %). ^{1}H NMR (300 MHz, $CDCl_3$, δ) 7.12 (d-d, J_{HH}=7.6, 1.2 Hz, Ar-*H*, 1 H), 7.04 (s, Ar-*H*, 1 H), 6.89 (d-d, J_{HH}=7.5, 0.9 Hz, Ar-*H*, 1 H), 6.60 (d-d, J_{HH}=17.6, 10.6 Hz, C*H*CH_2, 1 H), 5.56 (d-d, J_{HH}=17.6, 1.0 Hz, CHCH_2, 1 H), 5.03 (d-d, J_{HH}=10.9, 1.0 Hz, CHCH_2, 1 H), 3.06 (s, Ar-CH_2, 4 H).

3.7.6 Preparation of nitroxide thioacetate 11.

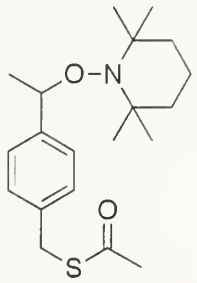

To a 50 mL round bottom flask was added TEMPO-benzyl chloride **2** (3.1 g, 10.5 mmol) potassium thioacetate (2.1 g, 16.5 mmol) and DMF (20 mL). The reaction was heated to 50 °C and stirred for 12 hours. The reaction was cooled, diluted with water (25 mL), and extracted with diethyl ether (3 x 75 mL). The combined organic layers were dried over $MgSO_4$, filtered over silica gel then solvent removed under reduced pressure. The crude product was recrystallized from methanol yielding the product as colorless crystals (3.2 g, 86% yield, mp 79-80 °C). ^{1}H NMR (300 MHz, $CDCl_3$, δ) 7.22 (m, 4 H, Ar-*H*), 4.75 (q, J_{HH}=6.59 Hz, 1 H, Ar-C*H*-(CH_3)-O), 4.11 (s, 2 H, Ar-CH_2-S), 2.35 (s, 3 H, S(O)CH_3), 1.46 (d, J_{HH}=6.70 Hz, 3 H, Ar-CH-CH_3), 1.33 (s, 3 H, C-*CH*$_3$), 1.15 (s, 3 H, C-*CH*$_3$), 1.01 (s, 3 H, C-*CH*$_3$), 0.66 (s, 3 H, C-*CH*$_3$). ^{13}C NMR (75 MHz, $CDCl_3$, δ) 195.32, 144.94, 135.85, 128.53, 126.90, 82.73, 59.74, 40.41, 33.34, 30.42, 23.56, 20.42, 17.29. HRMS-EI (m/z): $[M]^+$ calcd for $C_{20}H_{31}NO_2S$, 349.2076; found, 349.2052.

3.7.7 Preparation of nitroxide thiol 12

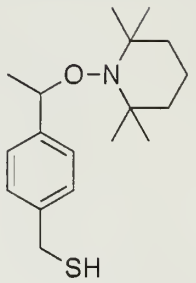

To a 50 mL round bottom flask was added LAH (0.4 g, 10 mmol) followed by THF (20 mL). The solution was cooled with an ice bath then nitroxide thioacetate **11** (2.8 g, 8 mmol) dissolved in THF (10 mL) was added drop wise. The reaction was stirred at room temperature and monitored by TLC until complete (15 minutes). The reaction was quenched with acetone, diluted with water (20 mL), and extracted with ether (3 x 50 mL). The organic layers were combined, dried with $MgSO_4$, and the solvent removed under reduced pressure giving the pure product as a colorless oil (2.3 g, 94 % yield). ^{1}H NMR (300 MHz, $CDCl_3$, δ) 7.21 (m, 4 H, Ar-*H*), 4.76 (q, J_{HH}=6.70 Hz, 1 H, Ar-C*H*-(CH_3)-O), 3.74 (d, J_{HH}=7.51 Hz, 2 H, Ar-CH_2-SH), 1.46 (d, J_{HH}=7.19 Hz, 3 H, Ar-CH-CH_3), 1.26 (s, 3 H, C-*CH*$_3$), 1.15 (s, 3 H, C-*CH*$_3$), 1.02 (s, 3 H, C-*CH*$_3$), 0.66 (s, 3 H, C-*CH*$_3$). ^{13}C NMR (75 MHz, $CDCl_3$, δ) 144.66, 139.49, 127.68, 126.88, 82.73, 59.68, 40.34, 29.29, 28.78, 23.56, 17.23. HRMS-EI (m/z): $[M+H]^+$ calcd for $C_{18}H_{30}NO_2S$, 308.2048; found, 308.1974.

3.7.8 Preparation of Thiol Nitroxide functionalized CdSe/ZnS Quantum Dot 13

TOPO covered CdSe/ZnS nanoparticles suspended in chloroform and thiol nitroxide **3** (400 mg) were stirred at room temperature for 24 hours. The nitroxide-functionalized particles were precipitated with methanol then centrifuged. The

supernatant was decanted and the particles redispersed in chloroform and the precipitation process repeated. A majority of the product dissolved in styrene for future polymerizations with a portion of the nanoparticles suspended in $CDCl_3$ for analytical analysis. ^{1}H NMR (300 MHz, $CDCl_3$, δ) 7.20, 4.71, 1.41, 1.19, 1.14, 0.96, 0.62.

3.7.9 General Procedure for the Preparation CdSe/ZnS-(PS-co-BCB) 14

Vinyl BCB **10** (0.3 g), styrene (0.2 g), and nitroxide functionalized CdSe/ZnS **13** in styrene (0.5 g) were added to a reaction tube equipped with a stir bar and N_2 inlet, purged with N_2, and subjected to three freeze-pump-thaw cycles. The mixture was heated at 125 °C for 12 h, allowed to cool, dissolved in THF, and precipitated into methanol. The product was recovered *via* filtration to afford a pale red powder (0.53 g, 53% yield). ^{1}H NMR (300 MHz, $CDCl_3$, δ) 7.12 (PS Ar-*H*), 6.71 (PS Ar-*H*), 3.10 (BCB CH_2-CH_2), 1.89 (PS C*H*), 1.46 (PS CH_2).

3.7.10 General procedure for removal of polymer from nanoparticle surface for molecular weight analysis.

25 mg of DMAP was added to 15 mg CdSe/ZnS-polymer product dissolved in THF (1 mL) then stirred at 50 °C for 24 hours. The solution was precipitated into methanol centrifuged for 10 minutes. The supernatant was decanted, and the residual white solid collected and dried by N_2 purge.

3.7.11 Preparation of Shell-cross-linked Quantum Dot 15

To a 3-neck round bottom flask equipped with magnetic stir bar, thermocouple adapter, reflux condenser, inlet adaptor, and addition funnel was added 1-octadecene (50 mL). CdSe/ZnS-(PS-*co*-BCB) composite material **14** (100 mg) was dissolved in 1,2,4-trichlorobenzene (20 mL) and added to the addition funnel. The system was degassed under vacuum for one hour, backfilled with argon, then the 1-octadecene heated to 240 °C. The CdSe/ZnS composite solution was added drop wise to the hot octadecene solution over 5 minutes, then stirred at 240 °C for an additional 40 minutes. After the reaction was cooled, the majority of the solvent was removed by Kugelrohr distillation (150 °C). The residue was dissolved in a minimal amount of chloroform, precipitated with methanol then centrifuged. The supernatant was decanted, and the shell cross-linked nanoparticles collected as a pale red solid (65 mg, 65% yield). ^{1}H NMR (300 MHz, $CDCl_3$, δ) 7.08 (PS Ar-*H*), 6.58 (PS Ar-*H*), 2.78 (CH_2-CH_2), 1.86 (PS C*H*), 1.44 (PS CH_2).

3.7.12 General Procedure for the Chemical Degradation Studies

The desired CdSe-polymer material (10 mg) was dissolved in chloroform (2 mL) followed by the addition of 1-octadecene (2.5 mL). The solution was transferred to a cuvette equipped with cap and stir bar and allowed to stir for 5 minutes. A solution of 4-dimethylaminopyridine (0.5 mL, 60 mg/mL) was added and the fluorescence spectrum (ex @ 450 nm) recorded immediately. The fluorescence intensity was monitored over 240 minutes.

3.8 References

(1) Zhang, Q.; Remsen, E. E.; Wooley, K. L. *J. Am. Chem. Soc.* **2000**, *122*, 3642-3651.

(2) Thurmound, K. B.; Kowalewski, T.; Wooley, K. L. *J. Am. Chem. Soc.* **1997**, *119*, 6656-6665.

(3) Thurmound, K. B.; Huang, H.; Clark, C. G.; Kowalewski, T.; Wooley, K. L. *Coll. Surf. B* **1999**, *16*, 45-54.

(4) Kang, Y.; Taton, T. A. *Angew. Chem. Int. Ed.* **2005**, *44*, 409-412.

(5) Harth, E.; Van Horn, B.; Lee, V. Y.; Germack, D. S.; Gonzales, C. P.; Miller, R. D.; Hawker, C. J. *J. Am. Chem. Soc.* **2002**, *124*, 8653-8660.

(6) Schlamp, M. C.; Peng, X. G.; Alivisatos, A. P. *J. App. Phys.* **1997**, *82*, 5837-5842.

(7) Peng, X. G.; Schlamp, M. C.; Kadavanich, A. V.; Alivisatos, A. P. *J. Am. Chem. Soc.* **1997**, *119*, 7019-7029.

(8) Wang, D.; He, J.; Rosenzweig, N.; Rosenzweig, Z. *Nano Lett.* **2004**, *4*, 409-413.

(9) Markoski, L. J.; Walker, K. A.; Deeter, G. A.; Spilman, G. E.; Martin, D. C.; Moore, J. S. *Chem. Mater.* **1993**, *5*, 248-250.

(10) Leiston-Belanger, J. M.; Russell, T. P.; Drockenmuller, E.; Hawker, C. J. *Macromolecules* **2005**, *38*, 7676-7683.

(11) Kirchhoff, R. A.; Bruza, K. J. *Prog. Polym. Sci.* **1993**, *18*, 85.

(12) Walker, K. A.; Markoski, L. J.; Moore, J. S. *Synthesis* **1992**, 1265-1268.

(13) Thomas, P. J.; Pews, R. G. *Synth. Commun.* **1991**, *21*, 2335-2340.

(14) Hong, R.; Fischer, N. O.; Verma, A.; Goodman, C. M.; Emrick, T.; Rotello, V. M. *J. Am. Chem. Soc.* **2004**, *126*, 739-743.

(15) Ruach-Nir, I.; Wagner, H. D.; Rubinstein, I.; Hodes, G. *Adv. Funct. Mater.* **2003**, *13*, 159-164.

CHAPTER 4

CADMIUM SELENIDE NANOPARTICLE-CONJUGATED POLYMER COMPOSITE MATERIALS

4.1 Rationale for CdSe-Conjugated Polymer Hybrid Materials

The dispersion of quantum dots in an electronically active matrix is expected to offer improved energy transfer between the matrix and quantum dot, by eliminating the inefficiencies of energy transfer associated with nanoparticle aggregation.[1-3] This chapter describes an approach taken to disperse CdSe nanoparticles in conjugated polymers. The method used here involves the direct functionalization of quantum dots with an electronically active ligand in a "graft-from" polymerization approach.

We chose initially to study poly(*p*-phenylene vinylene) (PPV) in conjunction with CdSe quantum dots. PPV is a conjugated polymer of interest for light emitting applications, since it is prepared readily by a number of polymerization techniques and exhibits an electroluminescence spectrum in the visible region of light.[4-10] The backbone can be modified with substitutents, such as phenyl, cyano, or alkyl ethers to change the band gap of the polymer.[11] Generally, electron donating groups reduce the band gap, red-shifting the fluorescence, while electron withdrawing groups widen the band gap, resulting in a photoluminescence blue shift.[5] To provide PPV with better solubility, di-*n*-octyl derivatives were prepared. Furthermore, CdSe nanoparticles blended PPV represented a majority of the quantum dot-conjugated polymer materials under investigation by a number of research groups, as discussed in Chapter 1.[12-16]

4.2 Growth of CdSe Nanoparticles in an Aryl Bromide Functionalized Ligand

The mild Heck coupling conditions described by Fu and coworkers[17] appeared attractive for use in conjunction with quantum dots. Palladium-catalyzed Heck couplings proceed effectively for aryl bromides and vinyl aromatic derivatives to give stilbene and substituted stillbenes. When applied to polymerization strategies. this coupling method can be used to afford PPV.[10,18]

Aryl bromide functionalized phosphine oxide **18** was prepared in 72 % overall yield according to **Scheme 14**.[19] Benzyl chloride **17** was prepared in 87 % yield from 4-bromobenzyl alcohol **16**. Nucleophilic substitution of di-*n*-octylphosphine oxide[20] on 4-bromobenzyl chloride **17** afforded the desired phosphine oxide ligand **18** in 85 % yield. Compound **18** was crystallized from hexanes and found to be 99.6% pure by high performance liquid chromatography in acetonitrile. The benzyl methylene group was seen as a doublet at δ 3.05 ppm in the ^{1}H NMR spectrum. High-resolution mass spectrometry confirmed the expected molecular weight (calcd 443.2078, found 443.2080). 4-Bromobenzyl chloride was preferred over 4-bromobenzyl bromide for the ligand synthesis since a large percentage of P-alkylation was observed during the nucleophilic substitution reaction with 4-bromobenzyl bromide.

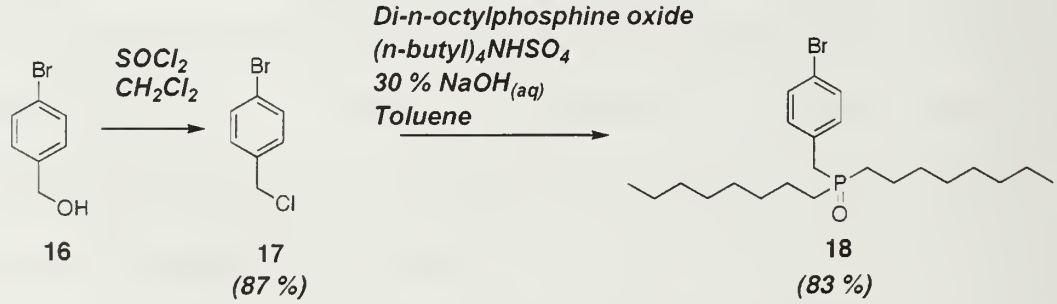

Scheme 14. Synthesis of aryl bromide phosphine oxide 18 from 4-bromobenzyl alcohol 16.

In experiments performed with Habib Skaff, ligand **18** was found to exhibit excellent thermal stability, a necessary property for application of new ligands to quantum dot syntheses performed at high temperatures. When compound **18** was used in place of TOPO (**Scheme 15**) in standard quantum dot synthesis.[21] aryl bromide functionalized, spherical CdSe nanocrystals **19** were obtained. Quantum dots prepared in aryl bromide ligand **18** were found to exhibit optical (UV/Vis and fluorescence) properties essentially identical to the traditional preparation in TOPO.

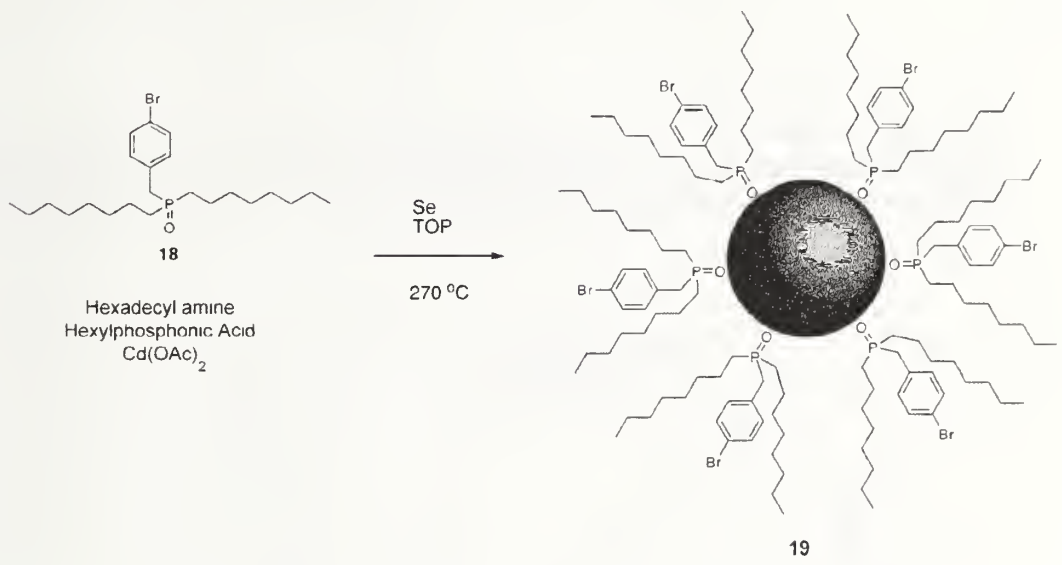

Scheme 15. The growth of aryl bromide functionalized CdSe quantum dots 19 in functional ligand 18.

Figure 28A shows a transmission electron microscopy (TEM) image of a typical sample of **18**-covered quantum dots. In addition, high-resolution TEM (**Figure 28B**) shows lattice planes, and electron diffraction reveals the crystalline nature of these materials (**Figure 28B inset**). UV-Vis and photoluminescence spectrophotometer confirmed the quantum confined nature of the particles and a chloroform solution quantum yield of 65% (**Figure 29**).[22]

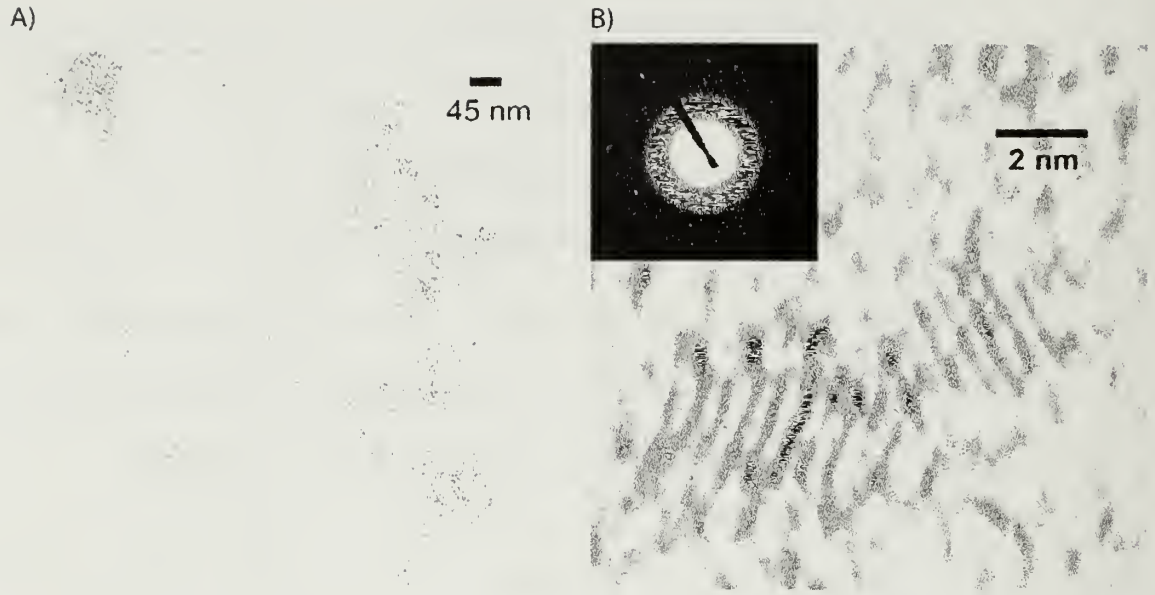

Figure 28. Transmission electron micrographs at A) 66,000 magnification and B) 600,000 magnification of functionalized CdSe nanoparticles 19. The electron diffraction pattern for these quantum dots is shown as the inset of panel B.

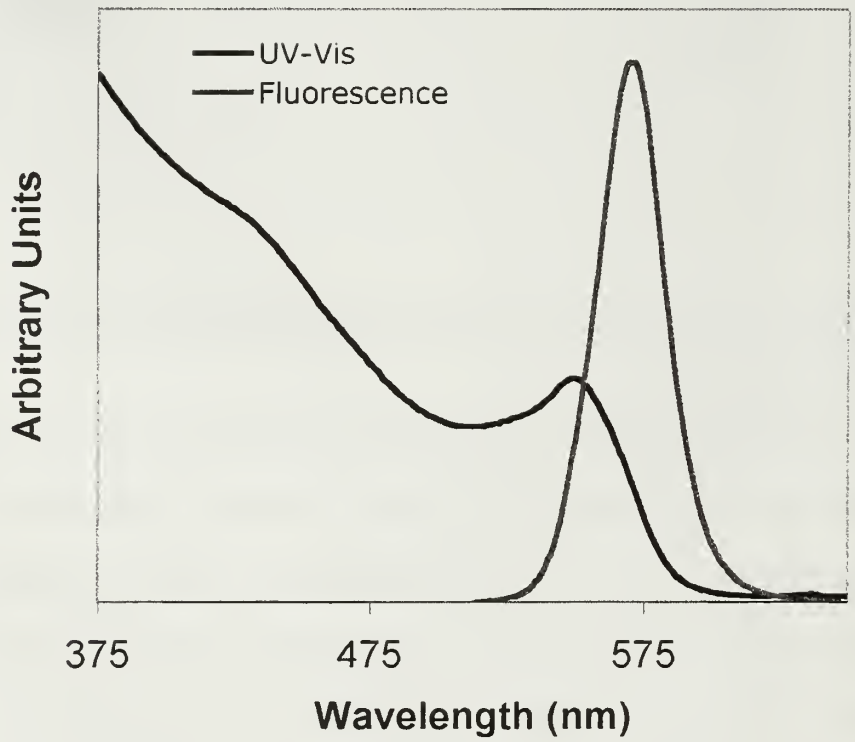

Figure 29. Solution state fluorescence spectrum (red curve) and UV-Vis absorption spectrum (blue curve) for aryl bromide functionalized quantum dots 19.

The aryl bromide ligand coverage was confirmed by ^{1}H NMR spectroscopy, as all resonances from **18** were present in the spectrum of **19**. ^{31}P NMR showed two resonances with a signal at δ 48.71 ppm corresponding to phosphorus of the functional ligand, while the phosphorus from TOPO (the oxidation product of TOP) appeared as a singlet at δ 46.08 ppm. Further analysis of the ^{1}H and ^{31}P NMR spectra for the aryl bromide functionalized CdSe **19** revealed the relative amounts of the ligands on the nanoparticle suface. Quantitiative ^{31}P NMR revealed that near equal amounts of aryl bromide **18** and TOPO were present. Using this information during the assignment of the ^{1}H NMR spectrum and integrations, it can be calculated that the aryl bromide phosphine oxide ligand **18** comprises ~ 33% of the ligands on the quantum dot surface, with ~ 33% tri-*n*-octyl phosphine oxide and ~ 33% hexadecylamine accounting for other surface ligands. This synthesis represented the first direct preparation of quantum dots containing functionalized ligands, where the functionality is obtained without the need for ligand exchange chemistry. Eliminating the ligand exchange step was found to be beneficial in the preparation of CdSe-PPV hybrid materials, in which surface oxidation that often accompanies ligand exchange would significantly hinder energy transfer events, and diminish photoluminescence quantum yield. For example, CdSe-PPV composite materials prepared with functional CdSe **19** obtained by ligand exchange of ligand **18** on TOPO CdSe exhibited properties similar to blended materials, rather than the unique properties discussed later in this chapter.

4.3 Monomer Synthesis for Heck Coupling Polymerizations from Aryl Bromide Functionalized CdSe Nanoparticles

4.3.1 Dibromo and Divinylbenzene Derivatives for the $A_2 + B_2$ Polymerization of Poly(p-phenylene vinylene)

Initial graft-from polymerization to prepared quantum dot-PPV composites, performed together with Habib Skaff, involved $A_2 + B_2$ Heck coupling of divinylbenzene and dibromobenzene derivatives to with aryl bromide-covered quantum dots.[18] 1,4-Divinyl-2,5-di-*n*-octylbenzene **23** was prepared according to **Scheme 16**. A Kumada coupling[23] of *n*-octyl magnesium bromide with *p*-dichlorobenzene **20** gave *p*-di-*n*-octylbenzene **21** in 85 % yield. Stirring compound **21** with bromine in the presence of catalytic iodine, with the exclusion of light, gave 1,4-dibromo-2,5-di-*n*-octylbenzene **22**, an A_2 monomer, in 92 % yield following purification by crystallization from ethanol.[23] Dibromide **22** was utilized in a Stille coupling[24] with tri-*n*-butyl vinyl tin to give the B_2 monomer, 1,4-divinyl-2,5-di-*n*-octylbenzene **23**, in 95 % yield after column chromatography on silica gel. The purity and identity of **23** was verified by ^{1}H NMR spectrometry, as the characteristic vinylic resonances were found at δ 6.94, 5.64 and 5.25 ppm, and a singlet representing the two identical aryl protons was found at δ 7.24 ppm, shifted downfield slightly from δ 7.35 ppm in dibromide **22**.

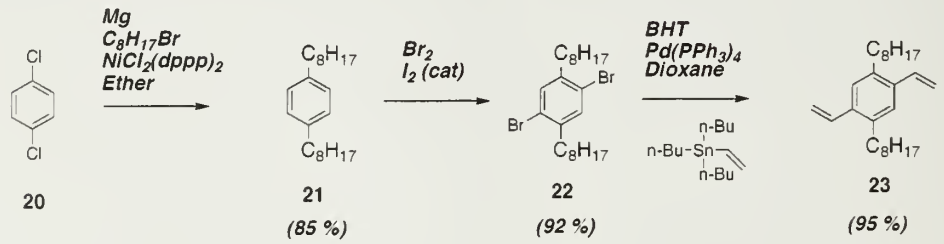

Scheme 16. Synthesis of A_2 monomer 1,4-dibromo-2,5-di-*n*-octylbenzene 22 and B_2 monomer 1,4-divinyl-2,5-di-*n*-octylbenzene 23.

4.3.2 Vinyl Bromide Derivatives for the AB Polymerization of Poly(*p*-phenylene vinylene)

The preparation of vinyl bromide derivatives for use as AB monomers, as shown in **Scheme 17**, represents an important improvement over the original synthesis of the PPV-quantum dot composite materials. The use of AB monomers eliminates the dependence on the demand for precise stoichiometric balance inherent in A_2+B_2 step growth polymerization.[25] Due to the small size scale of typical polymerizations (25-100 milligram quantities of monomer), and the difficulty associated with quantifying the number of aryl bromide equivalents on the quantum dot surface, it is advantageous to eliminate this need for stoichiometric balance.

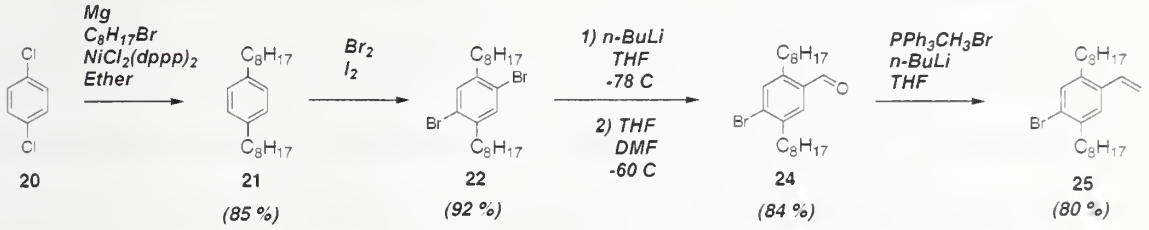

Scheme 17. Synthesis of AB monomer 4-bromo-2,5-di-*n*-octylstyrene 25 for the polymerization of PPV.

The synthesis of AB monomer **25** began with lithium-halogen exchange on 1,4-dibromo-2,5-dioctylbenzene **22** to give the mono-lithiated intermediate, as shown in **Scheme 17**.[26] This mono-lithium salt was quenched with dimethylformamide to give 4-bromobenzaldehyde **24** in 84 % yield following crystallization from ethanol to remove any dialdehyde or diaryl methanol side products. Wittig chemistry using **24** with methyl triphenylphosphonium bromide gave 1-bromo-2,5-di-*n*-octyl-4-vinylbenzne **25** in 80 % yield following crystallization from methanol. AB monomer **25** was characterized by ^{1}H NMR spectroscopy, which showed an aryl proton resonance at δ

7.30 and vinyl proton resonances at δ 6.88, 5.63, and 5.29 ppm. High-resolution mass spectrometry (calcd. 406.2235 g/mol, found 406.2201) verified the expected molecular weight of the product. Control polymerizations of monomer **25,** in the absence of quantum dots, were performed to give 30,000 g/mol poly(phenylene vinylene). These control polymerization were performed with 0.5 % $Pd(OAc)_2$ catalyst in DMF at 150 °C for 24 h. This high degree of polymerization (DP ~ 90) confirms the high purity of the monomers.[18,27]

Bunz and coworkers have applied a similar synthetic approach in the synthesis of 4-propynyl styrene derivatives[28] (**Scheme 18A)** for the preparation of poly(phenyleneethynylene-*alt*-phenylenevinylene). Others have utilized a Heck coupling between dibromobenzene derivatives and ethylene to afford di-substituted 4-bromostyrenes[29] (**Scheme 18B**), while Lahti and coworkers have employed multiple chemoselective steps[27] in the synthesis of mono-substituted 4-bromostyrene derivatives, as illustrated in **Scheme 18C**. Our preparation of monomer **3** represents a novel approach for the preparation of substituted aromatic vinyl bromides in four steps from commercially available material in 22 and 53% overall yield. The synthetic scheme presented here was readily scaled to more than 10 grams of monomer, yet still maintained the high purity required for condensation polymerization without the need for column chromatography.

A)

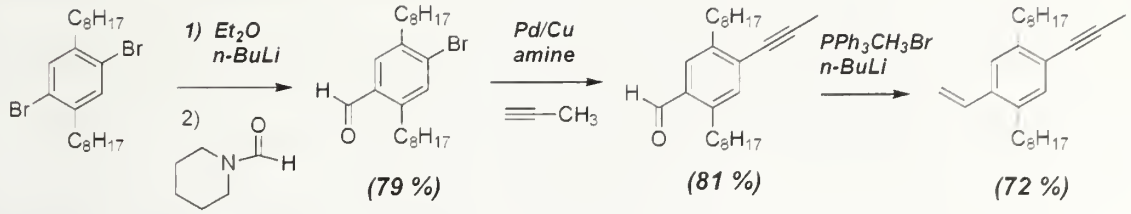

Brizius, G.; Pschirer, N. G.; Steffen, W.; Stitzer, K.; zur Loye, H. C.; Bunz, U. H. F. *J. Am. Chem. Soc.* **2000**, *122*, 12435-12440.

B)

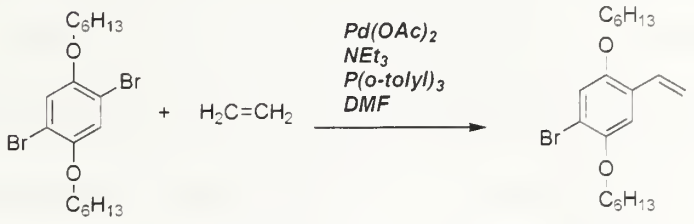

Detert, H.; Sugiono, E. *J. Prakt. Chem.* **1999**, *341*, 358-362.

C)

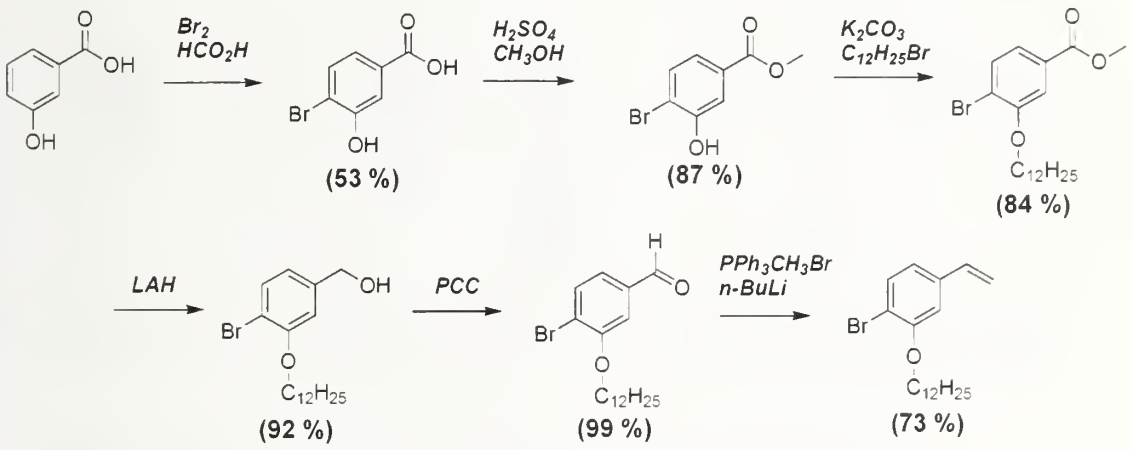

Pasco, S. T.; Lahti, P. M.; Karasz, F. E. *Macromolecules* **1999**, *32*, 6933-6937.

Scheme 18. Previous synthetic routes for the preparation of substituted 4-bromostyrene derivatives.

4.3.3 Vinyl-Bromide Derivatives for the Preparation of Poly(arylene vinylene)s

The synthesis in **Scheme 17** was readily adaptable to other AB monomers, such as 1-bromo-2,5-bis-octyloxy-4-vinylbenzene **30**, shown in **Scheme 19**. 1,4-Bis-*n*-octyloxybenzene **27** was prepared by Williamson ether synthesis of hydroquinone **26** and *n*-octylbromide in 60 % yield following recrystallization from ethanol.

Bromination of **27** was achieved in 66 % yield to give 1,4-dibromo-2,5-bis-octyloxy-benzene **28,** which was then converted to 4-bromo-2,5-bis-octyloxy-benzaldehyde **29**. This lithium-halogen exchange reaction and subsequent quenching with DMF proceeded as above, to give **29** in 79 % yield following crystallization from methanol. Again, a Wittig reaction of **29** with methyl triphenylphosphonium bromide afforded1-bromo-2,5-bis-octyloxy-4-vinylbenzene **30** in 57 % yield, with an overall yield of 22 %. ^{1}H NMR spectroscopy of monomer **30** showed vinylic resonances at δ 6.97, 5.72 and 5.27 ppm, and aryl resonances at δ 7.04 and 7.01 ppm. A high-resolution mass spectrometry signal at 438.2170 m/z confirmed the expected molecular weight of 438.2133 m/z for monomer **30**.

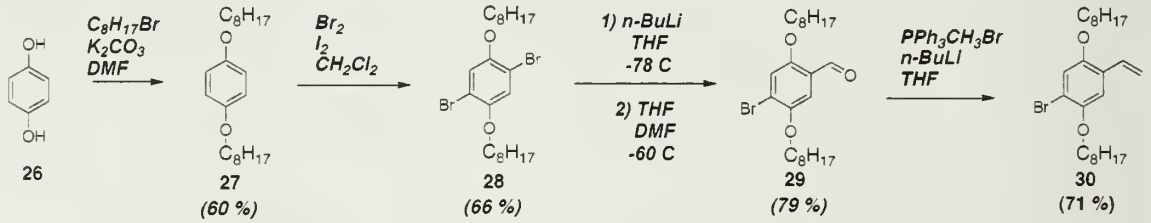

Scheme 19. Synthesis of AB monomer 4-bromo-2,5-bis-octyloxystyrene 30 for the polymerization of oxyPPV.

This approach can also be extended to carbazole derivatives, illustrated in **Scheme 20**. Polymers containing these groups typically exhibit excellent hole-transport properties and possess fluorescence emission spectra in the blue region of light.[30-32] It was initially hypothesized that these two characteristics would lead to more efficient energy transfer from the polymer to the quantum dot due to excellent overlap of the polymer emission with the absorbtion of the CdSe nanoparticle for Förster energy transfer and the ability of the carbazole to transfer holes away from the CdSe surface. Alkylation of 3,6-dibromocarbazole **31** with dodecyl bromide gave N-dodecyl-3,6-

dibromocarbazole **32** in 87 % yield. Carbazole **32** was stirred with *n*-butyl lithium at -78 °C (dry ice/acetone bath), then quenched with DMF to yield N-dodecyl-3-bromo-6-carbaldehydecarbazole **33**. In contrast to the benzene derivatives, characterization of the crude product by thin layer chromatography (TLC) and ^{1}H NMR spectroscopy revealed a small amount of starting material and dialdehyde carbazole. Compound **33** was isolated in 76 % yield following purification by column chromatography on silica gel followed by crystallization from methanol. The conversion of **33** to the N-dodecyl-3-bromo-6-vinylcarbazole **34** was accomplished under standard Wittig conditions in 80 % yield. The reaction was monitored by TLC, and the product purified by crystallization from ethanol. Overall, the synthesis of AB vinyl bromides by this method proved rapid and effective, and may be adaptable to a variety of other derivatives.

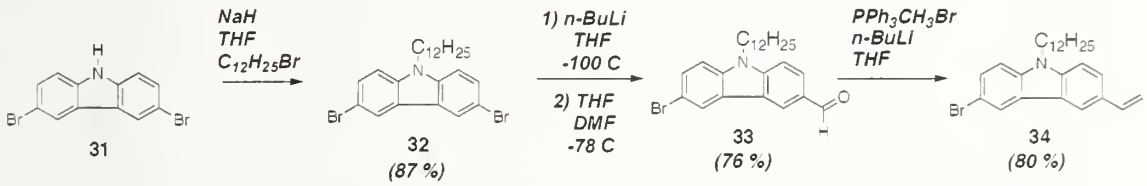

Scheme 20. Synthesis of AB monomer N-dodecyl-3-bromo-6-vinylcarbazole 34 for the polymerization of PKV.

4.4 Heck Coupling Polymerizations from Aryl Bromide Functionalized CdSe Nanoparticles

PPV-quantum dot composites were synthesized under palladium-catalyzed Heck coupling conditions in the presence of aryl bromide covered quantum dots **19**. A tetrahydrofuran solution of **19** was stirred at 50 °C for 24 hours in the presence of 1,4-di-*n*-octyl-2,5-divinylbenzene **22** and 1,4-dibromo-2,5-di-*n*-octylbenzene **23**, as well as

tris(dibenzylideneacetone)dipalladium ($Pd_2(dba)_3$), tri-*t*-butylphosphine, and N-methyldicyclohexylamine according to **Scheme 21**. The CdSe-PPV hybrid **35** was isolated by precipitation into methanol, which removed the Pd catalyst, base, and short chain oligomers of PPV. The quantum dot-PPV composite could be redissolved in many common organic solvents due to the solubilization provided by the alkyl chains on the PPV backbone.

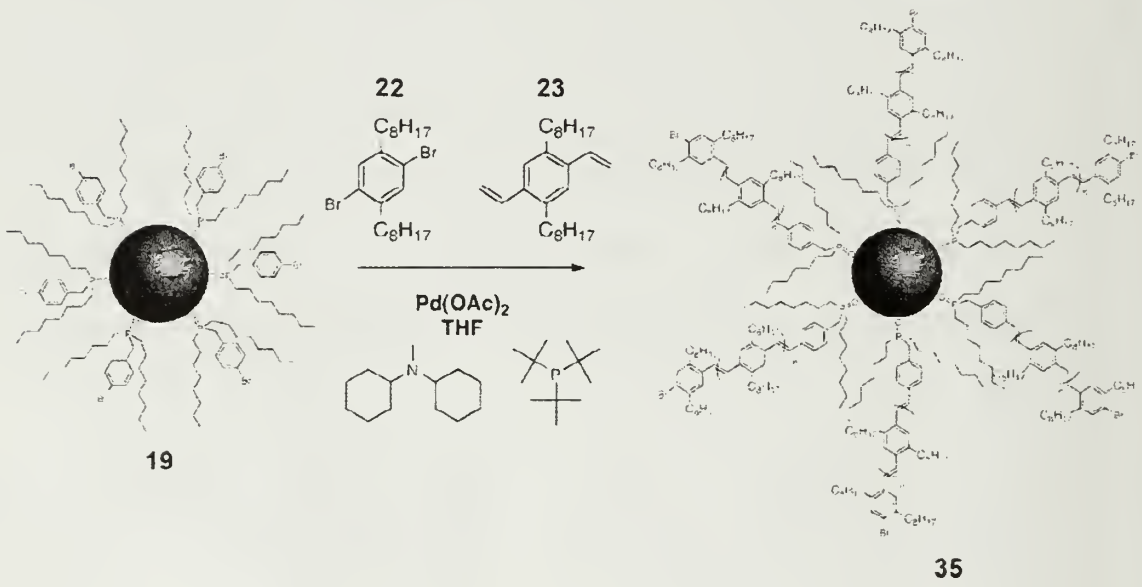

Scheme 21. The A_2+B_2 condensation polymerization of 22 and 23 from functional CdSe 19 for the preparation of CdSe-PPV 35.

Evidence of successful polymerization was shown by ^{1}H NMR spectroscopy of **35** where singlet resonances at δ 7.33 and 7.23 ppm were observed, corresponding to aromatic and vinylic resonances in the PPV backbone. The expected outcome of this polycondensation is a mixture of PPV connected to the quantum dots, and "free" or unconnected PPV that helps provide a matrix for the quantum dot-PPV material. Matrix assisted laser desorption ionization time-of-flight (MALDI-TOF) mass spectrometry gave molecular masses corresponding to PPV oligomers with and without phosphine oxide end groups. Importantly, quantum dot degradation was not observed

by UV/Vis, fluorescence, or TEM. Optical and morphological characterization of these materials is discussed later in the chapter.

While this method proved effective for the preparation of CdSe-PPV hybrid material **35**, improvement was desired in terms of PPV molecular weight control and reduction or elimination of palladium black impurities generated during the composite synthesis. Only lower oligomers were obtained in the A_2+B_2 polymeriation, and the use of higher amounts of catalyst (greater than 2 mg catalyst per 10 mg CdSe), designed to increase the degree of polymerization, proved ineffective. The higher catalyst loading resulted in nanoparticle degradation, as evidenced by the disappearance of the band-edge adsorption peak in the UV-Vis spectrum. Thus, AB monomer **25** was chosen to eliminate the stoichiometric dependence on molecular weight inherent in A_2+B_2 condensation polymerizations.

Improved conditions were also needed to suppress palladium black formation during the grafting-from polymerization reaction (**Figure 30**).[33,34] The formation of palladium black is characterized by the appearance of a red-black color in solution and the appearance of a broad absorption spectrum with a peak around 450 nm. This impurity can be removed by centrifugation, but suppressing its formation is far more desirable.

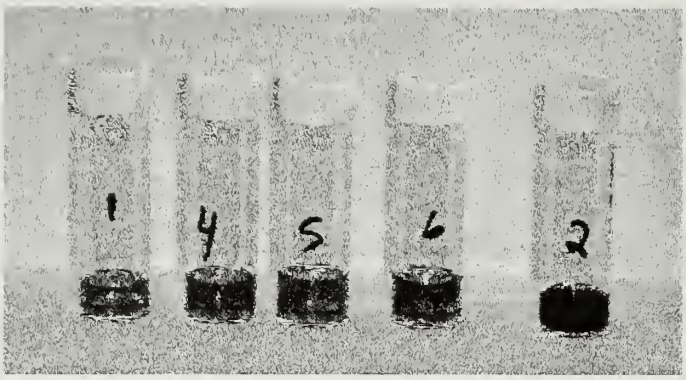

Figure 30. A photograph illustrating successful preparation of 35 (vials 4-6) and a polymerization that resulted in a large amount of palladium black (vial 2). Vial 1 represents the CdSe starting material 19.

For the optimization experiments described below, conjugated polymers were grafted from aryl bromide functional CdSe nanoparticles according to **Scheme 22**. Monomer **25**, N-methyldicyclohexylamine, aryl bromide CdSe nanoparticles **19**, palladium catalyst, and solvent were added to a heavy-walled reaction tube, equipped with a stir bar and Teflon valve, in a nitrogen atmosphere dry-box. The solutions were then stirred at room temperature to 120 °C for 12 to 48 h. Centrifugation of the cooled reaction solutions for 30 minutes at 3000 rpm removed insoluble material (*e.g.* palladium black or precipitated CdSe). The clear, red solutions were decanted and the composite material was precipitated with anhydrous methanol. The cloudy solutions were centrifuged for ca. 5 minutes then the light yellow supernatant decanted and the red precipitate was immediately redispersed in dry THF. Care must be taken to perform the precipitation as quickly as possible since the diminishment of the quantum dot's optical properties has been observed when the precipitated composites are stored an unnecessarily long time in the methanol solution. The CdSe-PPV composite in the precipitate was dissolved in THF for storage as a solution.

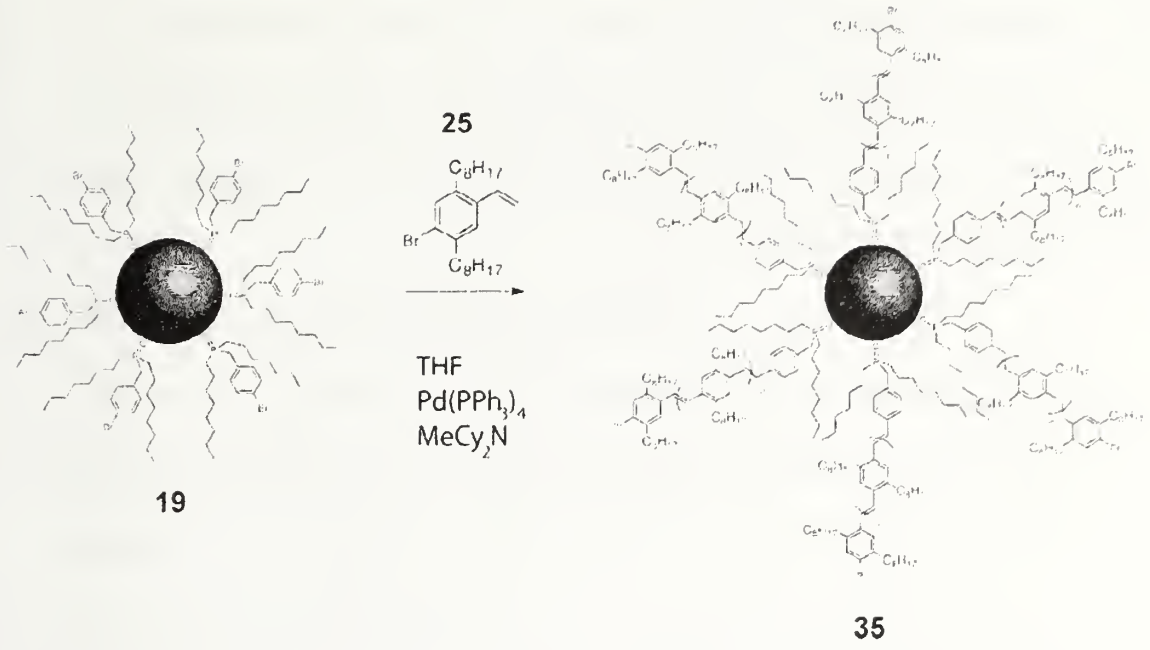

Scheme 22. The AB condensation polymerization of 25 from functional CdSe 19 for the preparation of CdSe-PPV 35.

The choice of palladium catalyst proved to be critically important to the success of these Heck-coupling polymerizations from aryl bromide-covered CdSe quantum dots **19**.[34] A balance must be found between the need for the highly active catalyst necessary to achieve the high monomer conversion required for an appreciable degree of polymerization without affecting the CdSe surface. It is spectulated that the palladium catalyst could compete with the nanoparticle for its phosphine oxide ligands, resulting in vacant cadmium atoms on the CdSe surface and subsequent oxidation. Our initial studies used a technique described by Fu and coworkers,[17] involving the *in situ* formation of bis(tri-*t*-butylphosphine)palladium (0) from tris(dibenzylidene acetone)dipalladium (II) and tri-*t*-butylphosphine. Optimization of the palladium catalyst explored the use of various ligands to facilitate the *in situ* formation of the Pd (0) active catalyst. No significant improvement in terms of nanoparticle stability during polymerization, as judged by a reduction or elimination of the quantum dot's band edge

absorption blue shift relative to the native aryl bromide CdSe, or an increase in PPV molecular weight was observed following the use of triphenylphosphine, tri-*o*-tolylphospine, bis(diphenylphosphino) ethane (DPPE), or bis(diphenylphosphino) propane (DPPP)) with Pd_2dba_3.

The preparation of CdSe-PPV composites was found to work better using tetrakis(triphenylphosphino)palladium ($Pd(PPh_3)_4$) as the source of Pd(0). The use of a preformed Pd(0) catalyst eliminates the side reactions associated with reduction of Pd(II) to Pd(0).[33,35] Conditions were optimized through a series of trial-and-error experiments to finally settle on the use of 2 mg ($Pd(PPh_3)_4$) per 10 mg of aryl bromide functionalized CdSe nanoparticles. This gave composites with higher degrees of polymerization without the formation of palladium black. Higher catalyst loadings resulted in a change of the bright red reaction solution to a dark red/black color and the appearance of a broad signal (400 – 900 nm) in the UV-Vis spectrum, indicating palladium black. Again, the introduction of additional phosphine ligands (e.g. PPh_3 or DPPE) served only to limit the molecular weight of the PPV grafted from the surface.

The success of $Pd(PPh_3)_4$ as the catalyst for these graft-from polymerizations left only optimization of reaction conditions such as temperature, solvent, and time. Higher reaction temperatures (e.g. 90 °C instead of 45 °C) resulted in higher degrees of polymerization. Higher DP is indicated by the red shift of the solution state fluorescence peak maxima from ~ 360 nm (PPV tetramer on average) for polymerizations at 45 °C to ~ 390 nm (PPV hexamer on average) for polymerizations at 90 °C. Moreover, the presence of higher oligomers in the composite is confirmed in the

MALDI-TOF spectrum, as oligomers from dimers to nonamers were detected, with hexamers representing the most probable oligomer, as shown in **Figure 31**.

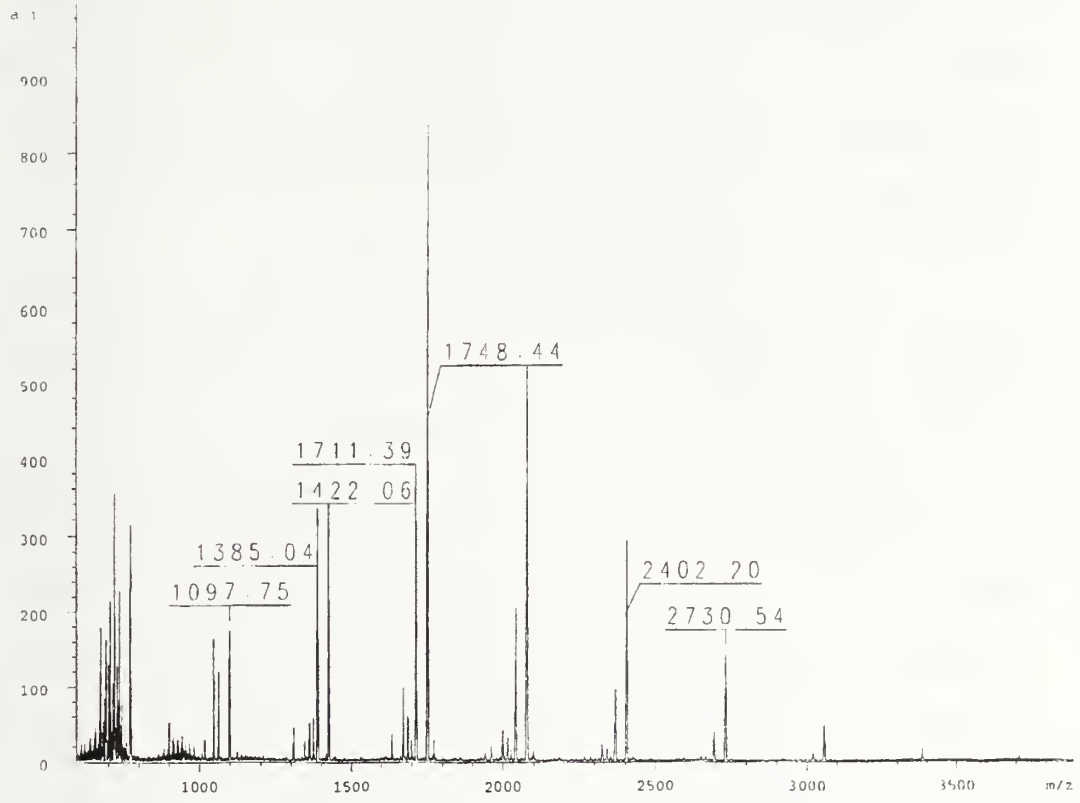

Figure 31. MALDI mass spectrum of PPV oligomers grafted from CdSe using optimized polymerization conditions. (1097, dimer; 1422, trimer; 1748, tetramer; 2076, pentamer; 2402, hexamer; 2730, heptamers; 3058, octamer; 3386, nonamer.)

Unfortunately, nanoparticle degradation was observed at temperatures above 90 °C, accompanied by the production of palladium black. The use of polar solvents such as DMF or dioxane, known to give faster reaction rates in Heck couplings,[34] resulted in either degradation of the quantum dot or an increase in palladium black formation. The use of less polar solvents, such as toluene or xylenes, was not effective in preparing the CdSe composite materials due to the formation of large amounts of palladium black, a the consequence of the lack of stabilization of the reactive intermediate within the catalytic cycle that is associated with polar solvents. Therefore, THF remained the

solvent of choice and is currently the only solvent known to be useable for the preparation of the CdSe-conjugated polymer composite materials by the graft-from method. Samples can be successfully stored in a nitrogen-purged THF solution in the dark with little or no degradation of optical properties for approximately two months. For comparison, identical storage conditions in toluene afford stable solutions for 1-2 weeks, while storage in chloroform leads to precipitation within a few days.

Optimization of conditions for growth of monomer **25** from quantum dots led to efforts to extend the technique to other monomers to give composites **36** (CdSe-oxyPPV) and **37** (CdSe-PKV), as shown in **Scheme 23.** Typical preparations of these composites were conducted on THF solutions of ~150 mg of monomer **30** or **34**, 10 mg phenyl bromide-functionalized CdSe nanoparticles, 2 mg $Pd(PPh_3)_4$, 100 mg N-methyldicyclohexylamine, stirred in a sealed vial under $N_{2(g)}$ for 16 h, and purified as described above for PPV-CdSe composite **35**. Typical ^1H NMR spectra of CdSe-oxyPPV **36** composites in $CDCl_3$ showed signals at δ 7.52 - 7.47 ppm and δ 7.17 ppm, corresponding to the aryl and vinyl protons, respectively. End-group analysis, performed by integrating backbone aromatic protons against alkyl protons (alkyl side chain and alkyl phosphine oxide), revealed an average degree of polymerization of ~4. In CdSe-PKV composite **37**, a broad signal in the ^1H NMR spectrum extending from δ 8.5-6.5 ppm of confirmed the presence of poly(carbazole vinylene), and end-group analysis (backbone aromatic protons against alkyl protons) also revealed a degree of polymerization of ~4. The characterization of these materials will be discussed later in the text.

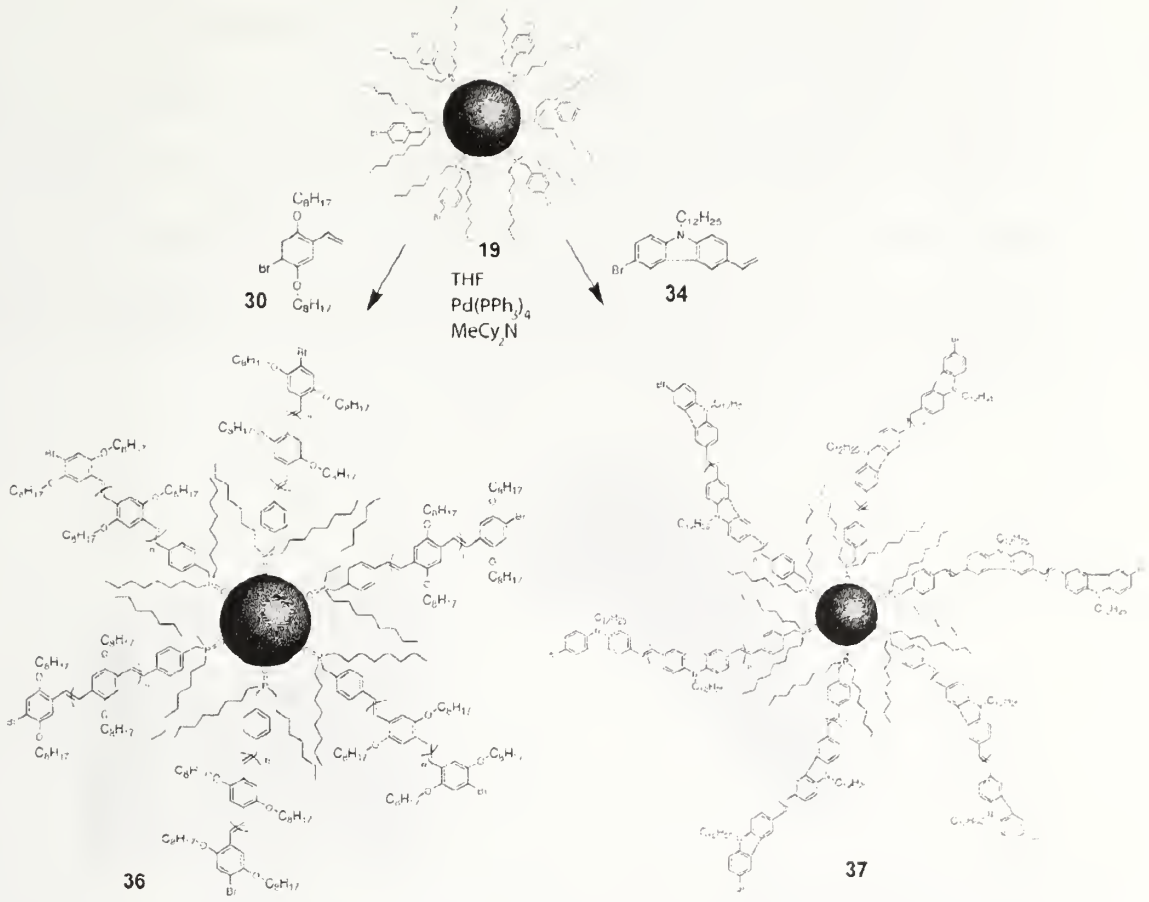

Scheme 23. The AB condensation polymerization of 30 from functional CdSe 19 for the preparation of CdSe-oxyPPV 36 and the polymerization of 34 for the preparation of CdSe-PKV 37.

4.5 Characterization of Cadmium Selenide-Conjugated Polymer Composites

4.5.1 Transmission Electron Microscopy of Composite and Blended Materials

Examples of aggregation common in nanoparticle blends are illustrated in **Figure 32A** and **Figure 32B**. These TEM images are representative of 5 wt % aryl bromide functionalized CdSe **19** or pyridine-functionalized CdSe **4** blended with oligomeric PPV (oligoPPV) prepared with monomers **22** and **23** with a DP ~ 4. In both cases, nanoparticle aggregation dominates the composite morphology. The TEM image of CdSe-PPV hybrid **35** (**Figure 32c**) reveals a drastically different morphology, as the

quantum dots are well-dispersed throughout the film. Composite **36** (**Figure 32d**) shows excellent dispersion in the substituted PPV matrix. TEM images of composite CdSe-PKV **37** (**Figure 32e**) show some clustering of particles, yet this clustering is rather minor relative to the gross aggregation found in blended samples. The dispersion that results from the graft-from technique is a consequence of the ligand terminated PPV attached to the nanoparticle.

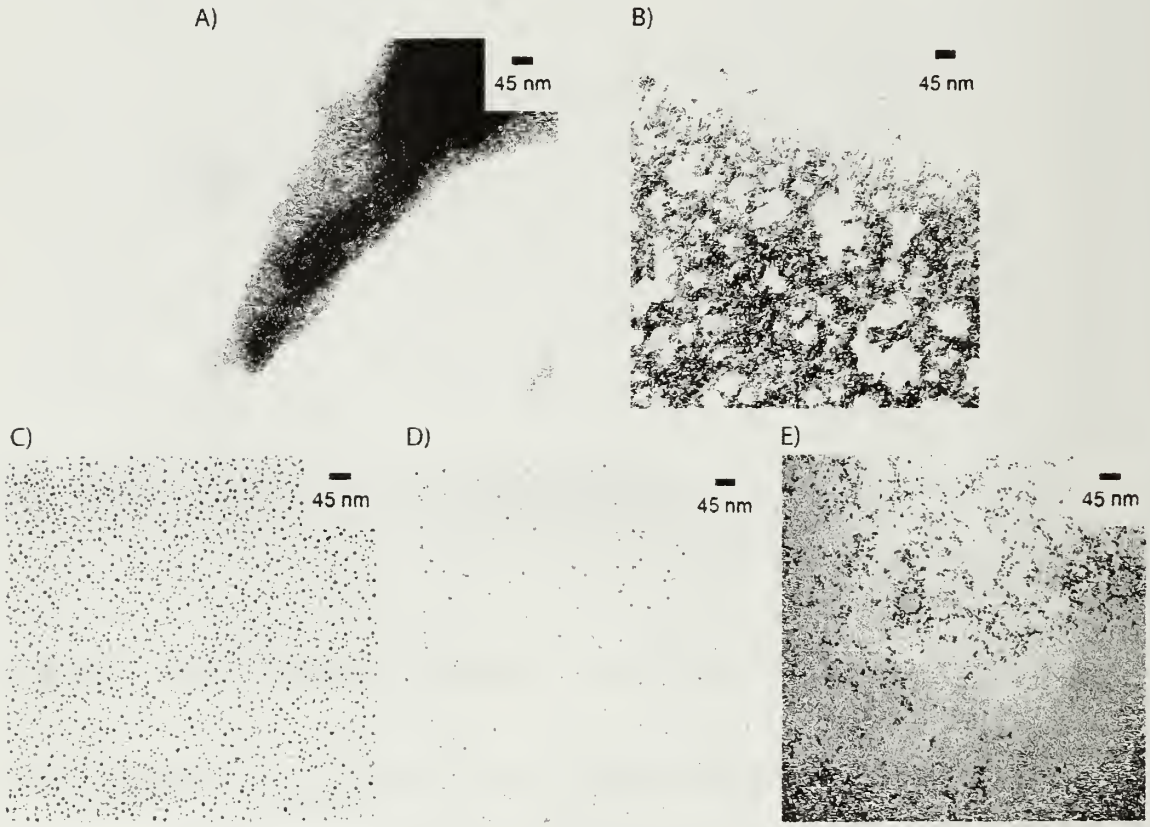

Figure 32. Transmission electron micrographs at 66,000 magnification of A) CdSe-DOPO-Br 19 blended with oligoPPV, B) pyridine covered CdSe 4 blended with oligoPPV, C) CdSe-PPV hybrid material 35, D) CdSe-oxyPPV 36, and E) CdSe-PKV 37.

4.5.2 Solution and Solid State Fluorescence Spectroscopy of Composite and Blended Materials

In the solid-state photoluminescence spectra of the CdSe nanoparticles blended with oligoPPV, high loadings of quantum dots are required to observe their solid-state fluorescence emission. This is illustrated in **Figure 33** for blends that utilize 10, 30, and 50 wt. % quantum dots in oligoPPV. In these blends, emission from oligoPPV dominates the photoluminescence spectrum, even at 50 wt %. Nanoparticle aggregation limits interfacial contact between polymer and quantum dots, and thereby precludes efficient energy transfer pathways. Moreover, this nanoparticle aggregation also leads to self-quenching of nanoparticle fluorescence. Another comparison of the CdSe nanoparticle-oligoPPV blend is shown in **Figure 34A**, where solution and solid-state photoluminescence of 5 wt % aryl bromide functionalized CdSe nanoparticles **19** blended with PPV are depicted. Again, both spectra are dominated by emission from PPV.

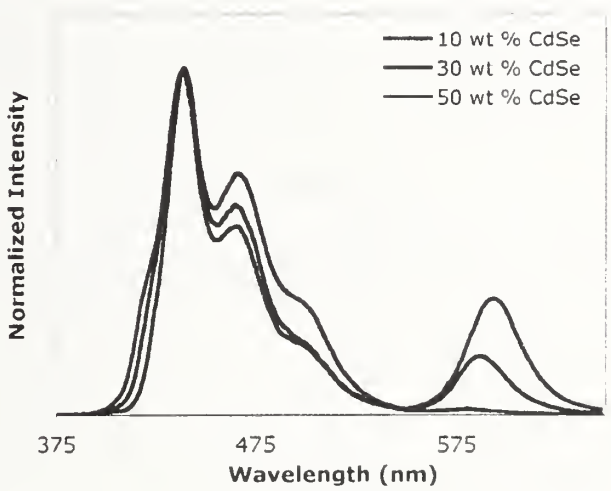

Figure 33. Solid state fluorescence emission spectra for blends of PPV with varying percentages of CdSe-DOPO-Br 19.

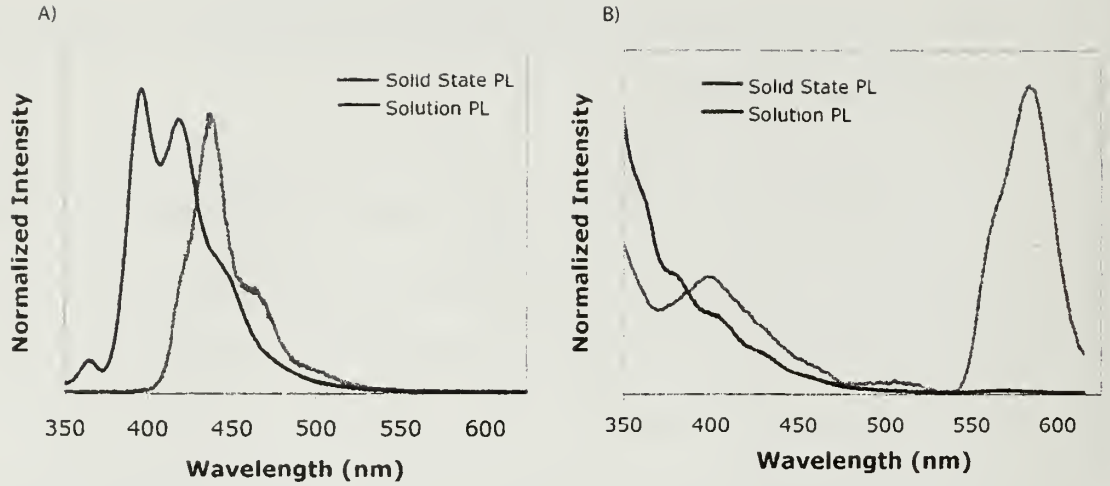

Figure 34. Solution (red curve) and solid-state (blue curve) fluorescence emission spectra for a) CdSe 19 blended with PPV and b) CdSe-PPV hybrid material 35 prepared with the A_2+B_2 approach.

In contrast to the oligoPPV-quantum dot blends, CdSe-PPV composite **35** was found to possess very different solid-state fluorescence spectra, as illustrated in **Figure 34B**. In dilute solution, PPV oligomers dominate the photoluminescence emission profile, and only a small fluorescence contribution from the quantum dots is seen. Conversely, in the solid-state, the photoluminescence emission spectrum is dominated by the quantum dots, with an almost complete quenching of PPV. Loss of PPV fluorescence in the solid-state, and emergence of a strong quantum dot emission, is observed even in cases of very low quantum dot loading (2-5 wt. %). This stands in contrast to the high weight loadings (50% or greater) typically used in quantum dot-conducting polymer composites. While the quantum yield of PPV is expected to diminish by self-quenching mechanisms in going from solution to the solid state, this alone does not explain the spectra of **Figure 34B**. However, this observation can be rationalized by the increased contact between PPV and quantum dots in the solid state relative to the more extended conformation of PPV around the dots in solution.

Photoluminescence emission from the quantum dots in the solid state is most pronounced in the composite materials. It is important to note that composite materials prepared by the ligand exchange reaction shown in **Scheme 24** were significantly different materials than those prepared by the "graft-from" method. While the products are expected to be very similar in chemical composition. the method of preparation has a profound impact upon the properties. These "graft-to" composites exhibited fluorescence profiles identical to blended materials and irreversible sedimentation of the nanoparticles was observed after 24-48 hours.

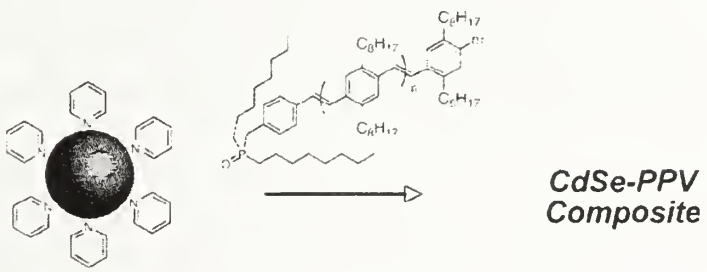

4

Scheme 24. Preparation of CdSe-PPV composite materials through ligand exchange chemistry.

A substantial increase in the CdSe fluorescence emission relative to the emission from PPV was observed following the use of optimized reaction conditions (**Figure 35**). The optimized polymerization conditions yield an increase the length of the PPV grafted from the nanoparticles, as shown by MALDI mass spectrometry of CdSe-PPV prepared using optimized conditions (**Figure 31**) and a red shift in the solution state fluorescence peak maxima to 393 nm (from the previous value of 340 nm). An explanation for these results can be found in the analysis of the energy levels for each of the separate components, illustrated in **Figure 36**. It is important to note that **Figure 36** represents an idealized case where discrete lines are drawn to represent a mixture of

polymer molecular weights and quantum dot sizes, corresponding to a range of band gaps. The ionization potential (IP) and electron affinity (EA) values are reported for fully conjugated polymers; therefore, a symmetric decrease in IP and increase in EA would be expected for oligomers that have not reached full conjugation.[11] However, the band gap nears convergence with a fully conjugated polymer when poly(arylene vinylene)s reach a DP=5.[36,37] thus the values presented in **Figure 36** offer a fair representation of the polymers that have been prepared. In the case of CdSe-PPV **35**, the ionization potential of the PPV (5.0 eV)[38] is above that of the CdSe core (5.25 eV),[39] facilitating energy transfer from the PPV to the CdSe. This analysis explains the enhancement of the CdSe emission relative to PPV emission in the solid state for composites composed of higher molecular weight PPV. The lower oligomers of PPV (e.g. trimers) have a larger band gap ($E_g \sim 2.8$)[40] and lower ionization potential (IP ~ 5.15) than hexameric PPV, resulting in a less efficient energy transfer from the PPV to the CdSe.

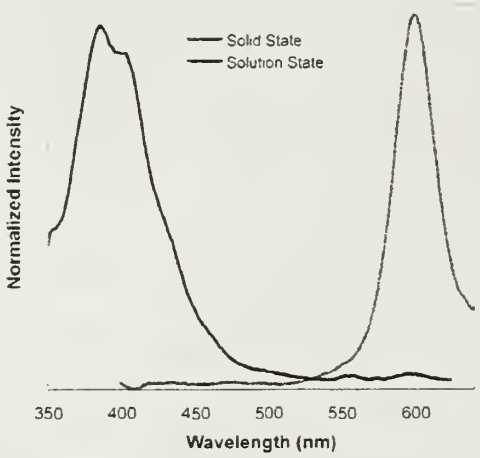

Figure 35. Solution (red curve) and solid-state (blue curve) fluorescence emission spectra for CdSe-PPV hybrid material 35 prepared with optimized conditions and an AB monomer

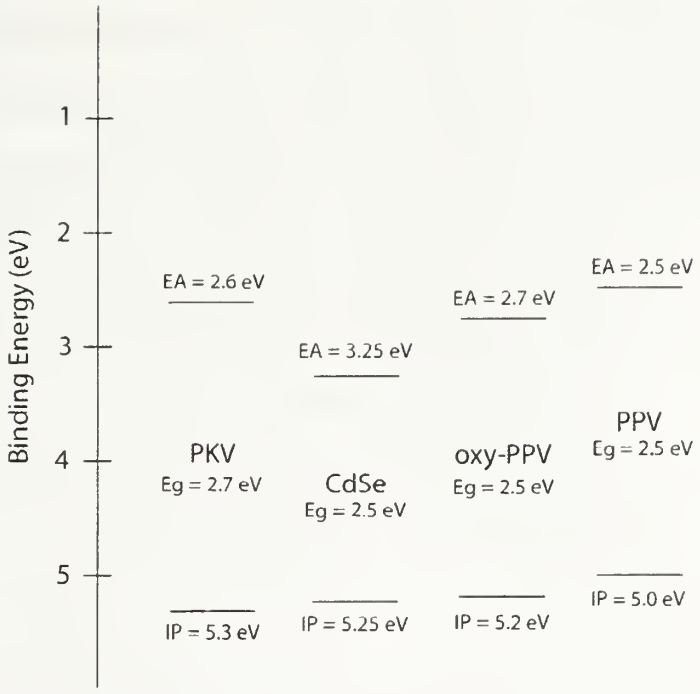

Figure 36. Energy levels for CdSe nanoparticles and the conjugated polymers grafted from the CdSe surface. All values were obtained from previous literature.[32,38,39,41]

Interesting comparisons are observed among the solid-state photoluminescence emission spectra of CdSe-PPV **35**, CdSe-oxyPPV **36**, and CdSe-PKV **37**. In contrast to CdSe-PPV **35**, the solid state photoluminescence emission spectrum of CdSe-oxyPPV (**Figure 37A**) exhibits fluorescence primarily from the conjugated polymer, along with the presence of a lower intensity signal corresponding to photoluminescence emission from the CdSe nanoparticles. This effect is more pronounced in CdSe-PKV, where emission from CdSe cannot be distinguished, as the spectrum is dominated by emission from the conjugated polymer (**Figure 37B**). While similar results are common for blended materials, the domination of the solid-state fluorescence spectra by the conjugated polymer was not expected for these composite materials. For CdSe-oxyPPV composite **36**, the IP of the oxyPPV (5.2 eV)[41] lies only slightly above that of the CdSe (5.25 eV). While this difference represents a theoretically favorable energy

transfer, small deviations (e.g. the effect of changing quantum dot size or polymer molecular weight) would result in energy transfer from the polymer to the quantum dot to become unfavorable. This serves as an explanation for **Figure 37A**, where emission from both the quantum dot core and conjugated polymer are clearly present. Another case is present when the energy levels for CdSe-PKV **37** are examined. The IP of PKV (5.3 eV)[32] is lower than the binding energy of CdSe (5.25 eV), representing a case where energy transfer from the conjugated polymer to the quantum dot is not favorable. Based upon this diagram and the solid-state photoluminescence spectra, the difference in IP must be sufficient for energy transfer in the case of CdSe-PPV **35**, while the small difference in IP leads to limited energy transfer events for CdSe-oxyPPV **36**. From the negligible CdSe emission from CdSe-PKV **37** and the lower IP of the conjugated polymer, energy transfer from the polymer to the particle is unfavorable.

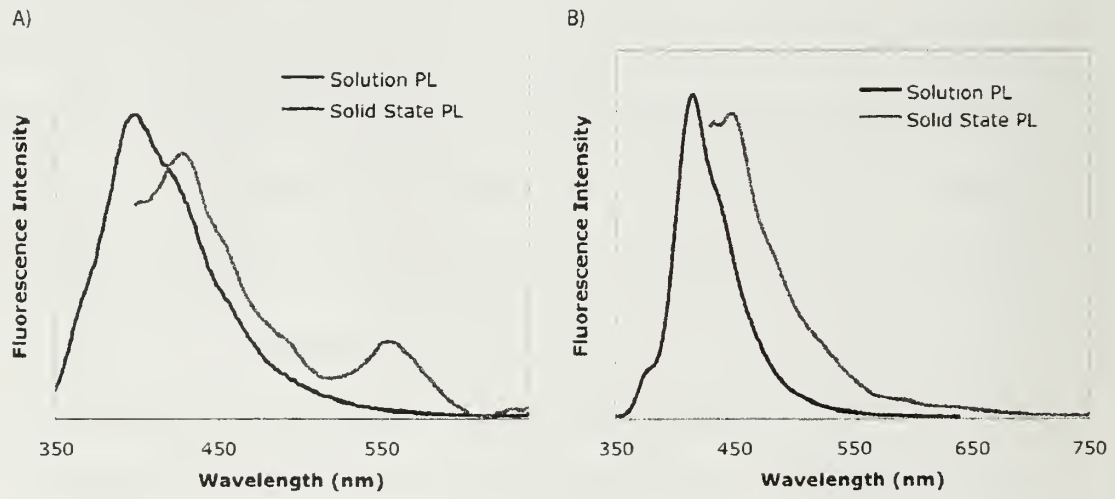

Figure 37. Solution (red curve) and solid-state (blue curve) fluorescence emission spectra for A) CdSe-oxyPPV 36 and B) CdSe-PKV 37.

4.5.3 Time-Resolved Solid-State Fluorescence Spectroscopy of CdSe-Conjugated Polymer Composites

Additional experimental evidence for the energy transfer events described above is shown in solid-state fluorescence spectra and time-resolved fluorescence spectra collected at Eastman Kodak Inc. (Rochester, NY) with Dr. Steve Switalski. The fluorescence emission from films of CdSe-PPV **35** and CdSe-oxyPPV **36** drop cast from chloroform solutions were examined as a function of time. The first set of experiments monitored the emission as the film was allowed to dry over 60 minutes, while the second experiment observed the fluorescence emission on the nanosecond time scale. These experiments were also valuable, as they offer corroborating evidence that the observation made in the Emrick lab were not the result of an instrumental artifact.

For the experiment illustrated in **Figure 38**, a CdSe-PPV solution was drop cast onto a quartz slide and allowed to dry until a visibly damp film was observed. The film was placed in the spectrometer and the time evolution of the fluorescence emission was monitored. The fluorescence spectrum at collected at time T=0 is dominated by the CdSe emission, with a weak fluorescence from PPV, features typically observed for these samples. As time progressed, an increase in the CdSe emission and concurrent decrease in the PPV emission was observed. This experiment was repeated with similar results acquired for each trial. A possible explanation for the increase in CdSe emission is the gradual removal of the solvent, which is functioning as a photoluminescence quenching agent. However, if this were the case, a similar increase in the photoluminescence intensity would be expected for the PPV. The quenching of the PPV emission with an increase in the CdSe fluorescence intensity as the film is allowed

to dry suggests that the solvent may be inhibiting energy transfer events from the PPV to the CdSe nanoparticle.

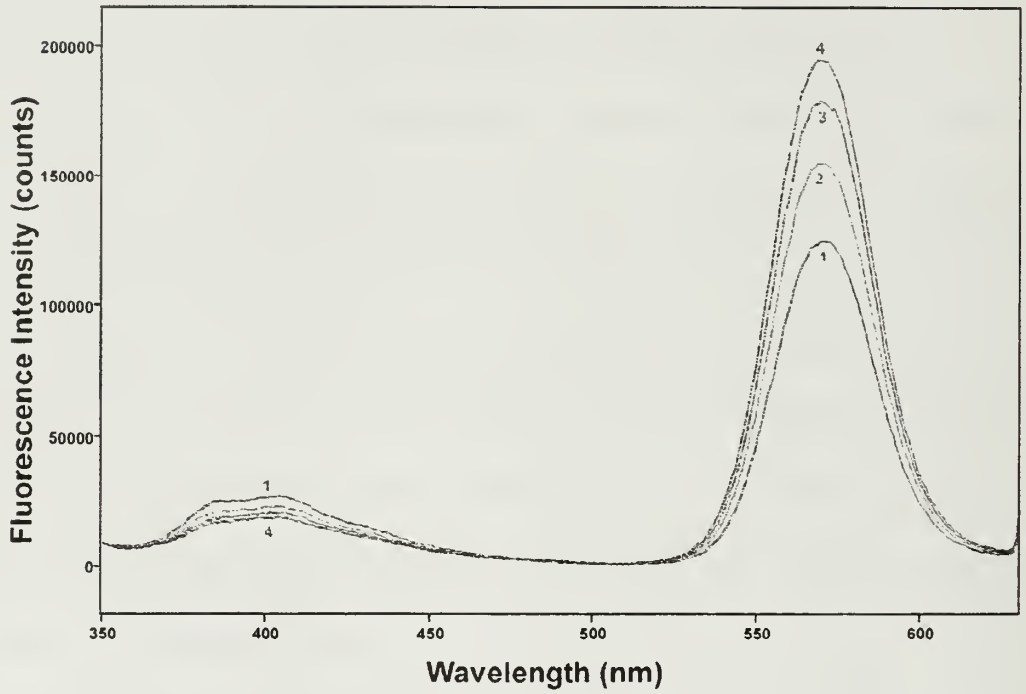

Figure 38. Solid state fluorescence emission spectra of CdSe-PPV 35 over a period of 30 minutes. Spectrum 1 was acquired at time = 0 minutes; spectrum 2, 5 minutes; spectrum 3, 15 minutes; spectrum 4, 30 minutes. (Data acquired at Eastman Kodak Company, Rochester, NY.)

A second set of experiments that monitored the lifetime of the fluorescence intensity on the nanosecond time scale was also performed at Kodak. **Figure 39** illustrates time-resolved fluorescence spectra collected from drop cast films of CdSe-PPV **35** and CdSe-oxyPPV **36**. This data, plotted on a logarithmic intensity scale, compares the fluorescence lifetime emission from three separate wavelengths, corresponding to emission from PPV (450 nm), the CdSe peak maximum (570 nm), and the CdSe peak shoulder (600 nm). In each sample, the CdSe lifetime is noticeably longer than that of the PPV emission. Notably, the CdSe emission at 600 nm is decaying at a slower rate the emission at 570 nm for both composite samples. This

observation reinforces our previous claim that energy transfer is highly dependent upon band gap structure, and energy transfer is more efficient for larger CdSe quantum dots.

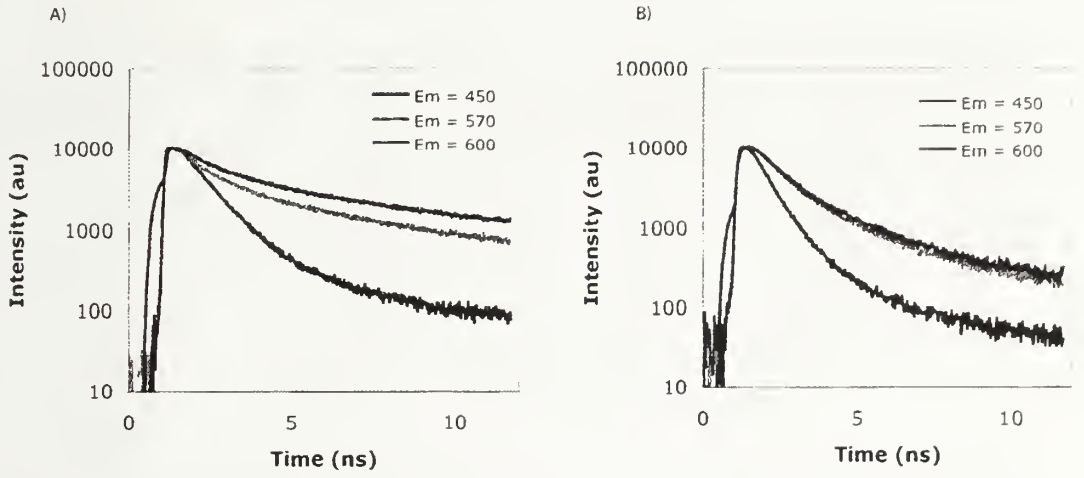

Figure 39. Time resolved fluorescence spectra from emissions at 450 nm (black spectra), 570 nm (red spectra) and 600 nm (blue spectra) for A) CdSe-PPV 35 and B) CdSe-oxyPPV 36. (Data acquired at Eastman Kodak Company, Rochester, NY.)

Another such comparison can be made in **Figure 40**, where the decay rates for PPV emission from both CdSe-PPV **35** and CdSe-oxyPPV **36** are compared on linear intensity scale. As expected, the decay rates for both PPV derivatives are on similar time scales. **Figure 40b** illustrates a completely different result, where the CdSe fluorescence decay from CdSe-oxyPPV **36** is comparable to fluorescence lifetimes typically associated with CdSe quantum dots.[42] However, the decay of the CdSe nanoparticle fluorescence lifetime is much slower from the CdSe-PPV composite **35**. This decay was fitted to a multi-exponental function, strongly indicates the existence of multiple energy transfer events. While more experimentation and modeling would be necessary to reinforce these claims, at this stage it can be speculated that energy transfer between the conjugated polymer attached to the quantum dot as well as energy transfer

from a PPV chain (unbound to any nanoparticle) first to the PPV ligand and then to the quantum dot is responsible for the multi-exponential decay.

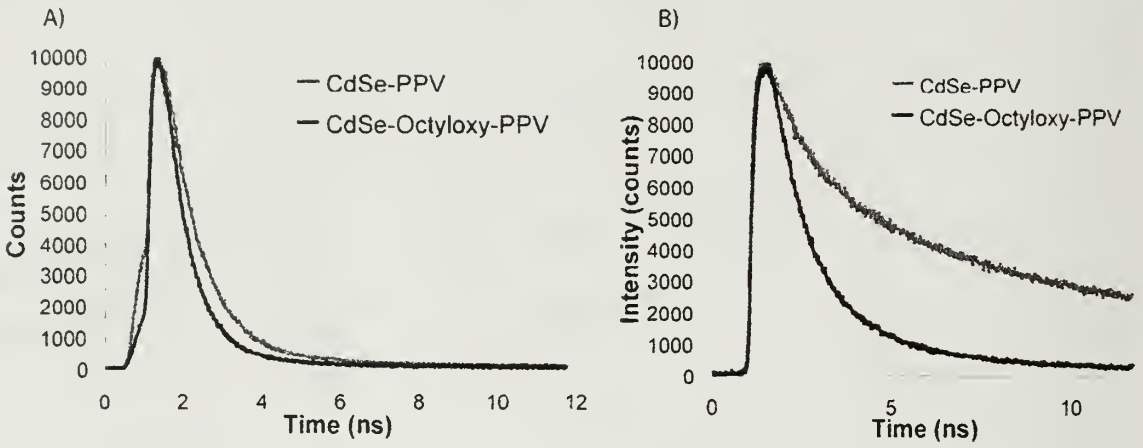

Figure 40. Time resolved fluorescence spectra from CdSe-PPV 35 (red spectra) and CdSe-oxyPPV 36 for emissions at A) 450 nm representing PPV emission and B) 570 nm, representing emission from CdSe. (Data acquired at Eastman Kodak Company, Rochester, NY.)

4.5.4 Single Molecule Fluorescence Spectroscopy of CdSe-PPV Hybrid Materials

Direct evidence for energy transfer was demonstrated through the use of single molecule fluorescence spectroscopy performed in collaboration with Prof. Mike Barnes in the Department of Chemistry at the University of Massachusetts, Amherst. In these experiments, the "molecule" of interest is a single quantum dot tailored with PPV ligands, isolated from dilute solution (~10^{-10} M) on clean glass cover slips using techniques developed in the Barnes laboratory.[43-45] Initially, control experiments on bulk films were performed, again verifying the data collected in the Emrick laboratory. The top of **Figure 41** represents the fluorescence spectra of oligoPPV and CdSe **19**, collected separately. The bottom of **Figure 41** represents the bulk film of CdSe-PPV composite **35** and 80 wt % CdSe **19** blended with oligoPPV. **Figure 42** compares the emission spectrum of a single CdSe-PPV nanostructure with the emission from single

TOPO-covered quantum dot. A single symmetric peak represents the TOPO-covered CdSe emission spectrum, while the CdSe-PPV spectrum shows a peak representing CdSe nanoparticle emission and a blue shoulder. As in the case of the bulk materials, no fluorescence emission associated with PPV was observed in the single molecule fluorescence spectrum of the CdSe-PPV **35**.

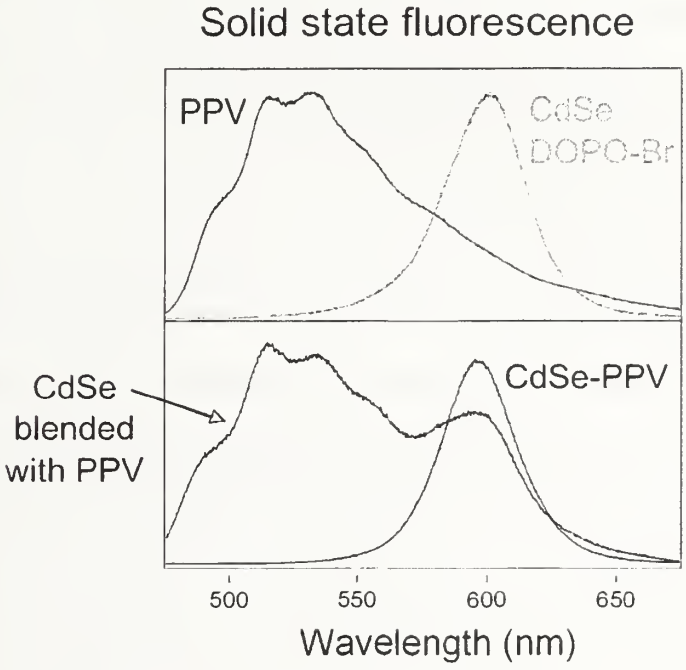

Figure 41. Bulk fluorescence measurements recorded from thin films in the Barnes laboratory.

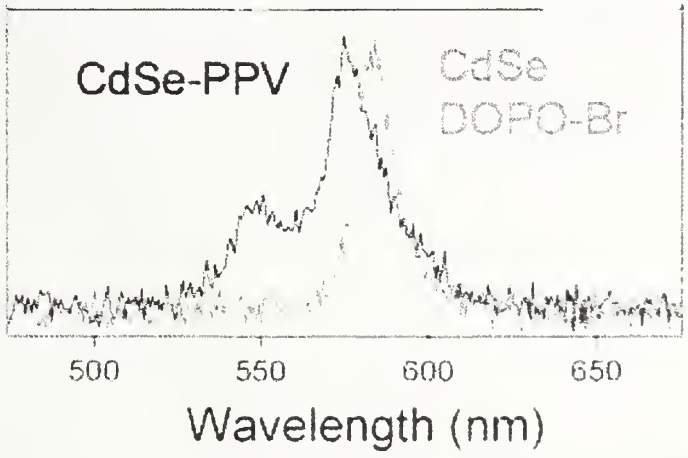

Figure 42. Representative fluorescence emission spectra from single molecules of CdSe-PPV 35 (black spectrum) and CdSe-DOPO-Br 19 (gray spectrum).

Interesting observations were made while monitoring the time evolution of single molecule fluorescence spectrum of both CdSe-PPV **35** and TOPO-covered CdSe. **Figure 43** compares the emission spectra as a function of time (3 frames/second) for a single TOPO-covered CdSe quantum dot and an individual CdSe-PPV nanostructure. The TOPO-covered sample exhibits a progressive blue shift over time, associated with photodegradation of the material. In contrast, the spectrum from CdSe-PPV showed much greater spectral stability than TOPO-CdSe, as the emission from the quantum dot was still present after 30 minutes for some particles. While reports of energy transfer within bulk blends of polyfluorene and TOPO-covered CdSe quantum dots have indicated Forster radii on the order of 8–10 nm, the architecture of the CdSe-PPV nanostructures leads to a Forster radius on the order of 1.5 nm, corresponding to energy transfer rates nearly 100 times larger than those of bulk films.[46] The blue shoulder observed in the single molecule fluorescence spectrum of composite **35** can be understood qualitatively as quenching of the PPV emission by energy transfer to the CdSe quantum dot. The blue shoulder on the CdSe composite spectrum is believed to be a spectral remnant of the PPV emission that resides very close to the CdSe emission, where energy transfer is much less efficient. This shoulder is not observed in bulk films due to the larger number of nanoparticles that are available to accept this energy transfer event.[47]

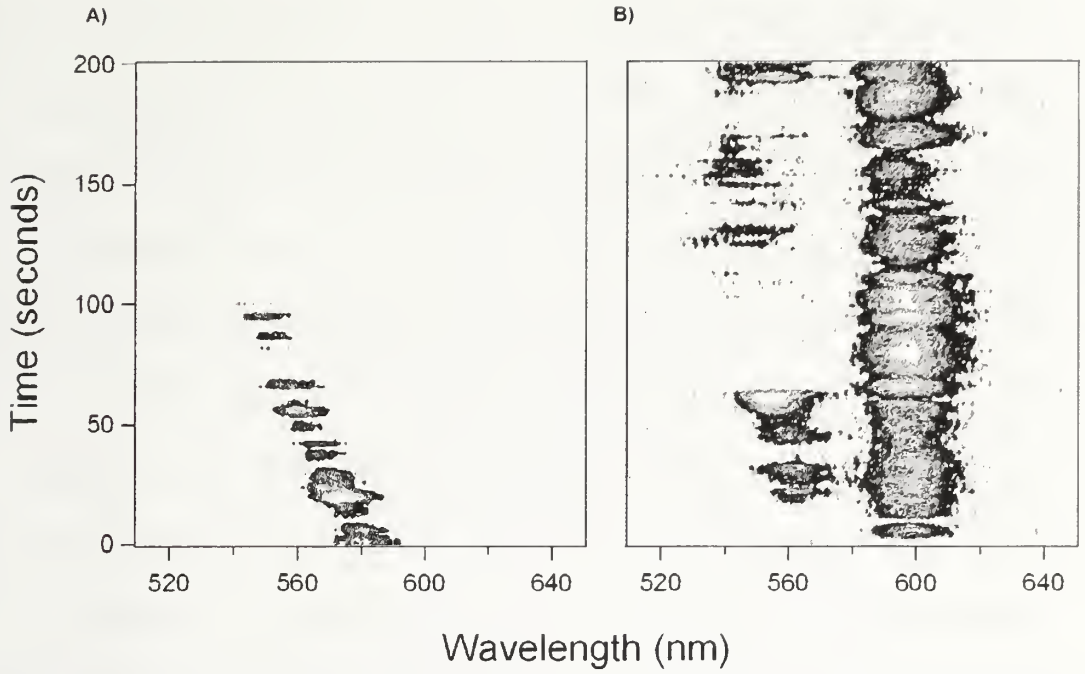

Figure 42. Time evolution spectra of a) TOPO-covered CdSe and b) CdSe-PPV 35. (Data collected by M. Odoi and N. Hammer.)

A second interesting observation from this time evolution experiment is the elimination of characteristic CdSe blinking.[48-50] The TOPO-covered sample exhibits the expected blinking behavior as evidenced in **Figure 44A** by the vertical gaps in emission intensity. Fluorescence blinking is inherent to quantum-confined CdSe nanoparticles, and is undesirable in device applications as blinking leads to a lower effective quantum yield since the nanoparticle is unable to fluoresce at all times. When a photon excites a quantum dot that already possesses an exciton in the core, a second electron-hole pair is formed. The two excitons annihilate one another with the ejection of an electron and the formation of a hole on the particle surface. While the charged particle cannot emit light, it can still absorb radiation and is considered to be in a "dark" state. Once the surface charge is quenched, the particle can once again emit light, and the particle is returned to its "bright" state. The time required to quench the surface charge is typically on the order of tenths of seconds to several seconds. However, in the

case CdSe-PPV, this blinking behavior is not observed at 300 millisecond intervals as shown **Figure 44B**. Time evolution experiments repeated with higher temporal resolution showed that this blinking behavior was not evident, even at 10 millisecond intervals, which are much shorter than the time scales typically associated with quantum dot blinking. While fluctuations in intensity are observed, the intensity never drops to zero, indicating that the quantum dots are always emitting some quantity of light during each exposure frame. It is believed that the PPV ligands function are incredibly effecient at quenching holes generated on the CdSe nanoparticle surface, returning the CdSe nanoparticle to its bright state on time scale shorter than 10 milliseconds. The reduction or elimination of quantum dot blinking may improve the external quantum efficiency achieved in light emitting devices from hybrid materials of conjugated polymers and quantum dots.

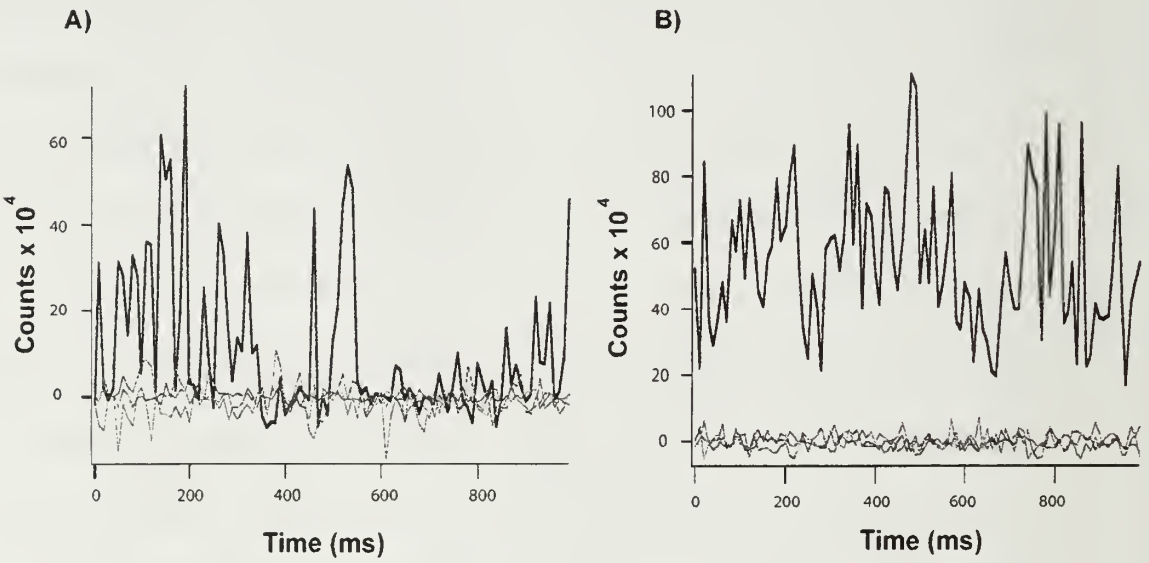

Figure 44. Time resolved fluorescence intensity of a) TOPO-covered CdSe and b) CdSe-PPV 35. (Data collected by M. Odoi and N. Hammer.)

4.6 Summary

Aryl bromide covered CdSe nanoparticles were prepared directly in the functional ligand, eliminating the need for ligand exchange chemistry. An improved synthetic strategy for three AB monomers was presented, and these monomers were incorporated in graft-from Heck coupling polymerizations from the surface of the aryl bromide-functionalized CdSe nanoparticles. Heck conditions were found that minimized the effect of the polymerization on the quantum dot, yet afforded the highest molecular weight to be grown from the nanoparticle surface without the generation of palladium black. The CdSe-PPV composite material was found to have a greatly different solid-state emission spectrum when compared to blends of CdSe and oligoPPV. The energy transfer events between the PPV chain and the CdSe core were investigated by time-resolved fluorescence spectroscopy and single molecule fluorescence spectroscopy.

4.7 Experimental Details

4.7.1 General Methods and Materials

Solvents were purchased from VWR and reagents were purchased from Aldrich and used as supplied unless otherwise noted. Tetrahydrofuan was dried over sodium/benzophenone and distilled before use. All reactions were run under a N_2 atmosphere unless otherwise noted. Nuclear magnetic resonance spectra were obtained on a Brüker DPX 300 MHz or a Brüker 400 MHz Spectrospin spectrometer. Chemical shifts are expressed in parts per million (δ) using residual solvent protons as the internal standard. $CHCl_3$ (δ 7.26 for ^1H, 77.23 for ^{13}C) was used as an internal standard for

$CDCl_3$. Gel permeation chromatography (GPC) measurements were performed in tetrahydrofuran (THF) at 1.0 mL/min using a Knauer K-501 Pump with a K-2301 refractive index detector and K-2600 UV detector, and a column bank consisting of two Polymer Labs PLGel Mixed D columns and one PLGel 50 Å column (1.5 x 30 cm) at 35 °C. Molecular weights are reported relative to polystyrene standards. Matrix assisted laser desorption ionization - time of flight (MALDI-TOF) mass spectrometry was performed on a Brüker Reflex III spectrometer on the CdSe composite samples solution cast from THF without the use of a matrix. High-resolution electron impact (EI) mass spectrometry was performed on a JOEL MStation JMS700 spectrometer. Fluorescence measurements were recorded on a Perkin-Elmer LS-55 fluorescence spectrophotometer from $CHCl_3$ solutions excited at 330, 370 and 400 nm excitation wavelengths with 7 nm (emission and excitation) slit widths. Solid-state fluorescence samples were prepared by drop casting from $CHCl_3$ (~ 5 mg/mL) solutions onto a glass cover slip. Solid-state fluorescence spectra were acquired with a front-surface assembly with 10 nm excitation slit widths and 15 nm emission slit widths. UV-Vis measurements were made on a Perkin-Elmer Lambda 25 spectrophotometer. Fluorescence spectra were normalized to the optical density at the excitation wavelength. Transmission electron microscopy and electron diffraction were performed on a JEOL 100CX microscope at 100,000 magnification (46 cm camera length). Single molecule fluorescence measurements were performed under ambient conditions on a Nikon TE300 inverted microscope with 1.4NA oil objective. Spectra were acquired by focusing the CdSe-PPV emission from the side-port of the microscope onto an Acton SP1220 dual-grating spectrograph and detected with a Roper Scientific Pixis 400B back-illuminated CCD.

4.7.2 Synthesis of 4-bromo-benzyl chloride 17

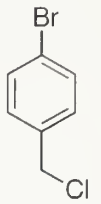

To a 500 mL, 2 neck round bottom flask equipped with a stir bar, septum, addition funnel and N_2 inlet was added 4-bromo-benzyl alcohol **16** (50.0 g, 267 mmol) and dichloromethane (150 mL). The solution was cooled to 0 °C then thionyl chloride (47.7 g, 400 mmol) in dichloromethane (50 mL) was added drop wise over 1 hour. The solution was stirred at room temperature for 12 hours, followed by the drop wise addition of saturated $NaHCO_3$ solution (200 mL). After complete addition, the solution was poured into a beaker containing additional $NaHCO_3$ solution (400 mL) and stirred rapidly for 2 hours. After extraction with dichloromethane (3 x 250 mL), the combined organic layers were dried over $MgSO_4$, treated with carbon black, filtered over silica gel. The solvent was evaporated yielding a colorless oil that crystallized at room temperature under reduced pressure to give colorless crystals (54.5 g, 263 mmol, 98 %). ^{1}H NMR (300 MHz, $CDCl_3$) 7.48 (d, J_{HH}= 8.4 Hz, Ar-*H*, 2 H), 7.27 (d, J_{HH}= 8.5 Hz, Ar-*H*, 2 H), 4.54 (s, Ar-CH_2-Cl, 2 H). ^{13}C NMR (75 MHz, $CDCl_3$, δ) 136.61, 132.06, 130.41, 122.62, 45.56.

4.7.3 Synthesis of *p*-bromobenzyl-DOPO 18

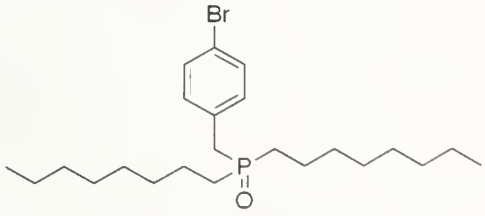

To a solution of di-*n*-octylphosphine oxide (21.9 g, 80.0 mmol), 4-bromobenzyl chloride **17** (18.5 g, 90.0 mmol), and tetra-*n*-butyl ammonium hydrogen sulfate (2.9 g, 8.5 mmol) in toluene (330 mL) was added 30 wt % aqueous NaOH solution (120 mL). The reaction was stirred overnight at 65 °C. The product was extracted with CH_2Cl_2, and the organic portions were combined and washed with water and brine, dried over $MgSO_4$, filtered, and concentrated to give a viscous liquid. The residue was crystallized from hexane to yield **1** as a white solid (24.7 g, 85%, mp 70-71 °C). ^{1}H NMR (300 MHz, $CDCl_3$) δ 7.45 (d, J_{HH}= 8.2 Hz, Ar-*H*, 2 H), 7.13 (d-d, J_{HH}= 8.5, 6.4 Hz, Ar-*H*, 2 H), 3.05 (d, J_{HH}= 13.8 Hz, Ar-C*H*$_2$-P, 2 H), 1.58 (m, P-C*H*$_2$-CH$_2$, 4 H), 1.32 (m, C*H*$_2$, 24 H), 0.88 (t, J_{HH}= 7.1 Hz, C*H*$_3$, 6 H) ppm. ^{13}C NMR (75 MHz, $CDCl_3$, δ) 132.08 (d), 131.68 (d), 131.32 (d), 121.07 (d), 35.90 (d), 31.95, 31.27 (d), 29.26, 29.20, 27.69 (d), 22.81, 21.83 (d), 14.28 ppm. HRMS-FAB (m/z): $[M+H]^+$ calcd for $C_{23}H_{41}BrOP$, 443.2078; found, 443.2080.

4.7.4 Synthesis of Aryl Bromide Functionalized CdSe nanoparticle 19

To a 3-neck, 50 mL round bottom flask equipped with reflux condenser, Ar inlet, septum, and thermocouple probe was added ligand **18** (4.48 g), cadmium acetate (0.21 g), 1-hexadecylamine (2.78 g), and hexylphosphonic acid (0.45 g). The flask was evacuated for 1 hour, then heated to 80 °C under vacuum. Once all the reactants formed a homogeneous liquid, the flask was backfilled with Ar, and the reaction was heated to 270 °C until a homogeneous, colorless solution was present. A solution of selenium (0.20 g) in tri-*n*-octyl phosphine (4 g) was quickly injected to the hot solution. The heating mantle was removed from the solution once an orange color was obtained

during the gradual color change from yellow to red. The solution was allowed to cool to room temperature, followed by particle precipitation with 10 mL anhydrous methanol. The solution was centrifuged and the supernatant decanted. The resulting solid was purified by dissolution in a minimal amount of THF precipitated into methanol, followed by centrifugation. The red powder was dried under N_2 purge and stored as a solution in THF or hexanes. ^{1}H NMR (300 MHz, $CDCl_3$) 7.46, 7.15, 3.05, 1.62, 1.57, 0.89.

4.7.5 Synthesis of *p*-di-*n*-octylbenzene 21

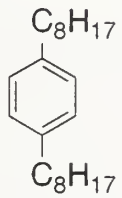

To a 3-neck, 1 L round bottom flask equipped with reflux condenser, N_2 inlet, addition funnel and stopper was added magnesium (12.42 g, 510 mmol) and diethyl ether (200 mL). The stirred solution was cooled to 0 °C with an ice bath and octyl bromide (104.40 g, 541 mmol) in diethyl ether (200 mL) was slowly added *via* addition funnel over 1 hour. The ice bath was removed and the solution heated to reflux for 3 hours. The solution was then cooled to 0 °C and diphenylphosphinopropane nickel dichloride (0.13 g) and *p*-dichlorobenzene **20** (29.97 g, 204 mmol) in diethyl either (200 mL) was added over 1 hour. The stirred solution was heated to reflux for 20 hours, cooled to 0 °C, then quenched with 2 N HCl (125 mL). The biphasic solution was poured into water (200 mL) and extracted with ether (3 x 150 mL). The combined organic layers were dried over $MgSO_4$, filtered and evaporated. The product was purified by Kugelrohr distillation (1 torr, 190 °C) to give a colorless liquid (53.6 g, 177

mmol, 87 %) ^{1}H NMR (300 MHz, $CDCl_3$, δ) 7.08 (s, Ar-*H*, 4 H), 2.58 (t, J_{HH}=7.3 Hz, Ar-C*H*$_2$, 4 H), 1.55 (m, Ar-CH$_2$-C*H*$_2$, 4 H), 1.29 (m, C*H*$_2$, 24 H), 0.88 (t, J_{HH}= 6.7 Hz, C*H*$_3$, 6 H). ^{13}C NMR (100 MHz, $CDCl_3$, δ) 140.29, 128.44, 35.81, 32.14, 31.85, 29.74, 29.64, 29.51, 22.91, 14.34.

4.7.6 Synthesis of 1,4-dibromo-2,5-di-*n*-octylbenzene 22

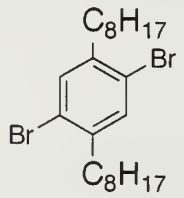

To a 100 mL round bottom flask equipped with a stir bar, septum and oil bubbler was added *p*-dioctylbenzene **21** (24.97 g, 82.6 mmol) and iodine (0.10 g, 0.4 mmol). The flask was wrapped with aluminum foil to exclude light and cooled to 0 °C. Bromine (27.07 g, 169.4 mmol) was added drop wise over 10 minutes and gas evolution was noted during the addition. The bubbler was removed after 2 hours and the reaction stirred at room temperature for 20 hours. 20 % $KOH_{(aq)}$ (50 mL) was added to the flask and then heated until a homogeneous solution was present. The solution was cooled and the solid material was collected by filtration. The product was obtained following recrystallization of the solid material from ethanol, yielding colorless crystals (32.56 g, 71 mmol, 86 %). ^{1}H NMR (300 MHz, $CDCl_3$, δ) 7.35 (s, Ar-*H*, 2 H), 2.63 (t, J_{HH}=7.9 Hz, Ar-C*H*$_2$, 4 H), 1.57 (m, Ar-CH$_2$-C*H*$_2$, 4 H), 1.28 (m, C*H*$_2$, 24 H), 0.88 (t, J_{HH}= 6.8 Hz, C*H*$_3$, 6 H). ^{13}C NMR (100 MHz, $CDCl_3$, δ) 141.54, 133.96, 123.27, 35.75, 32.10, 30.03, 29.60, 29.57, 29.45, 22.90, 14.34.

4.7.7 Synthesis of 1,4-divinyl -2,5-di-*n*-octylbenzene 23

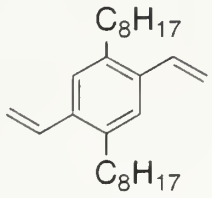

1,4-Dibromo-2,5-di-*n*-octylbenzene **22** (2.0 g, 4.4 mmol), tetrakis(triphenyl phosphine) palladium (0) (0.20 g, 0.17 mmol), and a few crystals of 2,6-di-*tert*-butyl-4-methylphenol were dissolved in anhydrous dioxane (40 mL) and stirred at room temperature under an inert atmosphere. Tri-*n*-butyl vinyl tin (3.1 g, 9.8 mmol) was added to the stirring solution, and the reaction was refluxed for 12 hours. The product was extracted with ether and washed with water, saturated ammonium chloride solution, brine, and dried over $MgSO_4$. The solvent was removed under reduced pressure and the crude product was purified by flash chromatography eluting with hexanes to yield the desired compound (1.34 g, 87%). ^{1}H NMR (300 MHz, $CDCl_3$, δ) 7.24 (s, Ar-*H*, 2 H), 6.94 (d-d, J_{HH}=17.4, 11.0 Hz, C*H*=CH_2, 2 H), 5.64 (d-d, J_{HH}= 17.4, 1.4 Hz, CH=CH_2, 2 H), 5.25 (d-d, J_{HH}=11.0, 1.4 Hz, CH=CH_2, 2 H), 2.63 (t, J_{HH}=7.7 Hz, Ar-CH_2, 2 H), 1.54 (quint, J_{HH}= 7.4 Hz, Ar-CH_2-CH_2, 4 H), 1.27 (m, CH_2, 24 H), 0.88 (t, J_{HH}= 6.9 Hz, CH_3, 6 H). ^{13}C NMR (75 MHz, $CDCl_3$, δ) 138.22, 135.81, 134.62, 126.80, 114.85, 33.32, 32.14, 31.56, 29.92, 29.71, 29.53, 22.92, 14.35.

4.7.8 Synthesis of 4-bromo-2,5-di-*n*-octylbenzaldehyde 24

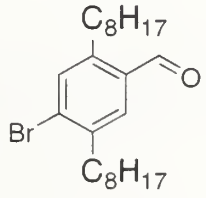

To a 500 mL, 2 neck round bottom flask equipped with a stir bar, nitrogen inlet and septum was added 1,4-dibromo-2,5-di-*n*-octylbenzene[23] **22** (15 g, 32.6 mmol). The flask was evacuated for 1 hour then backfilled with N_2. THF (400 mL) was added and the stirred solution cooled with a $CHCl_3$/dry ice bath (-60 °C). 2.7 M n-BuLi (39.1 mmol) in hexanes was added dropwise then stirred for 5 minutes. This solution was transferred by cannula to a stirred solution of DMF (5 mL) in THF (50 mL) at -60 °C. After the transfer was complete, the solution was allowed to warm to room temperature. The solution was filtered over silica gel and the solvent evaporated. The residue was crystallized with ethanol to give a white powder (9.6 g, 23.4 mmol, 72 %). ^{1}H NMR (400 MHz, $CDCl_3$, δ) 10.22 (s, C(O)*H*, 1 H), 7.64 (s, Ar-*H*, 1 H), 7.54 (s, Ar-*H*, 1 H), 2.93 (t, J_{HH}=7.8 Hz, Ar-CH_2, 2 H), 2.73 (t, J_{HH}=8.0 Hz, Ar-CH_2, 2 H), 1.60 (m, Ar-CH_2-CH_2, 4 H), 1.30 (m, CH_2, 24 H), 0.88 (t, J_{HH}= 5.6 Hz, CH_3, 6 H). ^{13}C NMR (100 MHz, $CDCl_3$, δ) 191.62, 144.74, 140.72, 135.20, 132.86, 13.2.53, 131.28, 35.81, 32.50, 32.08, 32.05, 31.80, 29.94, 29.70, 29.64, 29.59, 29.43, 22.88, 22.86, 14.32. HRMS-EI (m/z): [M]+ calcd for $C_{23}H_{37}BrO$, 408.2028; found, 408.2043.

4.7.9 Synthesis of 1-bromo-2,5-di-*n*-octyl-4-vinylbenzne 25

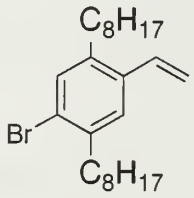

To a 100 mL, 2 neck round bottom flask equipped with a stir bar, nitrogen inlet and septum was added methyltriphenylphosphonium bromide (9.37 g, 26.2 mmol). The flask was evacuated for 1 hour then backfilled with N_2. THF (50 mL) was added and

the stirred solution cooled with an acetone/dry ice bath (-78 °C). 2.7 M n-BuLi (25.0 mmol) in hexanes was added dropwise then the flask warmed to room temperature. After 1 h, the solution was again cooled to -78 °C and 2,5-di-*n*-octyl-4-bromobenzaldehyde **24** (8.60 g, 21.0 mmol) in THF (25 mL) was added by syringe. The reaction was allowed to warm to room temperature and stirred for 2 hours. The solution was diluted with hexanes (100 mL) then filtered over silica gel. The solvent was removed and the white solid dissolved in methanol and crystallized to give colorless needles (7.3 g, 17.9 mmol, 85 %, mp 29 °C). ^{1}H NMR (400 MHz, $CDCl_3$, δ) 7.30 (s, Ar-*H*, 2 H), 6.88 (d-d, J_{HH}=17.4, 10.9 Hz, C*H*CH_2, 1 H), 5.63 (d-d, J_{HH}=17.4, 1.4 Hz, CHC*H*$_2$, 1 H), 5.29 (d-d, J_{HH}=11.0, 1.4 Hz, CHC*H*$_2$, 1 H), 2.68 (t, J_{HH}=7.8 Hz, Ar-C*H*$_2$, 2 H), 2.58 (t, J_{HH}=7.8 Hz, Ar-C*H*$_2$, 2 H), 1.61 (m, Ar-CH$_2$-C*H*$_2$, 4 H), 1.53 (m, Ar-CH$_2$-C*H*$_2$, 4 H), 1.28 (m, C*H*$_2$, 20 H), 0.89 (t, J_{HH}= 6.9 Hz, C*H*$_3$, 6 H). ^{13}C NMR (100 MHz, $CDCl_3$, δ) 139.84, 139.73, 135.70, 134.14, 133.45, 127.49, 123.73, 115.65, 36.07, 32.82, 32.12, 32.10, 31.18, 30.33, 29.76, 29.69, 29.65, 29.50, 29.46, 22.91, 14.34. HRMS-EI (m/z): [M]+ calcd for $C_{24}H_{39}Br$, 406.2235; found, 406.2201.

4.7.10 General Procedure for the Heck Coupling Polymerization of AB Monomers

In a N_2 filled drybox, N-methyldicyclohexylamine (0.10 g), palladium (II) acetate (7 mg), tri-*o*-tolylphosphine (18 mg), 2,5-dioctyl-4-bromostyrene **25** (0.15 g), one crystal of 3,5-di-*t*-butyl-4-hydroxy toluene, and DMF (1 mL) were added to a reaction vial equipped with a stir bar and Teflon valve. The reaction was sealed, removed from the drybox, and heated to 150 °C for 16 h. The solution was allowed to

cool then diluted with chloroform and precipitated into ethanol. A green solid was recovered following filtration. ^{1}H NMR (300 MHz, CD_2Cl_2, δ) 7.38 (Ar-*H*), 7.26 (Ar-C*H*=C*H*-Ar), 2.58 (Ar-CH_2), 1.68 (Ar-CH_2CH_2), 1.22 (alkyl CH_2), 0.89 (CH_2-CH_3) ppm. Size exclusion chromatography: M_n = 15100, M_w = 33300, PDI = 2.20.

4.7.11 Synthesis of 1,4-bis-octyloxy-benzene 27

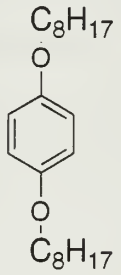

To a 500 mL, 2 neck round bottom flask equipped with a stir bar, nitrogen inlet and septum was added hydroquinone **26** (11.0 g, 100 mmol), potassium carbonate (82.8 g, 600 mmol) and DMF (300 mL). The stirred solution was heated to 80 °C then octyl bromide (42.4 g, 220 mmol) added *via* syringe. After 20 h, the reaction was allowed to cool, poured into water (400 mL) and extracted with diethyl ether (3 x 300 mL). The combined organic layers were dried over $MgSO_4$, filtered and evaporated. Pure product was obtained following crystallization with ethanol to give colorless flakes (19.9 g, 59.5 mmol, 60 %). ^{1}H NMR (300 MHz, $CDCl_3$, δ) 6.82 (s, Ar-*H*, 2 H), 3.90 (t, J_{HH}=6.6 Hz, Ar-O-CH_2, 4 H), 1.75 (quint, J_{HH}= 6.9 Hz, Ar-O-CH_2-CH_2, 4 H), 1.44 (m, CH_2, 4H), 1.30 (m, CH_2, 20 H), 0.88 (t, J_{HH}= 4.3 Hz, CH_3, 6 H). ^{13}C NMR (100 MHz, $CDCl_3$, δ) 153.42, 115.61, 68.89, 32.04, 29.62, 29.61, 29.47, 26.29, 22.88, 14.32.

4.7.12 Synthesis of 1,4-dibromo-2,5-bis-octyloxy-benzene 28

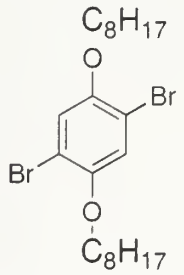

To a 100 mL round bottom flask equipped with a stir bar, septum and oil bubbler was added 1,4-bis-octyloxy-benzene **27** (10.0 g, 29.9 mmol), iodine (0.30 g, 1.4 mmol) and dichloromethane (15 mL). The flask was wrapped with aluminum foil to exclude light and cooled to 0 °C. Bromine (9.79 g, 61.3 mmol) was added drop wise over 10 minutes and gas evolution was noted during the addition. The bubbler was removed after 2 hours and the reaction stirred at room temperature for 20 hours. The solution was poured into 20 % $KOH_{(aq)}$ (50 mL) then extracted with dichloromethane (3 x 50 mL). The combined organic layers were dried over $MgSO_4$, filtered and evaporated. The product was obtained following three recrystallizations of the solid material from ethanol, yielding a white powder (9.5 g, 19.3 mmol, 66 %). ^{1}H NMR (300 MHz, $CDCl_3$, δ) 7.08 (s, Ar-*H*, 2 H), 3.94 (t, J_{HH}=6.5 Hz, Ar-O-C*H*$_2$, 4 H), 1.82 (quint, J_{HH}= 6.6 Hz, Ar-O-CH$_2$-C*H*$_2$, 4 H), 1.48 (m, C*H*$_2$, 4H), 1.30 (m, C*H*$_2$, 20 H), 0.89 (t, J_{HH}= 6.9 Hz, C*H*$_3$, 6 H). ^{13}C NMR (100 MHz, $CDCl_3$, δ) 150.30, 118.69, 111.35, 70.54, 32.02, 29.48, 29.43, 29.34, 26.15, 22.88, 14.33.

4.7.13 Synthesis of 4-bromo-2,5-bis-octyloxy-benzaldehyde 29

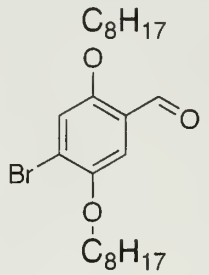

To a 250 mL, 2 neck round bottom flask equipped with a stir bar, nitrogen inlet and septum was added 1,4-dibromo-2,5-bis-octyloxy-benzene **28** (5.0 g, 10.2 mmol). The flask was evacuated for 1 hour then backfilled with N_2. THF (150 mL) was added and the stirred solution cooled with a $CHCl_3$/dry ice bath (-60 °C). 2.7 M n-BuLi (11.2 mmol) in hexanes was added dropwise then stirred for 5 minutes. This solution was transferred by cannula to a stirred solution of DMF (1.5 mL) in THF (50 mL) at -60 °C. After the transfer was complete, the solution was allowed to warm to room temperature. The solution was filtered over silica gel and the solvent evaporated. The residue was crystallized with ethanol to give a white powder (3.5 g, 7.9 mmol, 79 %, mp 54-55 °C). ^{1}H NMR (400 MHz, $CDCl_3$, δ) 10.41 (s, C(O)*H*, 1 H), 7.31 (s, Ar-*H*, 1 H), 7.22 (s, Ar-*H*, 1 H), 4.02 (m, Ar-O-C*H*$_2$, 4 H), 1.73 (m, Ar-O-CH$_2$-C*H*$_2$, 4 H), 1.47 (m, C*H*$_2$-CH$_3$, 4 H), 1.31 (m, C*H*$_2$, 20 H), 0.89 (t, J_{HH}=6.0 Hz, C*H*$_3$, 6 H). ^{13}C NMR (100 MHz, $CDCl_3$, δ) 189.09, 155.94, 150.03, 124.44, 121.12, 118.62, 110.76, 70.00, 69.63, 31.99, 31.97, 29.45, 29.41, 29.26, 29.21, 26.19, 26.14, 22.85, 22.84, 14.30, 14.28. HRMS-EI (m/z): [M]+ calcd for $C_{23}H_{37}BrO_3$, 440.1926: found, 440.1994.

4.7.14 Synthesis of 1-bromo-2,5-bis-octyloxy-4-vinylbenzene 30

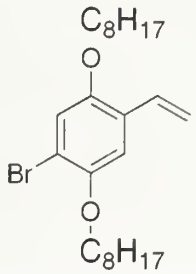

To a 100 mL, 2 neck round bottom flask equipped with a stir bar, nitrogen inlet and septum was added methyltriphenylphosphonium bromide (3.20 g, 9.0 mmol). The flask was evacuated for 1 hour then backfilled with N_2. THF (25 mL) was added and the stirred solution cooled with an acetone/dry ice bath (-78 °C). 2.7 M n-BuLi (8.6 mmol) in hexanes was added dropwise then the flask warmed to room temperature. After 1 h, the solution was again cooled to -78 °C and 4-bromo-2,5-bis-octyloxy-benzaldehyde **5** (3.30 g, 7.5 mmol) in THF (10 mL) was added *via* syringe. The reaction was allowed to warm to room temperature and stirred for 2 hours. The solution was diluted with hexanes (100 mL) then filtered over silica gel. The solvent was removed and the product was obtained following crystallization from methanol to give a white powder (1.9 g, 4.3 mmol, 57 %, mp 32 °C). ^{1}H NMR (400 MHz, $CDCl_3$, δ) 7.04 (s, Ar-*H*, 1 H), 7.01 (s, Ar-*H*, 1 H), 6.97 (d-d, J_{HH}=17.9, 11.3 Hz, C*H*CH_2, 1 H), 5.72 (d-d, J_{HH}=17.8, 1.4 Hz, CHCH_2, 1 H), 5.27 (d-d, J_{HH}=11.1, 1.3 Hz, CHCH_2, 1 H), 3.99 (t, J_{HH}=6.6 Hz, Ar-O-CH_2, 2 H), 3.91 (t, J_{HH}=6.5 Hz, Ar-CH_2, 2 H), 1.79 (m, Ar-O-CH_2-CH_2, 4 H), 1.47 (m, CH_2-CH_3, 4 H), 1.29 (m, CH_2, 20 H), 0.89 (t, J_{HH}= 6.9 Hz, CH_3, 6 H). ^{13}C NMR (100 MHz, $CDCl_3$, δ) 151.04, 149.87, 131.39, 126.92, 117.80, 114.81, 112.22, 111.97, 70.47, 69.60, 32.03, 29.54, 29.47, 26.30, 26.22, 22.89, 14.34. HRMS-EI (m/z): [M]+ calcd for $C_{24}H_{39}BrO_2$, 438.2133; found, 438.2170.

4.7.15 Synthesis of N-dodecyl-3,6-dibromocarbazole 32

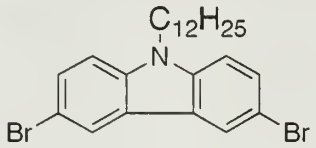

To a 50 mL, 2 neck round bottom flask equipped with a stir bar, nitrogen inlet and septum was added sodium hydride (0.24 g, 10.1 mmol), 3,6-dibromocarbazole **31** (3.00 g, 9.2 mmol) and DMF (30 mL). The solution was stirred at room temperature for 5 minutes then dodecylbromide (3.44 g, 13.8 mmol) was added *via* syringe. The reaction was stirred for 16 hours at 65 °C, allowed to cool, and then poured into 100 mL water. The solution was extracted with diethyl ether (3 x 75 mL) and the combined organic layers dried over $MgSO_4$, filtered and evaporated. The residue was purified by silica gel column chromatography (hexanes) then crystallized with methanol giving colorless needles (3.54 g, 8.0 mmol, 87 %, mp 58-59 °C). ^{1}H NMR (400 MHz, $CDCl_3$, δ) 8.14 (d-d, J_{HH}=2.1, 0.5 Hz, Ar-*H*, 2 H), 7.55 (d-d, J_{HH}=8.6, 2.0 Hz, Ar-*H*, 2 H), 7.28 (d, J_{HH}=0.4 Hz, Ar-*H*, 2 H), 4.24 (t, J_{HH}=7.1 Hz, N-C*H*$_2$, 2 H), 1.82 (quint, J_{HH}=6.8, N-CH$_2$-C*H*$_2$, 2 H), 1.31 (m, C*H*$_2$, 18 H), 0.88 (t, J_{HH}= 6.8 Hz, C*H*$_3$, 3 H). ^{13}C NMR (100 MHz, $CDCl_3$, δ) 139.47, 129.17, 123.60, 123.42, 112.10, 110.57, 43.52, 32.12, 29.79, 29.73, 29.66, 29.53, 29.04, 27.41, 22.90, 14.35. HRMS-EI (m/z): [M]+ calcd for $C_{24}H_{31}Br_2N$, 491.0823; found, 491.0811.

4.7.16 Synthesis of N-dodecyl-3-bromo-6-carbaldehydecarbazole 33

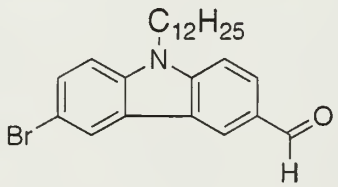

To a 250 mL, 2 neck round bottom flask equipped with a stir bar, nitrogen inlet and septum was added N-dodecyl-3,6-dibromocarbazole **32** (3.40 g, 7.7 mmol). The flask was evacuated for 1 hour then backfilled with N_2. THF (150 mL) was added and the stirred solution cooled with an acetone/dry ice bath (-78 °C). 2.7 M n-BuLi (7.8 mmol) in hexanes was added dropwise then stirred for 5 minutes. This solution was transferred by cannula to a stirred solution of DMF (1 mL) in THF (50 mL) in a $CHCl_3$/dry ice bath. After the transfer was complete, the solution was allowed to warm to room temperature. The solution was filtered over silica gel and the solvent evaporated. The residue was purified by silica gel column chromatography (3:2 hexanes/ethyl acetate) then crystallized with ethanol to give a white powder (2.3 g, 5.2 mmol, 68 %, mp 91-92 °C). ^{1}H NMR (400 MHz, $CDCl_3$, δ) 10.10 (s, C(O)*H*, 1 H), 8.56 (d, J_{HH}=1.1 Hz, Ar-*H*, 1 H), 8.27 (d, J_{HH}=1.7 Hz, Ar-*H*, 1 H), 8.04 (d-d, J_{HH}=8.6, 1.5 Hz, Ar-*H*, 1 H), 7.61 (d-d, J_{HH}=8.7 Hz, 1.9 Hz, Ar-*H*, 1 H), 7.48 (d, J_{HH}=8.5 Hz, Ar-*H*, 1 H), 7.33 (d, J_{HH}=8.8 Hz, Ar-*H*, 1 H), 4.32 (t, J_{HH}=7.2 Hz, N-CH_2, 2 H), 1.87 (quint, J_{HH}=7.2 Hz, N-CH$_2$-CH_2, 2 H), 1.23 (m, CH_2, 18 H), 0.89 (t, J_{HH}= 7.0 Hz, CH_3, 3 H). ^{13}C NMR (100 MHz, $CDCl_3$, δ) 191.68, 144.31, 139.92, 129.54, 128.98, 127.60, 124.80, 124.51, 123.63, 122.08, 113.29, 111.00, 109.44, 43.73, 32.08, 29.76, 29.70, 29.63, 29.50, 29.05, 27.38, 22.87, 14.33. HRMS-EI (m/z): [M]+ calcd for $C_{25}H_{32}BrNO$, 441.1667; found, 441.1589.

4.7.17 Synthesis of N-dodecyl-3-bromo-6-vinylcarbazole 34

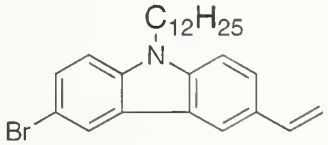

To a 50 mL, 2 neck round bottom flask equipped with a stir bar, nitrogen inlet and septum was added methyltriphenylphosphonium bromide (1.93 g, 5.4 mmol). The flask was evacuated for 1 hour then backfilled with N_2. THF (15 mL) was added and the stirred solution cooled with an acetone/dry ice bath (-78 °C). 2.7 M n-BuLi (5.2 mmol) in hexanes was added dropwise then the flask warmed to room temperature. After 1 h, the solution was again cooled to -78 °C and N-dodecyl-3-bromo-6-carbaldehydecarbazole **33** (2.00 g, 4.5 mmol) in THF (5 mL) was added by syringe. The reaction was allowed to warm to room temperature and stirred for 2 hours. The solution was diluted with hexanes (20 mL) then filtered over silica gel. The solvent was removed and the product obtained following recrystallization from methanol to give colorless crystals (1.7 g, 3.9 mmol, 86 %, 45-46 °C). ^{1}H NMR (400 MHz, $CDCl_3$, δ) 8.20 (d, J_{HH}=1.8 Hz, Ar-*H*, 1 H), 8.05 (d, J_{HH}=1.2 Hz, Ar-*H*, 1 H), 7.59 (d-d, J_{HH}=8.6, 1.5 Hz, Ar-*H*, 1 H), 7.52 (d-d, J_{HH}=8.6 Hz, 1.9 Hz, Ar-*H*, 1 H), 7.34 (d, J_{HH}=8.5 Hz, Ar-*H*, 1 H), 7.26 (d, J_{HH}=8.5 Hz, Ar-*H*, 1 H), 6.89 (d-d, J_{HH}=17.6, 10.9 Hz, C*H*CH_2, 1 H), 5.77 (d-d, J_{HH}=17.6, 0.6 Hz, CHC*H*$_2$, 1 H), 5.22 (d-d, J_{HH}=10.9, 0.6 Hz, CHC*H*$_2$, 1 H), 4.25 (t, J_{HH}=7.2 Hz, N-C*H*$_2$, 2 H), 1.83 (quint, J_{HH}=6.8 Hz, N-CH_2-C*H*$_2$, 2 H), 1.22 (m, C*H*$_2$, 18 H), 0.88 (t, J_{HH}= 7.0 Hz, C*H*$_3$, 3 H). ^{13}C NMR (100 MHz, $CDCl_3$, δ) 140.67, 139.58, 137.44, 129.40, 128.50, 124.80, 124.75, 123.28, 122.12, 118.72, 111.85, 111.57, 110.43, 109.12, 43.44, 32.12, 29.80, 29.75, 29.67, 29.54, 29.10, 27.42, 22.90, 14.35. HRMS-EI (m/z): [M]+ calcd for $C_{26}H_{34}BrN$, 439.1875; found, 439.1838.

4.7.18 General method for the preparation of CdSe-conjugated polymer composite materials

In a N_2 filled drybox, functionalized CdSe nanoparticles (10 mg in 1 mL THF), N-methyldicyclohexylamine (0.10 g), tetrakis(triphenylphosphine) palladium (2 mg), and 1-bromo-2,5-di-*n*-octyl-4-vinylbenzne **25** (0.15 g) were added to a glass tube equipped with a stir bar and Teflon valve. The reaction was sealed, removed from the drybox, and heated to 90 °C for 16 h. The solution was allowed to cool then centrifuged for 30 minutes. The supernatant was decanted and CdSe-PPV composite material was precipitated with the addition of methanol. The suspension was centrifuged and the supernatant was discarded. The red CdSe-PPV material was dried with a stream of N_2 and stored as a solution in THF. Characterization data for CdSe-PPV **35**: ^{1}H NMR (300 MHz, CD_2Cl_2, δ) 7.37 (Ar-*H*), 7.27 (Ar-C*H*=C*H*-Ar), 2.58 (Ar-CH_2), 1.68 (Ar-CH_2CH_2), 1.21 (alkyl CH_2), 0.88 (CH_2-CH_3) ppm. MALDI (m/z, % max. intensity) 1096 (dimer, 21 %), 1422 (trimer, 21 %), 1748 (tetramer, 40 %), 2076 (pentamer, 100%), 2402 (hexamer, 50 %), 2730 (heptamer, 36%), 3058 (octamer, 17 %), 3386 (nonamer, 6 %).

4.8 References

(1) Coe, S.; Woo, W. K.; Bawendi, M. G.; Bulovic, V. *Nature* **2002**, *420*, 800-803.

(2) Burda, C.; Green, T. C.; Link, S.; El-Sayed, M. A. *J. Phys. Chem. B* **1999**, *103*, 1783-1788.

(3) Greenham, N. C.; Peng, X.; Alivisatos, A. P. *Synth. Met.* **1997**, *84*, 545-546.

(4) Wang, Y. J.; Ma, J.; Jiang, Y. S. *J. Phys. Chem. A* **2005**, *109*, 7197-7206.

(5) Akcelrud, L. *Prog. Polym. Sci.* **2003**, *28*, 875-962.

(6) Shim, H. K.; Jin, J. I. In *Polymers For Photonics Applications I* 2002; Vol. 158, p 193-243.

(7) Cho, B. R. *Prog. Polym. Sci.* **2002**, *27*, 307-355.

(8) Scherf, U.; Riechel, S.; Lemmer, U.; Mahrt, R. F. *Curr. Opin. Solid State Mater. Sci.* **2001**, *5*, 143-154.

(9) Scherf, U. In *Carbon Rich Compounds Ii* 1999; Vol. 201, p 163-222.

(10) Pasco, S. T.; Lahti, P. M.; Karasz, F. E. *Macromolecules* **1999**, *32*, 6933-6937.

(11) Kim, D. Y.; Cho, H. N.; Kim, C. Y. *Prog. Polym. Sci* **2000**, *25*, 1089-1139.

(12) Mattoussi, H.; Radzilowski, L. H.; Dabbousi, B. O.; Thomas, E. L.; Bawendi, M. G.; Rubner, M. F. *J. Appl. Phys.* **1998**, *83*, 7965-7974.

(13) Dabbousi, B. O.; Bawendi, M. G.; Onitsuka, O.; Rubner, M. F. *App. Phys. Lett.* **1995**, *66*, 1316-1318.

(14) Gao, M. Y.; Richter, B.; Kirstein, S. *Adv. Mater.* **1997**, *9*, 802-&.

(15) Javier, A.; Yun, C. S.; Sorena, J.; Strouse, G. F. *J. Phys. Chem. B* **2003**, *107*, 435-442.

(16) Kumar, S.; Nann, T. *J. Mater. Res.* **2004**, *19*, 1990-1994.

(17) Littke, A. F.; Fu, G. C. *J. Am. Chem. Soc.* **2001**, *123*, 6989-7000.

(18) Mikroyannidis, J. A. *Macromolecules* **2002**, *35*, 9289-9295.

(19) Skaff, H.; Sill, K.; Emrick, T. *J. Am. Chem. Soc.* **2004**, *126*, 11322-11325.

(20) Williams, R. H.; Hamilton, L. A. *J. Am. Chem. Soc.* **1952**, *74*, 5418-5420.

(21) Peng, Z. A.; Peng, X. G. *J. Am. Chem. Soc.* **2001**, *123*, 183-184.

(22) Fluorescence quantum yield is reported relative to Rhodamine 6G and was calculated using the following equation. $Q = Q_R \frac{I}{I_R} \frac{OD_R}{OD} \frac{n^2}{n_R^2}$

(23) Rehahn, M.; Schluter, A. D.; Feast, W. J. *Synthesis* **1988**, 386-388.

(24) Milstein, D.; Stille, J. K. *J. Am. Chem. Soc.* **1979**, *101*, 4992-4998.

(25) Odian, G. *Principles of Polymerization*; 3rd ed.; Wiley-Interscience: New York, 1991.

(26) Jorgensen, M.; Krebs, F. C. *J. Org. Chem.* **2004**, *69*, 6688-6696.

(27) Liu, Y.; Lahti, P. M.; La, F. *Polymer* **1998**, *39*, 5241-5244.

(28) Brizius, G.; Pschirer, N. G.; Steffen, W.; Stitzer, K.; zur Loye, H. C.; Bunz, U. H. F. *J. Am. Chem. Soc.* **2000**, *122*, 12435-12440.

(29) Detert, H.; Sugiono, E. *J. Prakt. Chem.* **1999**, *341*, 358-362.

(30) Zhang, B. Z.; Fujiki, M.; Tang, H. Z.; Motonaga, M.; Torimitsu, K. *Macromolecules* **2002**, *35*, 1988-1990.

(31) Bruck, P. *J. Org. Chem.* **1970**, *35*, 2222-2227.

(32) Morin, J. F.; Drolet, N.; Tao, Y.; Leclerc, M. *Chem. Mater.* **2004**, *16*, 4619-4626.

(33) Reetz, M. T.; Westermann, E. *Angew. Chem. Int. Ed.* **2000**, *39*, 165-168.

(34) Beletskaya, I. P.; Cheprakov, A. V. *Chem. Rev.* **2000**, *100*, 3009-3066.

(35) Hu, J.; Liu, Y. *Langmuir* **2005**, *21*, 2121-2123.

(36) Schenk, R.; Gregorius, H.; Meerholz, K.; Heinze, J.; Mullen, K. *J. Am. Chem. Soc.* **1991**, *113*, 2634-2647.

(37) Scherf, U.; Mullen, K. *Synthesis* **1992**, 23-38.

(38) Colvin, V. L.; Schlamp, M. C.; Alivisatos, A. P. *Nature* **1994**, *370*, 354-357.

(39) Kucur, E.; Riegler, J.; Urban, G. A.; Nann, T. *J. Chem. Phys.* **2003**, *119*, 2333-2337.

(40) Bohnen, A.; Rader, H. J.; Mullen, K. *Synth. Met.* **1992**, *47*, 37-63.

(41) Schlamp, M. C.; Peng, X. G.; Alivisatos, A. P. *J. App. Phys.* **1997**, *82*, 5837-5842.

(42) Schlegel, G.; Bohnenberger, J.; Potapova, I.; Mews, A. *Phys. Rev. Lett.* **2002**, *88*, 137401.

(43) Barnes, M. D.; Krstic, P. S.; Kumar, P.; Mehta, A.; Wells, J. C. *Phys. Rev. B* **2005**, *71*.

(44) Gonzalez, J. I.; Lee, T. H.; Barnes, M. D.; Antoku, Y.; Dickson, R. M. *Phys. Rev. Lett.* **2004**, *93*.

(45) Kumar, P.; Mehta, A.; Mahurin, S. M.; Dai, S.; Dadmun, M. D.; Sumpter, B. G.; Barnes, M. D. *Macromolecules* **2004**, *37*, 6132-6140.

(46) Anni, M.; Manna, L.; Cingolani, R.; Valerini, D.; Creti, A.; Lomascolo, M. *App. Phys. Lett.* **2004**, *85*, 4169-4171.

(47) Odoi, M. Y.; Hammer, N. I.; Sill, K.; Emrick, T.; Barnes, M. D. *J. Am. Chem. Soc.* **2006**, *128*, 3506-3507.

(48) Kuno, M.; Fromm, D. P.; Hamann, H. F.; Gallagher, A.; Nesbitt, D. J. *J. Chem. Phys.* **2000**, *112*, 3117-3120.

(49) Krauss, T. D.; Brus, L. E. *Mater. Sci. Eng. B* **2000**, *69*, 289-294.

(50) Krauss, T. D.; Brus, L. E. *Phys. Rev. Lett.* **1999**, *83*, 4840-4843.

BIBLIOGRAPHY

Advincula, R. C. *J. Disp. Sci. Tech.* **2003**, *24*, 343-361.

Akcelrud, L. *Prog. Polym. Sci.* **2003**, *28*, 875-962.

Aldana, J.; Wang, Y. A.; Peng, X. G. *J. Am. Chem. Soc.* **2001**, *123*, 8844-8850.

Alivisatos, A. P. *J. Phys. Chem.* **1996**, *100*, 13226-13239.

Alivisatos, A. P. *Science* **1996**, *271*, 933-937.

Anni, M.; Manna, L.; Cingolani, R.; Valerini, D.; Creti, A.; Lomascolo, M. *App. Phys. Lett.* **2004**, *85*, 4169-4171.

Appell, D. *Nature* **2002**, *419*, 553-555.

Babes, L.; Denizot, B.; Tanguy, G.; Le Jeune, J. J.; Jallet, P. *J. Coll. Inter. Sci.* **1999**, *212*, 474-482.

Bailey, T. C.; Johnson, S. C.; Sreenivasan, S. V.; Ekerdt, J. G.; Willson, C. G.; Resnick, D. J. *J. Photopolym. Sci. Tech.* **2002**, *15*, 481-486.

Bakalova, R.; Ohba, H.; Zhelev, Z.; Nagase, T.; Jose, R.; Ishikawa, M.; Baba, Y. *Nano Lett.* **2004**, *4*, 1567-1573.

Bandaranayake, R. J.; Wen, G. W.; Lin, J. Y.; Jiang, H. X.; Sorensen, C. M. *Appl. Phys. Lett.* **1995**, *67*, 831-833.

Barnes, M. D.; Krstic, P. S.; Kumar, P.; Mehta, A.; Wells, J. C. *Phys. Rev. B* **2005**, *71*.

Barton, J. *Prog. Polym. Sci.* **1996**, *21*, 399-438.

Battaglia, D.; Peng, X. G. *Nano Lett.* **2002**, *2*, 1027-1030.

Becker, M. L.; Remsen, E. E.; Pan, D.; Wooley, K. L. *Bioconj. Chem.* **2004**, *15*, 699-709.

Beil, J. B.; Lemcoff, G.; Zimmerman, S. C. *J. Am. Chem. Soc.* **2004**, *126*, 13576-13577.

Beletskaya, I. P.; Cheprakov, A. V. *Chem. Rev.* **2000**, *100*, 3009-3066.

Benoit, D.; Chaplinski, V.; Braslau, R.; Hawker, C. J. *J. Am. Chem. Soc.* **1999**, *121*, 3904-3920.

Benoit, D.; Grimaldi, S.; Robin, S.; Finet, J. P.; Tordo, P.; Gnanou, Y. *J. Am. Chem. Soc.* **2000**, *122*, 5929-5939.

Blomberg, S.; Ostberg, S.; Harth, E.; Bosman, A. W.; Van Horn, B.; Hawker, C. J. *J. Polym. Sci., Part A: Polym. Chem.* **2002**, *40*, 1309-1320.

Bockstaller, M. R.; Lapetnikov, Y.; Margel, S.; Thomas, E. L. *J. Am. Chem. Soc.* **2003**, *125*, 5276-5277.

Bohnen, A.; Rader, H. J.; Mullen, K. *Synth. Met.* **1992**, *47*, 37-63.

Brizius, G.; Pschirer, N. G.; Steffen, W.; Stitzer, K.; zur Loye, H. C.; Bunz, U. H. F. *J. Am. Chem. Soc.* **2000**, *122*, 12435-12440.

Bruck, P. *J. Org. Chem.* **1970**, *35*, 2222-2227.

Brus, L. *Curr. Opin. Coll. Inter. Sci.* **1996**, *1*, 197-201.

Brus, L. *J. Phys. Chem. Solids* **1998**, *59*, 459-465.

Brust, M.; Walker, M.; Bethell, D.; Schiffrin, D. J.; Whyman, R. *Chem. Commun.* **1994**, 801-802.

Bunge, S. D.; Krueger, K. M.; Boyle, T. J.; Rodriguez, M. A.; Headley, T. J.; Colvin, V. L. *J. Mater. Chem.* **2003**, *13*, 1705-1709.

Burda, C.; Green, T. C.; Link, S.; El-Sayed, M. A. *J. Phys. Chem. B* **1999**, *103*, 1783-1788.

Calandra, P.; Longo, A.; Liveri, V. T. *J. Phys. Chem. B* **2003**, *107*, 25-30.

Carrot, G.; Rutot-Houze, D.; Pottier, A.; Degee, P.; Hilborn, J.; Dubois, P. *Macromolecules* **2002**, *35*, 8400-8404.

Carrot, G.; Scholz, S. M.; Plummer, C. J. G.; Hilborn, J.; Hedrick, J. *Chem. Mater.* **1999**, *11*, 3571-3577.

Chan, W. C. W.; Nie, S. M. *Science* **1998**, *281*, 2016-2018.

Chao, W. L.; Harteneck, B. D.; Liddle, J. A.; Anderson, E. H.; Attwood, D. T. *Nature* **2005**, *435*, 1210-1213.

Chiefari, J.; Chong, Y. K.; Ercole, F.; Krstina, J.; Jeffery, J.; Le, T. P. T.; Mayadunne, R. T. A.; Meijs, G. F.; Moad, C. L.; Moad, G.; Rizzardo, E.; Thang, S. H. *Macromolecules* **1998**, *31*, 5559-5562.

Chiu, J. J.; Kim, B. J.; Kramer, E. J.; Pine, D. J. *J. Am. Chem. Soc.* **2005**, *127*, 5036-5037.

Cho, B. R. *Prog. Polym. Sci.* **2002**, *27*, 307-355.

Chou, S. Y.; Krauss, P. R.; Renstrom, P. J. *Science* **1996**, *272*, 85-87.

Coe, S.; Woo, W. K.; Bawendi, M. G.; Bulovic, V. *Nature* **2002**, *420*, 800-803.

Colombani, D. *Prog. Polym. Sci.* **1997**, *22*, 1649-1720.

Colvin, V. L.; Schlamp, M. C.; Alivisatos, A. P. *Nature* **1994**, *370*, 354-357.

Corbierre, M. K.; Cameron, N. S.; Sutton, M.; Mochrie, S. G. J.; Lurio, L. B.; Ruhm, A.; Lennox, R. B. *J. Am. Chem. Soc.* **2001**, *123*, 10411-10412.

Corner, T. *Adv. Polym. Sci.* **1984**, *62*, 95-142.

Crouch, D. J.; O'Brien, P.; Malik, M. A.; Skabara, P. J.; Wright, S. P. *Chem. Commun.* **2003**, 1454-1455.

Dabbousi, B. O.; Bawendi, M. G.; Onitsuka, O.; Rubner, M. F. *App. Phys. Lett.* **1995**, *66*, 1316-1318.

Dao, J.; Benoit, D.; Hawker, C. J. *J. Polym. Sci., Part A: Polym. Chem.* **1998**, *36*, 2161-2167.

De Franceschi, S.; Kouwenhoven, L. *Nature* **2002**, *417*, 701-702.

Detert, H.; Sugiono, E. *J. Prakt. Chem.* **1999**, *341*, 358-362.

Dinsmore, A. D.; Hsu, M. F.; Nikolaides, M. G.; Marquez, M.; Bausch, A. R.; Weitz, D. A. *Science* **2002**, *298*, 1006-1009.

Dollefeld, H.; Hoppe, K.; Kolny, J.; Schilling, K.; Weller, H.; Eychmuller, A. *Phys. Chem. Chem. Phys.* **2002**, *4*, 4747-4753.

Duan, H.; Kuang, M.; Wang, D.; Kurth, D. G.; Mohwald, H. *Angew. Chem. Int. Ed.* **2005**, *44*, 1717-1720.

Eychmuller, A. *J. Phys. Chem. B* **2000**, *104*, 6514-6528.

Farmer, S. C.; Patten, T. E. *Chem. Mater.* **2001**, *13*, 3920-3926.

Fendler, J. H. *Chem. Mater.* **1996**, *8*, 1616-1624.

Fogg, D. E.; Radzilowski, L. H.; Dabbousi, B. O.; Schrock, R. R.; Thomas, E. L.; Bawendi, M. G. *Macromolecules* **1997**, *30*, 8433-8439.

Gao, H.; Zhao, Y.; Fu, S.; Li, B.; Li, M. *Colloid. Polym. Sci.* **2002**, *280*, 653-660.

Gao, M. Y.; Richter, B.; Kirstein, S. *Adv. Mater.* **1997**, *9*, 802-&.

Gao, M. Y.; Richter, B.; Kirstein, S. *Synthetic Metals* **1999**, *102*, 1213-1214.

Georges, M. K.; Veregin, R. P. N.; Kazmaier, P. M.; Hamer, G. K. *Macromolecules* **1993**, *26*, 2987-2988.

Gerion, D.; Pinaud, F.; Williams, S. C.; Parak, W. J.; Zanchet, D.; Weiss, S.; Alivisatos, A. P. *J. Phys. Chem. B* **2001**, *105*, 8861-8871.

Gerstner, E. *Nature* **2003**, *425*, 244-244.

Ginger, D. S.; Greenham, N. C. *Physical Review B* **1999**, *59*, 10622-10629.

Godovsky, D. Y. In *Biopolymers* 2000; Vol. 153, p 163-205.

Gonzalez, J. I.; Lee, T. H.; Barnes, M. D.; Antoku, Y.; Dickson, R. M. *Physical Review Letters* **2004**, *93*.

Gopidas, K. R.; Whitesell, J. K.; Fox, M. A. *J. Am. Chem. Soc.* **2003**, *125*, 14168-14180.

Gottfried, A. C.; Brookhart, M. *Macromolecules* **2003**, *36*, 3085-3100.

Gravano, S. M.; Dumas, R.; Liu, K.; Patten, T. E. *J. Polym. Sci, Part A* **2005**, *43*, 3675-3688.

Gray, M. K.; Zhou, H. Y.; Nguyen, S. T.; Torkelson, J. M. *Macromolecules* **2003**, *36*, 5792-5797.

Green, P. F.; Russell, T. P.; Jerome, R.; Granville, M. *Macromolecules* **1988**, *21*, 3266-3273.

Greenham, N. C.; Peng, X.; Alivisatos, A. P. *Phys. Rev. B* **1996**, *54*, 17628-17633.

Greenham, N. C.; Peng, X.; Alivisatos, A. P. *Synth. Met.* **1997**, *84*, 545-546.

Gruber, H. F. *Prog. Polym. Sci.* **1992**, *17*, 953-1044.

Harth, E.; Van Horn, B.; Lee, V. Y.; Germack, D. S.; Gonzales, C. P.; Miller, R. D.; Hawker, C. J. *J. Am. Chem. Soc.* **2002**, *124*, 8653-8660.

Hawker, C. J. *Acc. Chem. Res.* **1997**, *30*, 373-382.

Hawker, C. J.; Barclay, G. G.; Orellana, A.; Dao, J.; Devonport, W. *Macromolecules* **1996**, *29*, 5245-5254.

Hong, R.; Fischer, N. O.; Verma, A.; Goodman, C. M.; Emrick, T.; Rotello, V. M. *J. Am. Chem. Soc.* **2004**, *126*, 739-743.

Hsu, H. P.; Nadler, W.; Grassberger, P. *Macromolecules* **2004**, *37*, 4658-4663.

Hu, J.; Liu, Y. *Langmuir* **2005**, *21*, 2121-2123.

Huber, D. L. *Small* **2005**, *1*, 482-501.

Huynh, W. U.; Dittmer, J. J.; Alivisatos, A. P. *Science* **2002**, *295*, 2425-2427.

Ipe, B. I.; Lehnig, M.; Niemeyer, C. M. *Small* **2005**, *1*, 706-709.

Ito, T.; Okazaki, S. *Nature* **2000**, *406*, 1027-1031.

Javier, A.; Yun, C. S.; Sorena, J.; Strouse, G. F. *J. Phys. Chem. B* **2003**, *107*, 435-442.

Ji, J.; Coffer, J. L. *J. Phys. Chem. B* **2002**, *106*, 3860-3863.

Johnson, L. K.; Killian, C. M.; Brookhart, M. *J. Am. Chem. Soc.* **1995**, *117*, 6414-6415.

Jordi, M. A.; Seery, T. A. P. *J. Am. Chem. Soc.* **2005**, *127*, 4416-4422.

Jorgensen, M.; Krebs, F. C. *J. Org. Chem.* **2004**, *69*, 6688-6696.

Kalyuzhny, G.; Murrary, R. W. *J. Phys. Chem. B* **2005**, *109*, 7012-7021.

Kang, Y.; Taton, T. A. *Angew. Chem. Int. Ed.* **2005**, *44*, 409-412.

Karayigitoglu, C. F.; Tata, M.; John, V. T.; McPherson, G. L. *Coll. Surf. A* **1994**, *82*, 151-162.

Khairutdinov, R. F. *Coll. J.* **1997**, *59*, 535-548.

Kim, D. Y.; Cho, H. N.; Kim, C. Y. *Prog. Polym. Sci.* **2000**, *25*, 1089-1139.

Kim, H.; Achermann, M.; Balet, L. P.; Hollingsworth, J. A.; Klimov, V. I. *J. Am. Chem. Soc.* **2005**, *127*, 544-546.

Kim, S.; Bawendi, M. G. *J. Am. Chem. Soc.* **2003**, *125*, 14652-14653.

Kim, S. W.; Kim, S.; Tracy, J. B.; Jasanoff, A.; Bawendi, M. G. *J. Am. Chem. Soc.* **2005**, *127*, 4556-4557.

Kirchhoff, R. A.; Bruza, K. J. *Prog. Polym. Sci.* **1993**, *18*, 85.

Konya, Z.; Puntes, V. F.; Kiricsi, I.; Zhu, J.; Alivisatos, A. P.; Somorjai, G. A. *Nano Lett.* **2002**, *2*, 907-910.

Krauss, T. D.; Brus, L. E. *Phys. Rev. Lett.* **1999**, *83*, 4840-4843.

Krauss, T. D.; Brus, L. E. *Mater. Sci. Eng. B* **2000**, *69*, 289-294.

Kruse, T. M.; Souleimonova, R.; Cho, A.; Gray, M. K.; Torkelson, J. M.; Broadbelt, L. J. *Macromolecules* **2003**, *36*, 7812-7823.

Kucur, E.; Riegler, J.; Urban, G. A.; Nann, T. *J. Chem. Phys.* **2003**, *119*, 2333-2337.

Kumar, P.; Mehta, A.; Mahurin, S. M.; Dai, S.; Dadmun, M. D.; Sumpter, B. G.; Barnes, M. D. *Macromolecules* **2004**, *37*, 6132-6140.

Kumar, S.; Nann, T. *J. Mater. Res.* **2004**, *19*, 1990-1994.

Kuno, M.; Fromm, D. P.; Hamann, H. F.; Gallagher, A.; Nesbitt, D. J. *J. Chem. Phys.* **2000**, *112*, 3117-3120.

Lacoste, T. D.; Michalet, X.; Pinaud, F.; Chemla, D. S.; Alivisatos, A. P.; Weiss, S. *Proc. Nat. Acad. Sci.* **2000**, *97*, 9461-9466.

Lai, J. T.; Filla, D.; Shea, R. *Macromolecules* **2002**, *35*, 6754-6756.

Larson, D. R.; Zipfel, W. R.; Williams, R. M.; Clark, S. W.; Bruchez, M. P.; Wise, F. W.; Webb, W. W. *Science* **2003**, *300*, 1434-1436.

Leatherdale, C. A.; Kagan, C. R.; Morgan, N. Y.; Empedocles, S. A.; Kastner, M. A.; Bawendi, M. G. *Physical Review B* **2000**, *62*, 2669-2680.

Lee, J.; Sundar, V. C.; Heine, J. R.; Bawendi, M. G.; Jensen, K. F. *Adv. Mater.* **2000**, *12*, 1102-1105.

Lee, J. Y.; Thompson, R. B.; Jasnow, D.; Balazs, A. C. *Phys. Rev. Lett.* **2002**, *89*.

Leiston-Belanger, J. M.; Russell, T. P.; Drockenmuller, E.; Hawker, C. J. *Macromolecules* **2005**, *38*, 7676-7683.

Li, I.; Howell, B. A.; Matyjaszewski, K.; Shigemoto, T.; Smith, P. B.; Priddy, D. B. *Macromolecules* **1995**, *28*, 6692-6693.

Li, P. H.; Wang, L.; Li, H. J. *Tetrahedron* **2005**, *61*, 8633-8640.

Lin, Y.; Boker, A.; He, J.; Sill, K.; Xiang, H.; Abetz, C.; Li, X.; Wang, J.; Emrick, T.; Long, S.; Wang, Q.; Balazs, A.; Russell, T. P. *Nature* **2005**, *434*, 55-59.

Lin, Y.; Skaff, H.; Emrick, T.; Dinsmore, A. D.; Russell, T. P. *Science* **2003**, *299*, 226-229.

Link, S.; El-Sayed, M. A. *J. Phys. Chem. B* **1999**, *103*, 4212-4217.

Littke, A. F.; Fu, G. C. *J. Am. Chem. Soc.* **2001**, *123*, 6989-7000.

Liu, J.; Tanaka, T.; Sivula, K.; Alivisatos, A. P.; Fréchet, J. M. J. *J. Am. Chem. Soc.* **2004**, *126*, 6550-6551.

Liu, Y.; Lahti, P. M.; La, F. *Polymer* **1998**, *39*, 5241-5244.

Locklin, J.; Patton, D.; Deng, S.; Baba, A.; Millan, M.; Advincula, R. C. *Chem. Mater.* **2004**, *16*, 5187-5193.

Lopes, W. A.; Jaeger, H. M. *Nature* **2001**, *414*, 735-738.

Lover, T.; Henderson, W.; Bowmaker, G. A.; Seakins, J. M.; Cooney, R. P. *Inorg. Chem.* **1997**, *36*, 3711-3723.

Lowe, A. B.; Sumerlin, B. S.; Donovan, M. S.; McCormick, C. L. *J. Am. Chem. Soc.* **2002**, *124*, 11562-11563.

Malz, H.; Komber, H.; Voigt, D.; Pionteck, J. *Macromol. Chem. Phys.* **1998**, *199*, 583-588.

Manna, L.; Scher, E. C.; Alivisatos, A. P. *J. Am. Chem. Soc.* **2000**, *122*, 12700-12706.

Marcus, M. A.; Flood, W.; Stiegerwald, M.; Brus, L.; Bawendi, M. *J. Phys. Chem.* **1991**, *95*, 1572-1576.

Markoski, L. J.; Walker, K. A.; Deeter, G. A.; Spilman, G. E.; Martin, D. C.; Moore, J. S. *Chem. Mater.* **1993**, *5*, 248-250.

Matsuno, R.; Yamamoto, K.; Otsuka, H.; Takahara, A. *Chem. Mater.* **2003**, *15*, 3-5.

Matsuno, R.; Yamamoto, K.; Otsuka, H.; Takahara, A. *Macromolecules* **2004**, *37*, 2203-2209.

Mattoussi, H.; Cumming, A. W.; Murray, C. B.; Bawendi, M. G.; Ober, R. *J. Phys. Chem.* **1996**, *105*, 9890-9896.

Mattoussi, H.; Mauro, J. M.; Goldman, E. R.; Anderson, G. P.; Sundar, V. C.; Mikulec, F. V.; Bawendi, M. G. *J. Am. Chem. Soc.* **2000**, *122*, 12142-12150.

Mattoussi, H.; Radzilowski, L. H.; Dabbousi, B. O.; Fogg, D. E.; Schrock, R. R.; Thomas, E. L.; Rubner, M. F.; Bawendi, M. G. *J. Appl. Phys.* **1999**, *86*, 4390-4399.

Mattoussi, H.; Radzilowski, L. H.; Dabbousi, B. O.; Thomas, E. L.; Bawendi, M. G.; Rubner, M. F. *J. Appl. Phys.* **1998**, *83*, 7965-7974.

Maye, M. M.; Zheng, W.; Liebowitz, F. L.; Ly, N. K.; Zhong, C. J. *Langmuir* **2000**, *16*, 490-497.

Mayes, A. M.; Barker, J. G.; Russell, T. P. *J. Chem. Phys.* **1994**, *101*, 5213-5218.

Mayes, A. M.; Russell, T. P.; Bassereau, P.; Baker, S. M.; Smith, G. S. *Macromolecules* **1994**, *27*, 749-755.

McDonald, S. A.; Konstantantos, G.; Zhang, S.; Cyr, P. W.; Klem, E. J. D.; Levina, L.; Sargent, E. H. *Nature Mater.* **2005**, *4*, 138-141.

Mikroyannidis, J. A. *Macromolecules* **2002**, *35*, 9289-9295.

Milliron, D. J.; Alivisatos, A. P.; Pitois, C.; Edder, C.; Fréchet, J. M. J. *Adv. Mater.* **2003**, *15*, 58-61.

Milliron, D. J.; Alivisatos, A. P.; Pitois, C.; Edder, C.; Fréchet, J. M. J. *Adv. Mater.* **2003**, *15*, 58.

Milstein, D.; Stille, J. K. *J. Am. Chem. Soc.* **1979**, *101*, 4992-4998.

Misner, M. J.; Skaff, H.; Emrick, T.; Russell, T. P. *Adv. Mater.* **2003**, *15*, 221.

Mohanty, P. *Nature* **2005**, *437*, 325-326.

Morgan, N. Y.; Leatherdale, C. A.; Drndic, M.; Jarosz, M. V.; Kastner, M. A.; Bawendi, M. *Phys. Rev. B* **2002**, *66*, 075339.

Morin, J. F.; Drolet, N.; Tao, Y.; Leclerc, M. *Chem. Mater.* **2004**, *16*, 4619-4626.

Murray, C. B.; Kagan, C. R.; Bawendi, M. G. *Science* **1995**, *270*, 1335-1338.

Murray, C. B.; Kagan, C. R.; Bawendi, M. G. *Ann. Rev. Mater. Sci.* **2000**, *30*, 545-610.

Murray, C. B.; Norris, D. J.; Bawendi, M. G. *J. Am. Chem. Soc.* **1993**, *115*, 8706-8715.

Myung, N.; Ding, Z. F.; Bard, A. J. *Nano Lett.* **2002**, *2*, 1315-1319.

Nagasaki, Y.; Ishii, T.; Sunaga, Y.; Watanabe, Y.; Otsuka, H.; Kataoka, K. *Langmuir* **2004**, *20*, 6396-6400.

Nakamura, H.; Yamaguchi, Y.; Miyazaki, M.; Maeda, H.; Uehara, M.; Mulvaney, P. *Chem. Commun.* **2002**, 2844-2845.

Niemeyer, C. M. *Science* **2002**, *297*, 62-63.

Nikolaides, M. G.; Bausch, A. R.; Hsu, M. F.; Dinsmore, A. D.; Brenner, M. P.; Weitz, D. A. *Nature* **2002**, *420*, 299-301.

Nirmal, M.; Brus, L. *Acc. Chem. Res.* **1999**, *32*, 407-414.

Norris, D. J.; Efros, A. L.; Rosen, M.; Bawendi, M. G. *Phys. Rev. B* **1996**, *53*, 16347-16354.

Norris, D. J.; Sacra, A.; Murray, C. B.; Bawendi, M. G. *Phys. Rev. Lett.* **1994**, *72*, 2612-2615.

Odian, G. *Principles of Polymerization*; 3rd ed.; Wiley-Interscience: New York, 1991.

Odoi, M. Y.; Hammer, N. I.; Sill, K.; Emrick, T.; Barnes, M. D. *J. Am. Chem. Soc.* **2006**, *128*, 3506-3507.

Ohno, K.; Koh, K.; Tsujii, Y.; Fukuka, T. *Macromolecules* **2002**, *35*, 8989-8993.

Oneil, G. A.; Torkelson, J. M. *Trends Polym. Sci.* **1997**, *5*, 349-355.

Oneil, G. A.; Wisnudel, M. B.; Torkelson, J. M. *Macromolecules* **1996**, *29*, 7477-7490.

Oswald, P.; Pieranski, P.; Picano, F.; Holyst, R. *Phys. Rev. Lett.* **2002**, *8801*, art. no.-015503.

Otsuka, H.; Akiyama, Y.; Nagasaki, Y.; Kataoka, K. *J. Am. Chem. Soc.* **2001**, *123*, 8226-8230.

Pan, C.; Pelzer, K.; Philippot, K.; Chaudret, B.; Dassenoy, F.; Lecante, P.; Casanove, M. J. *J. Am. Chem. Soc.* **2001**, *123*, 7584-7593.

Park, S. J.; Taton, T. A.; Mirkin, C. A. *Science* **2002**, *295*, 1503-1506.

Pasco, S. T.; Lahti, P. M.; Karasz, F. E. *Macromolecules* **1999**, *32*, 6933-6937.

Pathak, S.; Choi, S. K.; Arnheim, N.; Thompson, M. E. *J. Am. Chem. Soc.* **2001**, *123*, 4103-4104.

Patten, T. E.; Matyjaszewski, K. *Acc. Chem. Res.* **1999**, *32*, 895-903.

Peng, X. G.; Manna, L.; Yang, W. D.; Wickham, J.; Scher, E.; Kadavanich, A.; Alivisatos, A. P. *Nature* **2000**, *404*, 59-61.

Peng, X. G.; Schlamp, M. C.; Kadavanich, A. V.; Alivisatos, A. P. *J. Am. Chem. Soc.* **1997**, *119*, 7019-7029.

Peng, Z. A.; Peng, X. G. *J. Am. Chem. Soc.* **2001**, *123*, 183-184.

Peng, Z. A.; Peng, X. G. *J. Am. Chem. Soc.* **2002**, *124*, 3343-3353.

Penner, R. M. *Acc. Chem. Res.* **2000**, *33*, 78-86.

Priddy, D. B. In *Polym. Synth.* 1994; Vol. 111, 67-114.

Qi, D.; Fischbein, M.; Drndic, M.; Selmic, S. *Appl. Phys. Lett* **2005**, *86*, 093103.

Qu, L. H.; Peng, X. G. *J. Am. Chem. Soc.* **2002**, *124*, 2049-2055.

Qu, L. H.; Peng, Z. A.; Peng, X. G. *Nano Letters* **2001**, *1*, 333-337.

Reetz, M. T.; Westermann, E. *Angew. Chem. Int. Ed.* **2000**, *39*, 165-168.

Rehahn, M.; Schluter, A. D.; Feast, W. J. *Synthesis* **1988**, 386-388.

Rogach, A. L.; Katsikas, L.; Kornowski, A.; Su, D. S.; Eychmuller, A.; Weller, H. *Berichte Der Bunsen-Gesellschaft-Physical Chemistry Chemical Physics* **1996**, *100*, 1772-1778.

Roovers, J. In *Star and Hyperbranched Polymers* New York, 1999, p 285-341.

Ruach-Nir, I.; Wagner, H. D.; Rubinstein, I.; Hodes, G. *Adv. Funct. Mater.* **2003**, *13*, 159-164.

Russell, J. T.; Lin, Y.; Boker, A.; Long, S.; Carl, P.; Zettl, H.; He, J.; Sill, K.; Tangirala, R.; Emrick, T.; Littrell, K.; Thiyagarajan, P.; Cookson, D.; Fery, A.; Wang, Q.; Russell, T. P. *Angew. Chem. Int. Ed.* **2005**, *44*, 2420-2426.

Ryu, D. Y.; Shin, K.; Drockenmuller, E.; Hawker, C. J.; Russell, T. P. *Science* **2005**, *308*, 236-239.

Schenk, R.; Gregorius, H.; Meerholz, K.; Heinze, J.; Mullen, K. *J. Am. Chem. Soc.* **1991**, *113*, 2634-2647.

Scherf, U. In *Carbon Rich Compounds II* 1999; Vol. 201, p 163-222.

Scherf, U.; Mullen, K. *Synthesis* **1992**, 23-38.

Scherf, U.; Riechel, S.; Lemmer, U.; Mahrt, R. F. *Curr. Opin. Solid State Mater. Sci.* **2001**, *5*, 143-154.

Schlamp, M. C.; Peng, X. G.; Alivisatos, A. P. *J. App. Phys.* **1997**, *82*, 5837-5842.

Schlegel, G.; Bohnenberger, J.; Potapova, I.; Mews, A. *Phys. Rev. Lett.* **2002**, *88*, 137401.

Schmelz, O.; Mews, A.; Basche, T.; Herrmann, A.; Mullen, K. *Langmuir* **2001**, *17*, 2861-2865.

Schmidt, G.; Malwitz, M. M. *Curr. Opin. Coll. Inter. Sci.* **2003**, *8*, 103-108.

Schulte-Frohlinde, V.; Holovatch, Y.; von Ferber, C.; Blumen, A. *Phys. Lett. A* **2004**, *328*, 335-340.

Selmarten, D.; Jones, M.; Rumbles, G.; Yu, P.; Nedeljkovic, J.; Shaheen, S. *J. Phys. Chem. B* **2005**, *109*, 15927-15932.

Service, R. F. *Science* **2002**, *298*, 2322-2323.

Service, R. F. *Science* **2005**, *309*, 36-36.

Shenhar, R.; Norsten, T. B.; Rotello, V. M. *Adv. Mater.* **2005**, *17*, 657-669.

Shim, H. K.; Jin, J. I. In *Polymers For Photonics Applications I* 2002; Vol. 158, 193-243.

Sill, K.; Emrick, T. *Chem. Mater.* **2004**, *16*, 1240-1244.

Skaff, H.; Emrick, T. *Chem. Commun.* **2003**, 52-53.

Skaff, H.; Emrick, T. *Angew. Chem. Int. Ed.* **2004**, *43*, 5583-5386.

Skaff, H.; Ilker, M. F.; Coughlin, E. B.; Emrick, T. *J. Am. Chem. Soc.* **2002**, *124*, 5729-5733.

Skaff, H.; Sill, K.; Emrick, T. *J. Am. Chem. Soc.* **2004**, *126*, 11322-11325.

Stalmach, U.; de Boer, B.; Post, A. D.; van Hutten, P. F.; Hadziioannou, G. *Angew. Chem. Int. Ed.* **2001**, *40*, 428-430.

Stathatos, E.; Lianos, R.; Zakeeruddin, S. M.; Liska, P.; Gratzel, M. *Chem. Mater.* **2003**, *15*, 1825-1829.

Sun, Y. G.; Xia, Y. N. *Science* **2002**, *298*, 2176-2179.

Tachibana, Y.; Nazeeruddin, M. K.; Gratzel, M.; Klug, D. R.; Durrant, J. R. *Chem. Phys.* **2002**, *285*, 127-132.

Templeton, A. C.; Hostetler, M. J.; Kraft, C. T.; Murray, R. W. *J. Am. Chem. Soc.* **1998**, *120*, 1906.

Teredesai, P. V.; Deepak, F. L.; Govindaraj, A.; Sood, A. K.; Rao, C. N. R. *J. Nanosci. Nanotech.* **2002**, *2*, 495-498.

Thomas, P. J.; Pews, R. G. *Synth. Commun.* **1991**, *21*, 2335-2340.

Thompson, R. B.; Ginzburg, V. V.; Matsen, M. W.; Balazs, A. C. *Science* **2001**, *292*, 2469-2472.

Thorn-Csanyi, E.; Kraxner, P. *Macromol. Rapid Commun.* **1995**, *16*, 147-153.

Thurmound, K. B.; Huang, H.; Clark, C. G.; Kowalewski, T.; Wooley, K. L. *Coll. Surf. B* **1999**, *16*, 45-54.

Thurmound, K. B.; Kowalewski, T.; Wooley, K. L. *J. Am. Chem. Soc.* **1997**, *119*, 6656-6665.

Tian, S.; Liu, J.; Zhu, T.; Knoll, W. *Chem. Mater.* **2004**, *16*, 4103-4108.

Tseng, G. Y.; Ellenbogen, J. C. *Science* **2001**, *294*, 1293-1294.

von Werne, T.; Patten, T. E. *J. Am. Chem. Soc.* **1999**, *121*, 7409-7410.

von Werne, T.; Patten, T. E. *J. Am. Chem. Soc.* **2001**, *123*, 7497-7505.

Walker, K. A.; Markoski, L. J.; Moore, J. S. *Synthesis* **1992**, 1265-1268.

Wang, D.; He, J.; Rosenzweig, N.; Rosenzweig, Z. *Nano Lett.* **2004**, *4*, 409-413.

Wang, F.; Han, M. Y.; Mya, K. Y.; Wang, Y.; Lai, Y. H. *J. Am. Chem. Soc.* **2005**, *127*, 10350-10355.

Wang, S. P.; Mamedova, N.; Kotov, N. A.; Chen, W.; Studer, J. *Nano Lett.* **2002**, *2*, 817-822.

Wang, X.; Zhuang, J.; Peng, Q.; Li, Y. D. *Nature* **2005**, *437*, 121-124.

Wang, X. S.; Dykstra, T. E.; Salvador, M. R.; Manners, I.; Scholes, G. D.; Winnik, M. A. *J. Am. Chem. Soc.* **2004**, *126*, 7784-7785.

Wang, X. S.; Winnik, M. A.; Manners, I. *Angew. Chem. Int. Ed.* **2004**, *43*, 3703-3707.

Wang, Y.; Tang, Z. Y.; Correa-Duarte, M. A.; Liz-Marzan, L. M.; Kotov, N. A. *J. Am. Chem. Soc.* **2003**, *125*, 2830-2831.

Wang, Y. A.; Li, J. J.; Chen, H. Y.; Peng, X. G. *J. Am. Chem. Soc.* **2002**, *124*, 2293-2298.

Wang, Y. J.; Ma, J.; Jiang, Y. S. *J. Phys. Chem. A* **2005**, *109*, 7197-7206.

Watson, K. J.; Zhu, J.; Ngyen, S. T.; Mirkin, C. A. *J. Am. Chem. Soc.* **1999**, *121*, 462-463.

Weimer, M. W.; Chen, H.; Giannelis, E. P.; Sogah, D. Y. *J. Am. Chem. Soc.* **1999**, *121*, 1615-1616.

Wendland, M. S.; Zimmerman, S. C. *J. Am. Chem. Soc.* **1999**, *121*, 1389-1390.

Williams, R. H.; Hamilton, L. A. *J. Am. Chem. Soc.* **1952**, *74*, 5418-5420.

Yan, H. *Science* **2004**, *306*, 2048-2049.

Yu, D.; Wang, C.; Sionnest, P. G. *Science* **2003**, *300*, 1277-1280.

Yu, D.; Wang, C. J.; Guyot-Sionnest, P. *Science* **2003**, *300*, 1277-1280.

Yu, H.; Li, J. B.; Loomis, R. A.; Gibbons, P. C.; Wang, L. W.; Buhro, W. E. *J. Am. Chem. Soc.* **2003**, *125*, 16168-16169.

Yu, W. W.; Falkner, J. C.; Shih, B. S.; Colvin, V. L. *Chem. Mater.* **2004**, *16*, 3318-3322.

Zeng, Q. H.; Yu, A. B.; Lu, G. Q.; Paul, D. R. *J. Nanosci. Nanotech.* **2005**, *5*, 1574-1592.

Zhang, B. Z.; Fujiki, M.; Tang, H. Z.; Motonaga, M.; Torimitsu, K. *Macromolecules* **2002**, *35*, 1988-1990.

Zhang, Q.; Remsen, E. E.; Wooley, K. L. *J. Am. Chem. Soc.* **2000**, *122*, 3642-3651.

Zhang, Q.; Xu, T.; Butterfield, D.; Misner, M. J.; Ryu, D. Y.; Emrick, T.; Russell, T. P. *Nano Lett.* **2005**, *5*, 357-361.

Zhou, Q.; Wang, S.; Fan, X.; Advincula, R.; Mays, J. *Langmuir* **2002**, *18*, 3324-3331.

Zhu, T.; Vasilev, K.; Kreiter, M.; Mittler, S.; Knoll, W. *Langmuir* **2003**, *19*.